E. E. ZUKOSKI

in

Thermodynamics of Aircraft Gas Turbine Engines (1978)

2. AFTERBURNERS

2.1 Introduction

The simple gas turbine cycle can be designed to have good performance characteristics at a particular operating or design point. However, a particular engine does not have the capability of producing a good performance for large ranges of thrust, an inflexibility that can lead to problems when the flight program for a particular vehicle is considered. For example, many airplanes require a larger thrust during takeoff and acceleration than they do at a cruise condition. Thus, if the engine is sized for takeoff and has its design point at this condition, the engine will be too large at cruise. The vehicle performance will be penalized at cruise for the poor off-design point operation of the engine components and for the larger weight of the engine. Similar problems arise when supersonic cruise vehicles are considered.

The afterburning gas turbine cycle was an early attempt to avoid some of these problems. Afterburners or augmentation devices were first added to aircraft gas turbine engines to increase their thrust during takeoff or brief periods of acceleration and supersonic flight. The devices make use of the fact that, in a gas turbine engine, the maximum gas temperature at the turbine inlet is limited by structural considerations to values less than half the adiabatic flame temperature at the stoichiometric fuel-air ratio. As a result, the gas leaving the turbine contains most of its original concentration of oxygen. This oxygen can be burned with additional fuel in a secondary combustion chamber located downstream of the turbine where temperature constraints are relaxed. The increased total temperature produced at the nozzle by this additional heat addition results in an increased exit velocity and thrust.

The advantage of using the afterburning gas turbine engine cycle is that the weight of the augmented engine is much less than the weight of a turbojet engine producing the same maximum thrust. This advantage is partially offset by the low thermal efficiency of the augmented turbojet cycle, which is characterized by values of specific fuel consumption much higher than those for the gas turbine cycle. However, when the afterburner is used for a small part of a flight, the weight reduction is more important than the increase in fuel consumption.

In the middle 1960s, an augmented gas turbine engine, the General Electric GE4, was selected as the cycle to be used on the Boeing supersonic transport. It was an afterburning turbojet engine and the afterburner was used not only during takeoff or transonic acceleration, but also during the

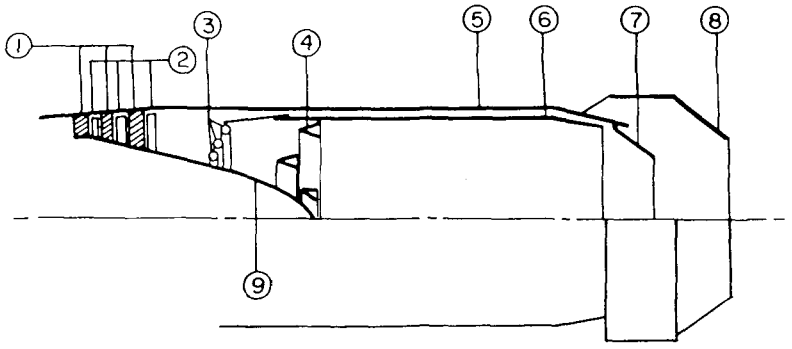

Fig. 2.1 General Electric J-79 afterburner: (1) turbine nozzles, (2) turbine blades, (3) fuel injection rings, (4) three annular V-gutter flameholders, (5) afterburner case, (6) perforated liner, (7) and (8) primary and secondary nozzle flaps, and (9) diffuser inner cone.

Mach 2.7 cruise. At these speeds, afterburning is required even during cruise to obtain a reasonable air specific thrust.

Finally, with the advent of the turbofan engines in the late 1960s and the variable-cycle engines in the 1970s, the afterburner must be viewed as one of an increasing number of devices that can be used to enhance the flexibility of the basic gas turbine cycle. The aim of these systems is to optimize engine performance over the widest possible range of operating conditions. Augmentation can be used in both fan and core streams. In some flight regimes, afterburning in the bypass airstream alone is advantageous and in others, where maximum augmentation is required, afterburning in both the bypass and core engine exhaust streams is desirable. Under some circumstances, mixing the fan and core engine exhaust streams prior to afterburning may produce a large enough performance gain to more than offset total pressure losses and increased engine weight associated with the mixing process.

An afterburner for the gas turbine engine cycle is very similar to a ramjet engine. Gas leaving the turbine is diffused, liquid fuel is added through fuel injection tubes or rings, the combustion process is initiated in the wakes of a number of flame stabilizers, and heat is added along the flame surfaces spreading from these stabilization positions. Nozzles with variable-area throats are necessary to accommodate the large total temperature changes produced by afterburning.

These elements of the afterburner are illustrated in Fig. 2.1 for the turbojet cycle and in Fig. 2.2 for the turbofan cycle. The turbojet engine is a sketch of the General Electric J79 engine and the turbofan engine is a sketch of the Pratt & Whitney F100 engine. In the latter case, afterburning is accomplished without mixing core and fan streams and the inner contour of the nozzle is shown in closed (11) and open (12) positions. In both engines, a combustion chamber liner with an aircooling passage is used to protect the outer, pressure vessel wall from heat transfer by convection and radiation.

To illustrate typical afterburner operating conditions, performance curves are shown in Fig. 2.3 for a turbofan engine, the Pratt & Whitney TF30 engine. This engine is similar to that shown in Fig. 2.2 and the core and turbine gas streams are not mixed. The specific fuel consumption (SFC) and

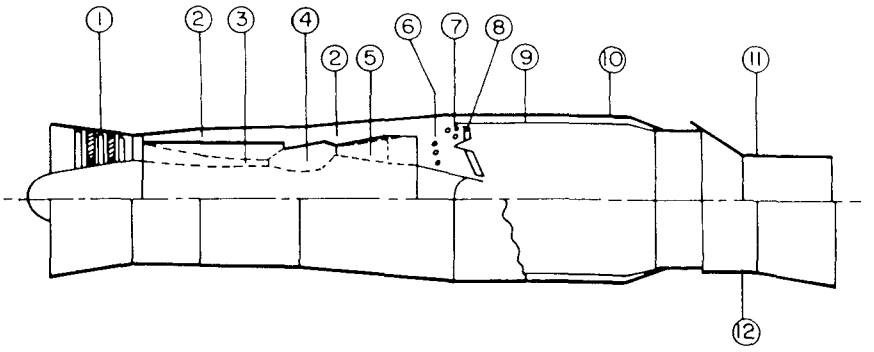

Fig. 2.2 Pratt & Whitney F100-PW-100 augmented turbofan engine: (1) three-stage fan; (2) bypass air duct, core engine compressor (3), burner (4), and turbine (5); (6) fuel injectors for core engine gas stream; (7) fuel injectors for bypass airstream; (8) flame stabilizer for afterburner; (9) perforated afterburner liner; (10) afterburner case; nozzle closed to minimum area (11) and opened to maximum area (12).

thrust F are shown as ratios of their values to their values with no afterburning and as a function of afterburner fuel-air ratio. Afterburner total pressure ratio π_{AB} and combustion efficiency η_{AB} are also given. The two curves on each plot correspond to operating altitudes of about 12 and 14.6 km and a flight Mach number of 1.4. Flow conditions at afterburner entrance for the core stream and for the two altitudes were, for the core stream: total pressure of 1.05 and 0.69 atm, total temperatures of about 900 K for both, inlet velocities of 180 and 230 m/s; for the fan stream: total temperature was about 400 K. At these conditions, thrust augmentation of about 60% can be achieved at a cost of an increase of 120% in specific fuel consumption. The performance decreases as the altitude is increased. Note that the afterburner total pressure ratio with no heat addition is about 0.94; the 6% loss represented by this ratio accounts for some diffusion loss in addition to the flameholder drag losses.

For this engine, fuel is injected through orifices with diameters of about 0.15 cm in a number of concentric rings of fuel injection tubes, which are similar to those shown in Fig. 2.2. Afterburner fuel-air ratio is increased by adding fuel first to the core flow near the interface between the core flow and fan airstream, then to the fan air, and finally to the rest of the core flow. Because the fan air contains the most oxygen and the lowest temperature, afterburning in the stream produces the largest performance gain. However, the low temperature of this stream makes vaporization of the fuel and hence afterburning most difficult. The addition of fuel in the order suggested here first produces a high temperature at the outer edge of the core stream where it can act as a pilot for the fan air combustion process. The rapid fall in combustion efficiency at 14.6 km and for low fuel-air ratios is due to the problem of burning in the cold fan streams where vaporization of the fuel is very poor.

The purpose of this chapter is to discuss the engineering information available concerning afterburner components and to indicate some of the current design practices. Some problem areas will be more thoroughly described than others. The supplementary reading list at the end of this

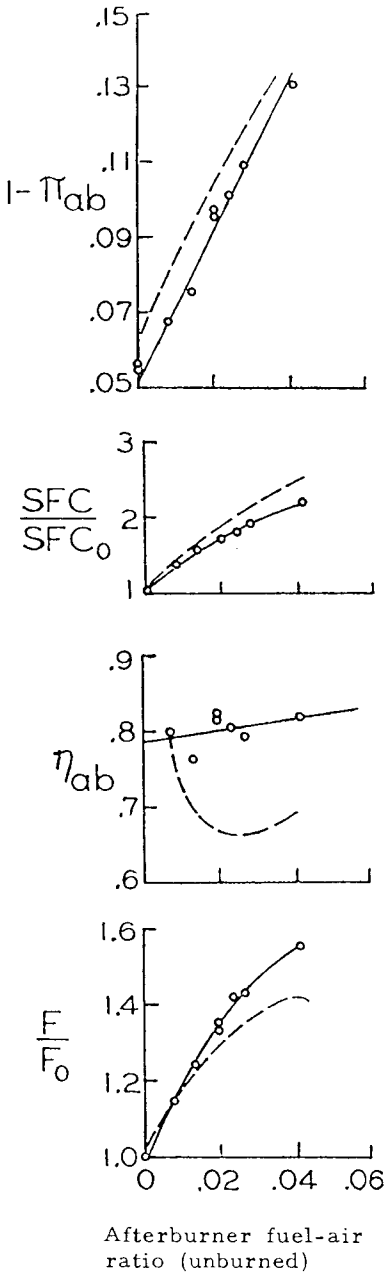

Fig. 2.3 Afterburner performance characteristics for the TF30-P-3 engine. Engine characteristics: $\pi_c = 17$, $\pi_c' = 2.1$, bypass ratio $\alpha = 1.0$, flameholder blockage 0.38, flight Mach number 1.4. Solid curves are for an altitude of 12 km and dashed curves for 14.6 km (data from Ref. 1).

chapter contains references to review articles covering a number of subjects concerning afterburners omitted here.

2.2 Diffuser

The heat that can be added to a compressible flow in a constant-area duct before choking occurs and the pressure loss accompanying this heat addition depend on the Mach number of the flow entering the burner. As the inlet Mach number decreases, the maximum heat addition increases and the total pressure loss decreases. In addition, the flame stabilization process

becomes more difficult as the gas speed increases. Hence, it is desirable to have as low a Mach number as possible at the burner inlet, which leads to the use of a diffuser between the turbine exit plane and the afterburner itself.

The minimum Mach number at the burner inlet is usually fixed by the requirement that the diameter of the afterburner section of the engine not exceed that of the engine components located upstream of the afterburner. This limitation arises from the desire to minimize the drag of the engine due to frontal area and nozzle exit area and the desire to minimize the weight of the afterburner itself.

The desire to minimize weight also results in the requirement that the diffuser be kept as short as possible without producing flow separation from the inner body. Relatively large divergence angles can be used because the blockage of the flow, produced by the flameholder and fuel injection systems, reduces the tendency of the flow to separate from the diffuser cone. Finally, the general problem of producing a steady, uniform, and unseparated flow at the diffuser outlet is often complicated by the presence of a large swirl component in the gas leaving the turbine (15–20% tangential component) and the interaction of this swirling flow with the struts required to support the rear engine bearing.

In augmented turbofan engines in which the two gas streams are to be mixed before afterburning is initiated, the diffuser is usually combined with the mixer. For example, the fan and core streams can be ducted together to form a series of adjacent radial slots with fan air and core air in alternate slots. This geometry has the advantage that mixing will occur in a distance much smaller than required with the undisturbed annular geometry shown in Fig. 2.2. By keeping the cross-sectional areas of each stream almost constant, pressure losses in mixers of this type can be minimized.

2.3 Fuel Injection, Atomization, and Vaporization

The goal of the fuel injection system is to produce a specified distribution of fuel vapor in the gas stream entering the afterburner. In most engines, fuel is introduced in a staged manner so that the heat addition rate can be increased gradually from zero to the desired value. Because ignition, flame stabilization, and flame spreading are easiest to achieve when the fuel-air ratio is close to the stoichiometric value, staging is usually produced by adding fuel to successive annular stream tubes so that the mixture ratio in each tube is nearly stoichiometric. Each stream tube has its own set of fuel injectors and control system, which can be activated independently. For example, see the six injectors used in the F100 engine shown in Fig. 2.2.

The most remarkable fact concerning the fuel systems for afterburners is their simplicity. In many engine systems, fuel is supplied to a circular tube that lies with its axis perpendicular to the gas stream. Fuel is injected into the gas though small-diameter holes located in the sides of the tube such that the liquid jet enters the gas stream in a direction perpendicular to the undisturbed flow direction. The liquid jet penetrates some distance into the gas stream before its momentum is dissipated. During this penetration

process, the airstream tears the jet apart and produces droplets with diameters of micrometer size. Heat transfer from the hot gas stream then vaporizes the droplets.

Given the wide range of values of the mass flows of fuel required, it is remarkable that reasonably thorough mixing of the fuel with the air can be achieved with this simple injection system. In some recent engines, efforts are being made to use simple variable-area injection ports that may possibly give better preparation of the fuel-air mixture.

The whole area of fuel penetration, atomization, and vaporization is not well understood from first principals and one of the time-consuming parts of an afterburner development program is to determine the optimum distribution of the locations for injector tubes, injector ports, and port diameters. In the following paragraphs, a very brief analysis is made of several aspects of the fuel injection problem with the aim of illustrating some of the important scaling parameters rather than of furnishing design procedures.

Penetration

The trajectory of a fluid jet injected into a high-speed airstream can be crudely analyzed by treating the boundaries of the jet and the resulting droplet stream as a solid body and applying the continuity and momentum conservation laws. The force applied to the surface of the stream tube in the direction of the flow (see Fig. 2.4) will be proportional to the dynamic pressure of the gas $\rho_\infty v_\infty^2/2$ and some cross-sectional area, say $\bar{w} \times h$ (where $\bar{w}$ is an average width and h the penetration distance). This force must be balanced by the momentum flux of the injectant stream with mass flux $\dot{m}_j$. If we assume that the fluid is accelerated to a velocity v_∞ at the exit of the control volume and that it enters with *no* momentum flux in the direction of

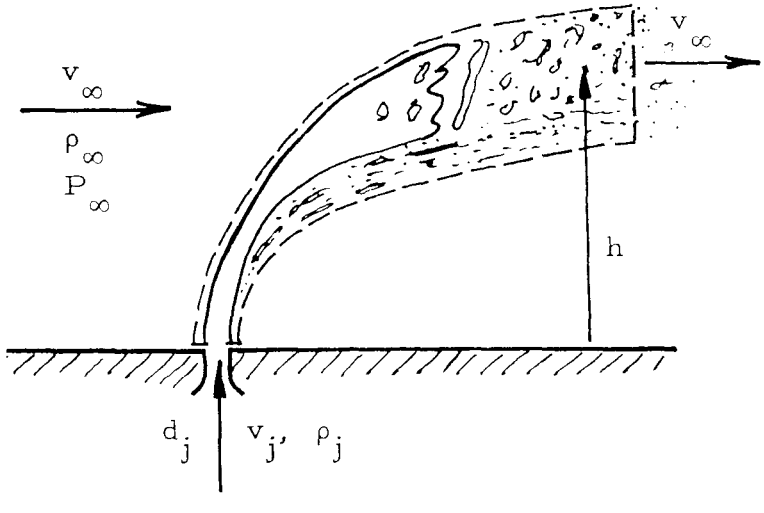

Fig. 2.4 Estimate of penetration distance.

flow, the force balance gives

$$\rho_\infty v_\infty^2 (wh) \propto \dot{m}_j v_\infty$$

so that

$$\dot{m}_j / [\rho_\infty v_\infty (wh)] = \text{const} \tag{2.1}$$

The actual penetration distance is obtained by assuming $w \propto d_j$ and $\dot{m}_j \propto (\pi d_j^2/4)\rho_j v_j$; it is given by

$$\frac{h}{d_j} \propto \sqrt{\frac{\rho_j}{\rho_\infty}} \left(\frac{\rho_j v_j^2}{\rho_\infty v_\infty^2} \right)^{\frac{1}{2}}$$

Note that the denominator of Eq. (2.1) is proportional to the mass flux of air through the region fed by the injector. Thus, if the injector flow rate is changed in order to keep h fixed (as some other parameter such as flight altitude is varied), the overall fuel-air ratio in the stream tube fed by the injector will be held fixed.

Experimental work by Schetz and Padhye[2] suggests that an analysis of this type does predict a reasonable dependence of penetration distance h on the dynamic pressure ratio $\rho_j v_j^2 / \rho_\infty v_\infty^2$. Penetration distances of tens of diameters can be achieved with dynamic pressure ratios between 1 and 2.

Atomization

The breakup of the injected fuel stream into small droplets depends on the dynamic pressure parameters listed above and, in addition, on the viscosities of the fuel and gas streams and on the interfacial tension of the fuel-gas system. The physical process of atomization of the fluid jet probably involves the production of waves on the fluid-gas interface, the shedding of long ligaments of fluid as the waves break, and then the breakup of the ligaments into droplets. The overall process is sufficiently complex that no model or set of scaling parameters has been generally accepted. The problem is complicated by the necessity for measuring and describing a distribution of drop sizes rather than a single drop diameter.

To give the flavor of the results obtained in experiments, the results of Ingebo and Foster[3] will be described. They worked with the volume-median droplet diameter defined as

$$D_{30} = \left(\sum_i n_i D_i^3 / \sum_i n_i \right)^{\frac{1}{3}}$$

where n_i is the number of particles with diameter D_i. They found that D_{30} depended on the injector diameter d_j and two dimensionless parameters, a Reynolds number,

$$Re \equiv \rho_l v_\infty d_j / \mu_l$$

based on the gas stream velocity v_∞, the injector diameter d_j, the liquid density and viscosity ρ_l and μ_l, and a Weber number,

$$We \equiv \sigma_j / \rho_\infty v_\infty^2 d_j$$

based on fuel surface tension σ_j and dynamic pressure of the gas. The relationship for D_{30} found by these authors was

$$D_{30}/d_j = 4(We/Re)^{\frac{1}{4}} \tag{2.2}$$

For a gas stream with a speed of about 200 m/s, temperature of 900 K, pressure of 3 atm, and a gasoline-like fuel jet, the Reynolds and Weber numbers for a millimeter diameter injector port are about 2×10^5 and 10^{-3}, respectively. Using these values in the above equation we find $D_{30} \approx 40$ μm.

Equation (2.2) indicates that there is *no* dependence of atomization on the injection velocity v_j, but that there is an inverse one-quarter power dependence of D_{30} on the gas stream density and, hence, pressure. Thus, as the pressure decreases, droplet diameter will increase slowly. Finally, D_{30} is proportional to the square root of the port diameter d_j.

Evaporation

The evaporation rate of the droplets formed in the injection process is a strong function of the gas and droplet temperatures and the relative velocity of the droplets with respect to the air. For most conditions of interest here, the pressure of the vapor at the surface of the drop will be close to the equilibrium value fixed by the surface temperature of the drop. Vapor is removed from this region by diffusion and forced convection; and the heat required to produce the evaporation is transferred to the surface by conduction from within the drop and by conduction and forced convection from the gas stream. The drop radius and the temperature distribution within the drop will be functions of time. Transport of vapor and heat occur by diffusion and forced convection, both of which may be either laminar or turbulent.

The simplest situation to analyze for this complex problem is the case in which molecular transport processes for mass and heat are dominant and for which the temperature changes within the drop can be ignored. This quasisteady situation is most likely to occur for small (e.g., 10 μm diam) drops moving at a small velocity with respect to the gas stream. Under these conditions, the rate of change of mass M of a droplet is given by

$$\dot{M} = -4\pi r(\rho_v \mathscr{D}) \tag{2.3}$$

where r is the droplet radius and ρ_v and $\mathscr{D}$ the vapor density and diffusion coefficient at the particle surface. Since the particle mass is $(4/3)\pi r^3 \rho_l$,

$$\frac{r\,\mathrm{d}r}{\mathrm{d}t} = \frac{\rho_v \mathscr{D}}{\rho_l}$$

and the time t_e required for complete evaporation of a particle of initial radius r_0 is

$$t_e = r_0^2 / \left(\overline{\rho_v \mathscr{D} / \rho_l}\right) \tag{2.4}$$

where the denominator is the value averaged over the evaporation time of the droplet. Clearly, the time for complete evaporation will be much longer for large drops.

The term in the denominator of Eq. (2.4) is a strong function of the temperature; in order to determine its value, an energy balance for the droplet must also be used. The vapor density at the droplet surface ρ_v is only a function of temperature and, since $\mathscr{D} \propto 1/P$ holds roughly, $\overline{\rho_v \mathscr{D}}$ will be proportional to $1/P$, the inverse of the local static pressure. Thus, as the pressure in the region of injection falls, the time required for evaporation of small droplets of a *fixed* temperature will decrease.

For the simple situation under investigation here, the energy balance reduces to

$$-\dot{M}L = \dot{q}$$

where L is the heat of vaporization, $(-\dot{M})$ the rate of generation of vapor, and $\dot{q}$ the heat transferred by conduction to the drop. $\dot{q}$ is given by $4\pi rk(T_\infty - T_p)$, where k is the coefficient of thermal conductivity and T_∞ and T_p the temperatures of the gas far from the drop and the temperature of the drop, respectively. Given these results, the energy balance given above reduces to

$$\frac{T_\infty - T_p}{T_\infty} = \left(\frac{\rho_v}{\rho_g}\right)\left(\frac{\rho_g \mathscr{D} C_{pg}}{k_g}\right)\left(\frac{L}{C_{pg} T_\infty}\right) \tag{2.5}$$

Note that ρ_v is an exponential function of T_p. Here the vapor density at the particle surface has been normalized by ρ_g, the density of the gas stream evaluated at T_p. The second and third terms on the right-hand side of Eq. (2.5) are almost independent of pressure and temperature. (The second term is the Lewis number.) However, the first term is a very strong function of temperature and is inversely proportional to pressure because the gas density is proportional to P/T_p. Hence, Eq. (2.5) can be written in the form

$$\left(T_\infty - T_p\right) = f\left\{T_p\right\}/P_\infty \tag{2.6}$$

where f increases exponentially with T_p.

If P_∞ is reduced, e.g., by increasing the altitude at which the engine is flying, the droplet temperature must adjust to satisfy this equality. Two regimes of interest can be defined. In the first, let the gas temperature be much greater than the particle temperature. Then a drop in P_∞ must be accompanied by a drop in T_p. Because of the strong dependence of f on T_p, a small change in T_p will be required to satisfy the equation. Hence, the

temperature difference $(T_\infty - T_p)$ will not change appreciably and, consequently, the conduction term and thus the evaporation rate will not change appreciably. For this example, the increase in the diffusion coefficient resulting from a reduction in the pressure is offset by a reduction in the vapor pressure (due to reduced T_p) so that the vapor diffusion and evaporation rates are held almost constant. For this case then, the evaporation time t_e of Eq. (2.4) will not be affected directly by the pressure.

In the second regime, assume that T_∞ is almost equal to T_p. Then, when P_∞ is forced to drop, the small change in T_p needed to balance Eq. (2.6) will make an appreciable difference in the temperature difference $(T_\infty - T_p)$. Thus, the heat-transfer rate and consequently the evaporation rate will increase as the pressure falls.

If the simplified results presented above are combined, it is found that as the pressure in the afterburner falls, say as a result of the increase in altitude of an engine operating at a fixed Mach number, the simple injector discussed here is capable of supplying the required fuel flow to the appropriate volume of space. However, as the pressure decreases, the droplet diameter will increase. In addition, for the first vaporization regime discussed above, the evaporation rate will be independent of the pressure but will decrease rapidly as the drop radius increases. Hence, the effect of the reduction in pressure will be to increase the initial diameter of the droplets and to decrease the evaporation rate. In the second regime, the effect of the increase in the initial radius of the drops will be offset by the increase in the diffusion rates.

Also note that the evaporation rate depends on the diameter of the injector part d_j. It is clear from Eq (2.2) that D_{30} is proportional to $\sqrt{d_j}$ and consequently that the evaporation time given in Eq. (2.4) is directly proportional to d_j. Hence, more rapid evaporation could be achieved by using injection ports of a smaller diameter. However, the number and location of the injector ports would need to be changed to keep the fuel distribution unchanged. In addition, the smaller holes would be more subject to blockage by dirt and pyrolized fuel.

In real systems, the observed effect of a pressure decrease is that combustion efficiency falls off badly when the pressure is reduced below some limiting value, often on the order of 1 atm. This pressure limit is a major restriction on the operating range for an afterburner.

2.4 Ignition

The fuel-air mixture produced by the injection process has a flame propagation velocity that is much lower than the gas speed in the combustion chamber. Thus, unless sources of continuous ignition are present in the chamber, the burning gas ignited by a temporary process will be blown out of the engine as soon as the ignition is stopped. In most afterburner systems, the continuous source of ignition is the wake of a bluff body (called the flameholder) held with its axis perpendicular to the flow. Hot gas, trapped in the first few diameters of the flameholder wake, mixes with the combustible mixture flowing over the wake and acts as the source of ignition. The

process of flame stabilization is the subject of the next section; here the process of the initiation of the stabilization process will be discussed. This ignition process need only start the stabilization process and may then be turned off. Furthermore, it has been found that once the stabilization process has been established in a relatively short length of flameholder, say 5 diam, the process will spread to the rest of the stabilizer system if the wakes of the stabilizers form a continuous pathway. Finally, fuel is usually added in sequence to a number of annular stream tubes to prevent pressure surges during afterburner ignition and to allow modulation of the afterburner thrust. Hence, once one region is "lit," it can act as a source of ignition for adjacent regions when fuel is added to them. Thus, the purpose of the ignition system is to establish a stabilized flame in a relatively small part of the flame stabilizer system. The bluff-body flameholder system will then furnish a path for the further spreading of the stabilized flame as additional fuel is added.

Three general systems have been used: the hot-streak technique, spark or arc ignition, and the pilot burner technique. In the hot-streak system, fuel is injected for a short period into the gas stream of the core engine just upstream of the turbine. The combustible flow formed by this process produces a very hot stream of burning gas that is positioned radially to coincide with the primary fuel-air injection stream tube for the afterburner. Combustion occurs in this stream by autoignition (because of the high temperatures present upstream of the turbine) and the flame stabilization process is initiated when the hot burning gas fills the initial wake region of the flameholders. The hot streak can be maintained for only a brief period to prevent thermal damage to the turbine.

Ignition and initiation of the flame stabilization process can also be initiated by producing a high-energy electric arc in the primary stream tube. In this case, ignition is usually produced by placing the arc in a region of the wake of the flameholder system that is particularly sheltered and that may have its own fuel supply system. Stabilization is initiated locally by the heat from the arc and spreads by the mechanism described above.

The pilot burner system is similar to the arc system and may use an arc to initiate combustion. In this system, a small can burner (similar to that used in the core-engine primary burner) is located in the primary stream tube. This system furnishes a continuous source of hot combustion products that act in a manner similar to the hot-streak system to start the stabilization process once fuel injection is started.

The energy required to initiate the flame stabilization process comes primarily from chemical reactions initiated in the premixed fuel-air stream by the ignition system. At present, the amount of energy required (e.g., joules supplied to the arc discharge or total mass of fuel injected into the hot streak) to achieve ignition cannot be calculated for a particular design. However, some trends can probably be determined by examination of experimental results concerned with the ignition of the flowing streams of fuel-air mixtures.

Studies with various sources of ignition such as arcs, hot surfaces, and hot gas streams indicate that the energy required is a strong function of the

fuel-air ratio, fuel properties, local pressure and temperature, and residence time of the combustible gas in the system. The energy required is smallest for mixture ratios near the stoichiometric value and increases very rapidly as the mixture ratio is decreased below 0.5–0.7 of the stoichiometric ratio. Also, it decreases with increases in the pressure, temperature, oxygen mole fraction, and residence time of the flow in the ignition region. The exact values required are very sensitive to the particular device being studied. Thus, the calculation of the conditions required to produce ignition for a particular system cannot yet be carried out, even for very idealized experimental conditions.

Based on these results, one expects ignition in afterburner systems to be most easily achieved in gases with fuel-air ratios close to the stoichiometric value in the most sheltered regions of the stabilization system, where residence times are longest and when pressures and temperatures are highest.

Ignition is usually harder to achieve than stabilization. Because velocities and temperatures do not change a great deal at the afterburner inlet, the primary problem for afterburner ignition systems is the high-altitude relight problem. The difficulty here is associated with the low pressure in the afterburner that affects both the preparation of the fuel (by the injector system) and the ignition process directly. The operating regime for the engine is often plotted, as shown in Fig. 2.5, on an altitude vs Mach number

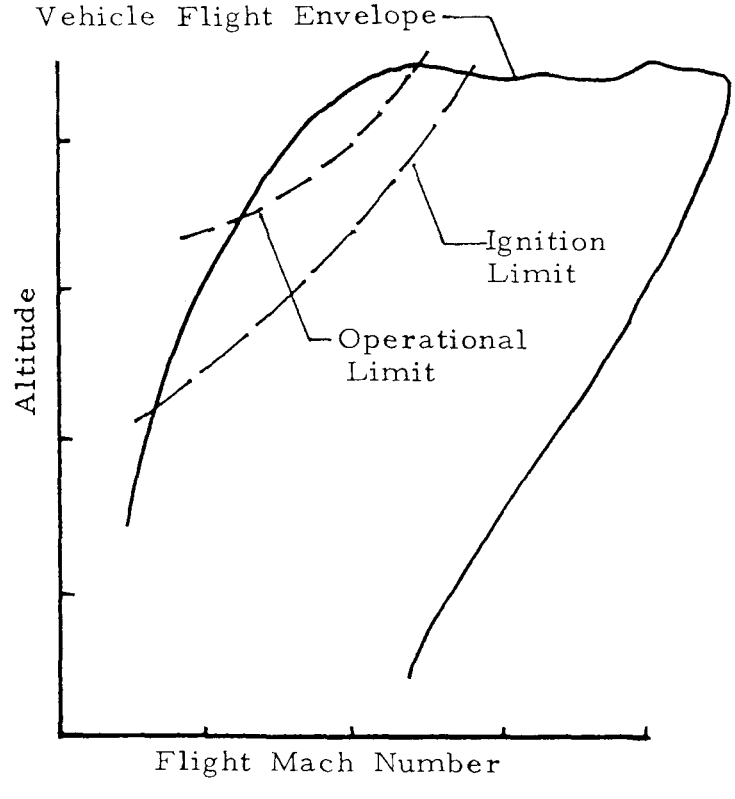

Fig. 2.5 Flight envelope for an afterburner.

map. The boundary called the ignition curve is the altitude (i.e., the pressure) limit above which ignition is no longer possible. Afterburner operation above this altitude is possible (for this example) if the afterburner is ignited at a lower altitude.

2.5 Stabilization Process

The purpose of the flame stabilization process is to establish a continuous source of ignition in a fuel-air mixture whose velocity is much greater than the turbulent flame speed for the mixture. Laminar flame speeds in mixtures of typical hydrocarbon fuels with air heated by partial combustion are in the range of a few meters per second. If the flow is turbulent, this speed may be as large as a few tens of meters per second, although the meaning of the term *turbulent flame speed* is poorly defined. These turbulent speeds are still much less than the gas speeds encountered in the flame stabilization region of afterburner systems where gas speeds of hundreds of meters per second are typically encountered. Hence, a continuous source of ignition is required to start the combustion process. Once started, the combustion wave can spread from its point of ignition across the fuel-air mixture produced by the injection system in a wave-like manner similar to the propagation of an oblique shock wave across a supersonic flow.

One of the most important parameters of the stabilization process is the state of the fuel in the fuel-air mixture. In the core flow, temperatures are high enough to insure that most of the fuel is vaporized. However, in the fan stream, temperatures can be so low that only a small fraction of the fuel will be vaporized and the stabilization mechanism will have the additional job of vaporizing the fuel used in producing a stable flame. In existing systems, this problem is usually avoided by starting the afterburning process in the core stream. The hot gas generated in the core is then used to stabilize the flame in the fan stream. The first part of the following discussion is restricted to the vaporized fuel example.

The ignition process, usually called flame stabilization in afterburner systems, is typically achieved in a mixture of fuel *vapor* and air by allowing the hot products of combustion to mix with the unburned fuel-air mixture. The steady flow of hot gas required for this process is usually obtained by setting up a recirculating flow of burned material. When a bluff-body flameholder is used (Fig. 2.6a), hot gas is generated by the recirculation of burning material in the wake of the bluff body and supplies the energy and the mass of products of combustion required to ignite the unburned material flowing past the wake. This process is described and analyzed in detail in the following sections.

The processes occurring in the wake of the bluff body also occur in the wake of a step or in a wall recess. Figures 2.6b and 2.6c show that heat transfer from the gas to walls of the cavity reduces the gas temperature in the recirculation zone and makes stabilization more difficult.

The wake region required to produce the recirculation zone described above can also be produced by injecting a secondary gas stream into the unburned flow, as shown in Figs. 2.6d and 2.6e. Again, a wake region with strong recirculation is formed by the interaction of the two streams. In these

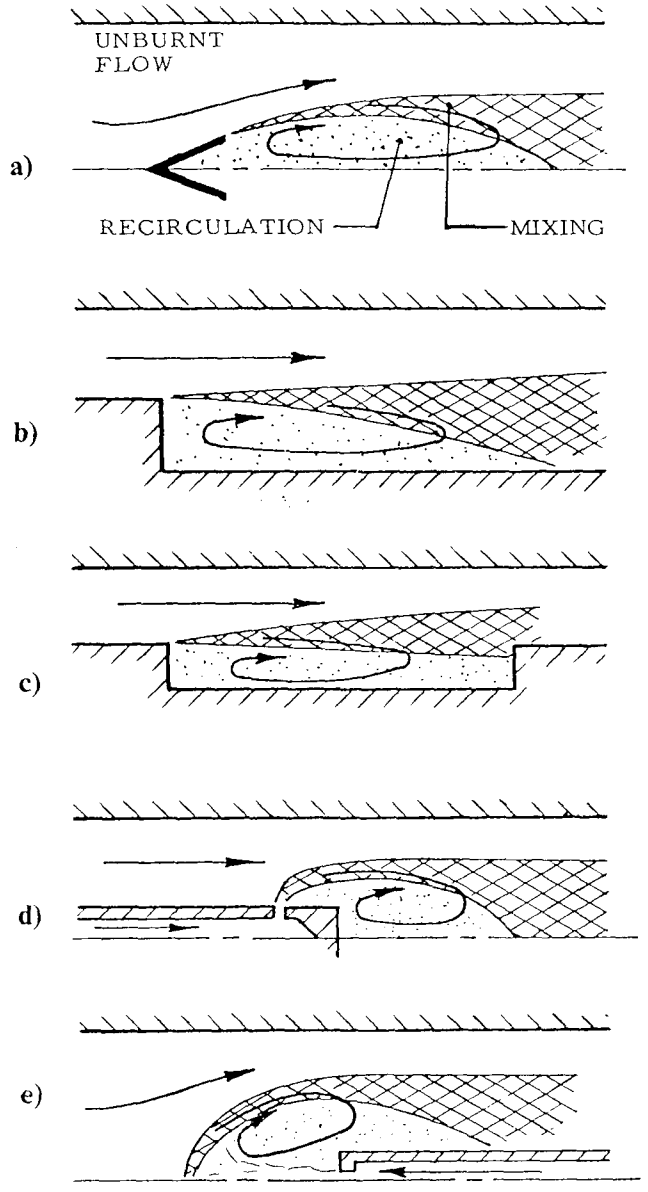

Fig. 2.6 Flame stabilization schemes for mixtures of fuel vapor and air.

examples, the fluid entering the recirculating wake is made up in part of the injected fluid. Hence, the fuel-air ratio of the recirculation zone gas can be changed by changing the fuel-air ratio of the injectant. This process can result in a powerful control over the stabilization process, as will be described later in this chapter.

The configurations shown schematically in Fig. 2.6 can be used in either axisymmetric or two-dimensional geometries. The latter configuration is the most common.

The performance of a flame stabilization system is usually presented in the form of a map on which the boundaries of a stabilization parameter are

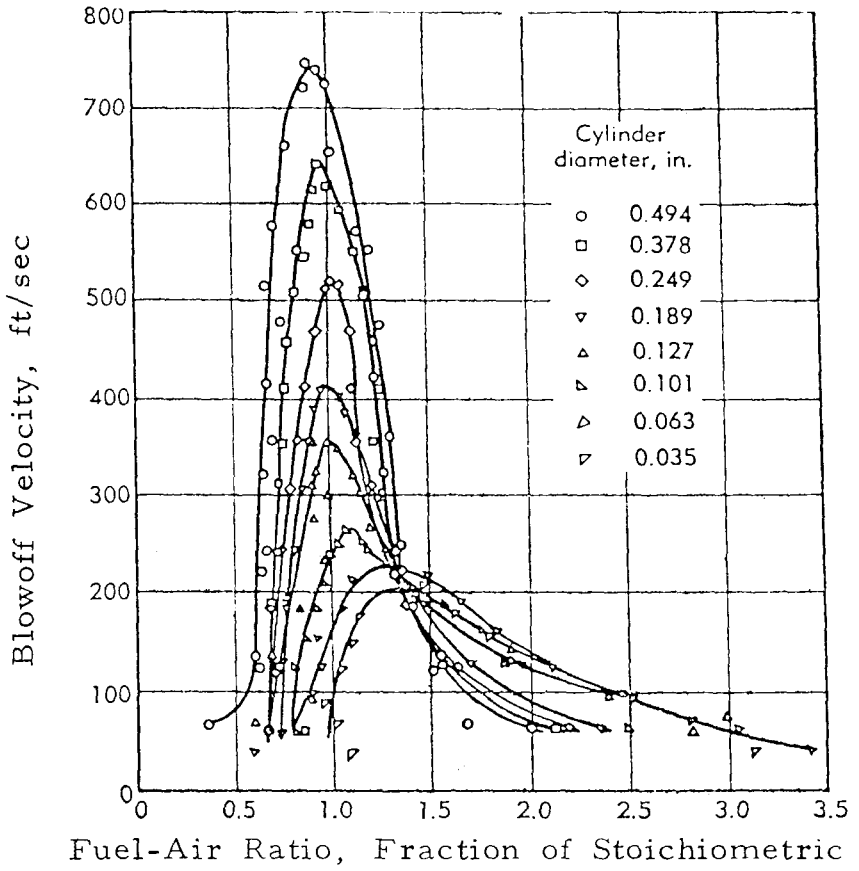

Fig. 2.7 Stability limit curves for circular cylinders, vaporized hydrocarbon fuel-air mixture at 1 atm and 60°C (data from Ref. 4).

given as a function of the fuel-air ratio. An elementary map of this type is shown in Fig. 2.7 where the velocity at which the stabilization process fails (called here the blowoff velocity) is presented as a function of the fuel-air ratio with the flameholder scale as a parameter. The experimental data of Haddock[4] were obtained in a mixture of vaporized gasoline and air and with circular cylinders used as flameholders. For each flameholder, flame stabilization was found to be possible for the range of values of the fuel-air ratio within the curves shown in Fig. 2.7. For example, stabilization was possible with the $\frac{1}{2}$-in. (1.3-cm) diam cylinder for fuel-air ratios between 0.70 and 1.15 times the stoichiometric value when the gas speed approaching the cylinder was about 600 ft/s (183 m/s). As the gas speed increased, the fuel-air ratio range for which stabilization could be achieved decreased and the peak value of about 740 ft/s (226 m/s) occurred for values close to stoichiometric. Flameholders with diameters between $\frac{1}{2}$ and $\frac{1}{8}$ in. (1.27 and 0.32 cm) had clearly turbulent wakes and exhibited similar behavior. The blowoff velocities increase regularly as the holder scale increases.

The three remaining curves are for holders with laminar wakes. The peak blowoff velocity for these examples is progressively shifted toward fuel-air

ratios greater than stoichiometric as the flameholder scale is reduced. This behavior is a result of a molecular diffusion process that is usually of no importance in flameholder systems operating in gas turbine engines. However, note that even for the largest flameholder, the lean stability limit is well above 0.5 of stoichiometric and that values above 0.8 are required to stabilize flames in high-speed flows.

It is clear from these data that the velocity at which stabilization can be maintained is a strong function of the flameholder scale, fuel-air ratio, and wake condition (laminar or turbulent). Other experiments show that it also depends upon the fuel characteristics; the temperature, pressure, and oxygen content of the unburnt gas stream; and a number of geometric factors describing the flameholder-duct system. The nature of these dependencies and their origin will be discussed in later paragraphs of this section. The stability limits obtained with the other systems shown in Fig. 2.6 follow a pattern similar to that described above when mixtures of fuel vapor and air are used. However, when a large fraction of the fuel is not vaporized, the picture is quite different.

The bluff-body flame stabilization process that occurs in fuel-vapor-air mixtures will be treated in detail in the following subsection. Briefer descriptions will be given of the scaling parameters for the stabilization by secondary injection (illustrated in Fig. 2.6d) and of bluff-body stabilizers operating in unvaporized fuel-air mixtures.

Flame Stabilization by Bluff Bodies in Premixed Flow

The mechanism of flame stabilization by bluff-body flameholders is still a subject of some contention and the mechanism described here is that developed at the California Institute of Technology by F. E. Marble, E. E. Zukoski, and a number of co-workers at the Jet Propulsion Laboratory (e.g., see Refs. 5–8).

This approach is based on a picture of the wake of a two-dimensional flameholder shown in Fig. 2.8. Figure 2.8a was taken in the flame stabilization region of a circular cylinder. The line of sight is along the cylinder. Figure 2.8b is a highly simplified drawing of the velocity field for the same region. The mixing zones are illuminated in Fig. 2.8a by light from the combustion process occurring there. Chemiluminescence and hence chemical reaction is almost absent in the recirculation zone.

The wake of the flameholder can be divided into two regions: the recirculation zone that is characterized by strongly recirculating flow and the mixing zone that separates the recirculation zone from the unburned mixture. The temperature of the recirculation zone gas is typically within 5–10% of the adiabatic flame temperature corresponding to the mixture ratio of the approach stream and is independent of gas speed and the flameholder-duct geometry. Chemical reaction appears to be almost complete in this volume and the residence of gas is 5–10 times the time required by the flow at the cold side of the mixing region to pass over the recirculation zone. This long residence time insures that, if any chemical

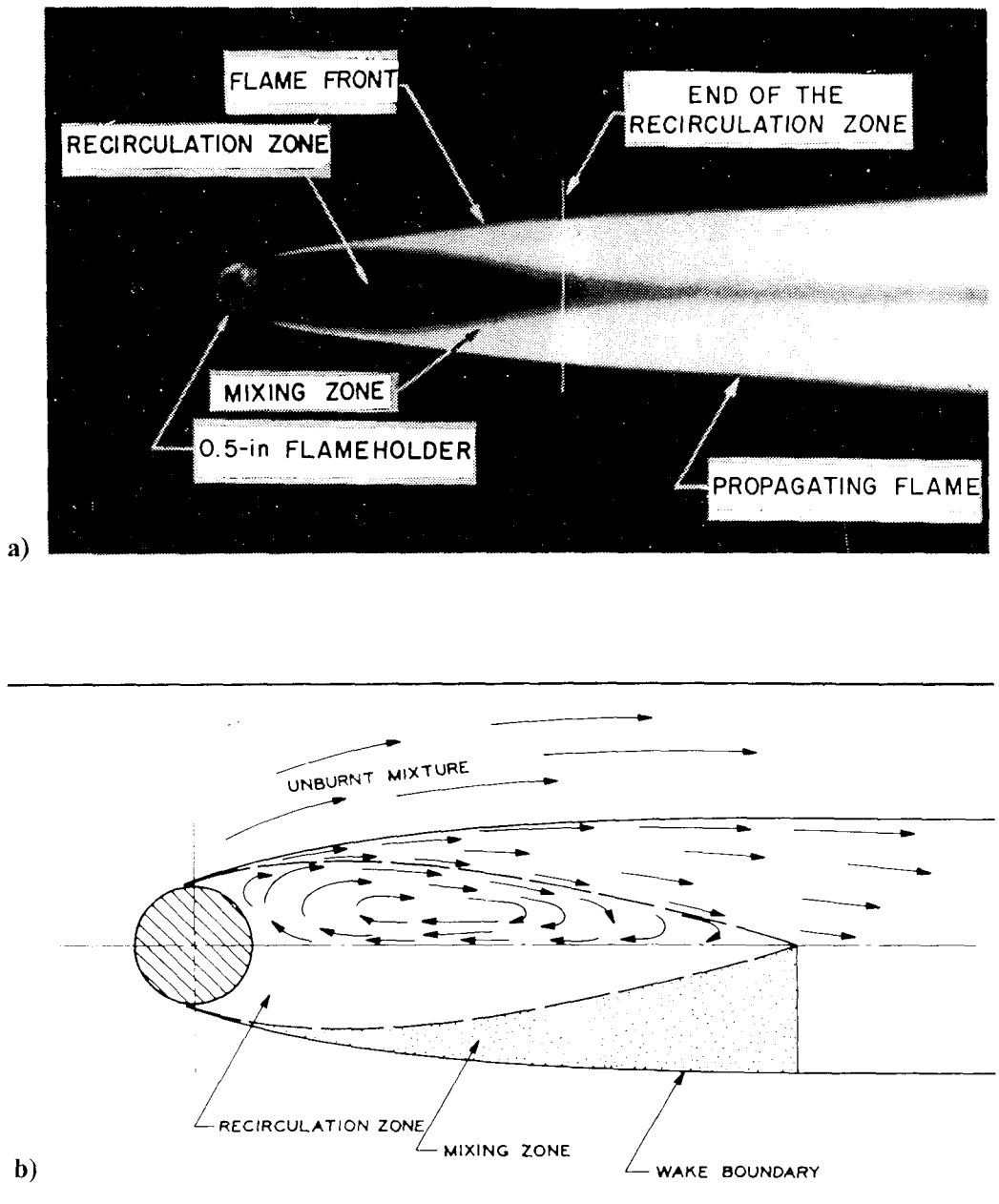

Fig. 2.8 Flame stabilization region of a circular cylinder used as a bluff-body flameholder.

reaction takes place in the wake at all, it will be most nearly complete in the recirculation zone.

The mixing zones on either side of the recirculation zone are turbulent regions of very strong shear, steep temperature gradients, and vigorous chemical reaction. These regions thicken almost linearly and their junction forms the downstream end of the recirculation zone.

The process leading to the formation of a self-propagating chemical reaction takes place in the mixing zone. This region is fed by turbulent mixing processes with cool combustible gas from the approach stream and with very hot burned material from the recirculation zone. Thus, if no chemical reaction were present, the mixing zone gas would still be at a high temperature at the inner edge (or recirculation zone side) of the region. Downstream of the end of the recirculation zone, the cool, unburned gas continues to be entrained into the wake, but no more hot gas is added; hence, if no chemical reaction is present, the temperature will fall.

Chemical reaction is initiated in the mixing zone by heat and species transfer from the hot burned gases to the unburned material. The total heat and species transferred to any particle of unburned gas and its reaction rate will depend largely on the time this particle spends in contact with hot burned gas. Thus, the temperature, species concentration, and consequently, the local chemical reaction rate of the unreacted material will depend strongly on the residence time of this unburned material in the mixing zone.

For a sufficiently long residence time, a chemical reaction will be started in the mixing zone flow and will continue as this gas moves on downstream to form the wake. If this reaction is vigorous enough in the wake region, then the quenching action of the continuing entrainment of cool unburned gas will be overcome and a propagating flame will be produced.

It is reasonable to suppose that the residence time of the unburned gas in the mixing zone will be proportional to $L_e/\bar{v}$, where $\bar{v}$ is a suitably chosen average speed in the mixing zone and L_e the scale of the recirculation zone. Hence, when the velocity of the flow increases, $\bar{v}$ will increase proportionately and the residence time will decrease. When the residence time is too short, the chemical reaction in the wake will be quenched and no propagating flame will be stabilized. Thus, flame extinction or blowoff occurs due to failure of the ignition process and not as a direct result of cooling of the recirculation zone gas.

The important parameters of the system as indicated by this discussion are: $\bar{v}$, an average gas velocity in the mixing zone; τ, a time characterizing the period required to achieve ignition in the mixing zone; and L_e, the length of the recirculation zone that is effective in igniting the mixing zone. The dimensionless parameter of interest is then $\bar{v}\tau/L_e$. There is good evidence that the mixing layer flowfields are roughly similar, i.e., have similar velocity, composition, and temperature fields. Thus, if similar systems are compared with the same chemical parameters but under different fluid dynamic conditions, the stability parameter must take on a particular value at blowoff condition, i.e.,

$$(\bar{v}\tau/L_e)_{\text{blowoff}} = \beta_c$$

Because of the similarity of the turbulent mixing zones of bluff-body flameholders, the parameters L_e and $\bar{v}$ used in this expression can be replaced without loss of generality by the maximum length of the recirculating flow L and the unburned gas speed at the edge of the mixing zone V_2.

Then the blowoff condition given above can be rewritten as

$$\frac{\bar{v}\tau}{L_e} = \left(\frac{\bar{v}}{V_2}\frac{L}{L_e}\right)\left(\frac{V_2\tau}{L}\right) = \beta_c$$

When $\bar{v}/V_2$ and L/L_e can be assumed to be constants (for similar turbulent mixing regions), the stability criterion becomes

$$V_2\tau/L = \text{const}$$

at the flame extinction or blowoff condition.

A number of experiments have verified the usefulness of this relationship. However, an independent calculation of the characteristic chemical time τ has not been developed; consequently, it is necessary to experimentally determine τ from a set of flame blowoff experiments. In these experiments, V_{2c} and L are determined at the blowoff state and τ is obtained from $\tau_c \equiv L/V_{2c}$. Given this definition, the flame blowoff criteria is

$$(V_{2c}\tau_c/L)_{\text{blowoff}} = 1 \tag{2.7}$$

where the unknown constant β_c has been absorbed in the measured quantity τ_c. One of the great advantages of this approach is that all of the dependence on the chemical parameters is naturally lumped in τ_c and all of the dependence on the fluid dynamic parameters in L/V_{2c}.

When τ_c has been determined experimentally for a single duct-flameholder configuration and for the desired ranges of the chemical parameters, it can be used to predict stability limits for any other duct-flameholder configuration and the *same* range of chemical parameters. Thus, τ_c is a scaling parameter.

A number of experiments with a wide range of flameholder-duct configurations have shown that the values of τ_c do depend on a number of chemical parameters such as the fuel type, fuel-air ratio, gas temperatures, and degree of vitiation, but are substantially independent of the geometry and scale of the flameholder-duct configuration and of the gas speed so long as the flow in the mixing region is turbulent. A few typical results are summarized in Table 2.1. The top two flameholders are circular cylinders with their axis held perpendicular to the flow and the latter three are cylindric bodies with their axis parallel to the flow and several types of axisymmetric noses. The third body is the two-dimensional analog of the fourth. The large differences in the flowfield produced by these bodies is illustrated in Fig. 2.9. Note that values of the critical times evaluated at the stoichiometric ratios are about the same regardless of geometry.

In addition, for flames in which mixing length similarity does not hold, values of τ_c determined by the integration of local velocity measurements along a path in the mixing zones again confirmed the validity of this approach. For example, see the work of Broman and Zukoski.[8]

The fluid dynamic and chemical aspects of the stability criterion will be discussed separately in the following subsections.

Table 2.1 Dependence of Ignition Time τ_c Obtained at the Stoichiometric Fuel-Air Ratio on Flameholder Geometry and Gas Speed

Flameholder Geometry	D or d, in.	τ_c, 10^{-4} s
	1/8	3.09
	3/16	2.85
	1/4	2.80
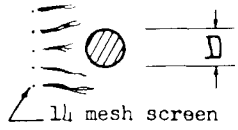	1/4	3.00
	1/4	2.38
	3/8	2.70
	1/2	2.65
	3/4	2.58
	1/4	3.46
	3/8	3.12
	1/2	3.05
	3/4	3.03
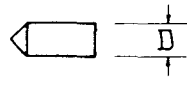	3/4	3.05
	3/4	2.70

Fluid dynamic parameters. The flame stabilization criterion given in Eq. (2.7) is not immediately useful, even when the characteristic τ_c is known as a function of the chemical parameters, because the recirculation zone length L and the gas speed in the flow over the wake V_2 are not simply related to the scale of the flameholder and the velocity far upstream. To illustrate the dependence of these parameters on other fluid dynamic variables, consider the case of a two-dimensional flameholder of height d located on the centerline of a rectangular duct of height H and subject to a flow with an upstream velocity V_1. The fluid dynamic parameters used in this model need to be connected with these parameters, which are the ones usually specified. These two sets of parameters are illustrated in Fig. 2.10. In a formal way, the stability criterion can be written as

$$\frac{V_{2c}\tau_c}{L} = 1 \quad \text{or} \quad \frac{V_{1c}\tau_c}{H} = \left(\frac{V_1}{V_2}\right)\left(\frac{L}{W}\right)\left(\frac{W}{H}\right) \tag{2.8}$$

where W is the width of the wake near the downstream end of the

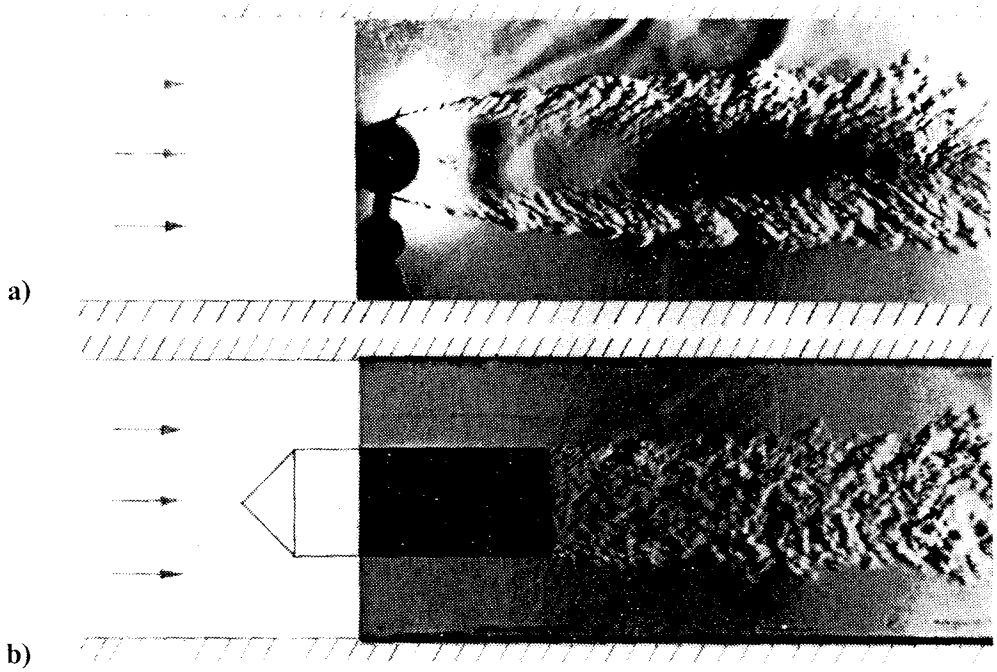

Fig. 2.9 Spark schlieren photographs of flames stabilized on: a) circular cylinder viewed from the side and b) on axisymmetric body with axis parallel to flow. [The recirculation zone, clearly outlined in a) is not visible in b).]

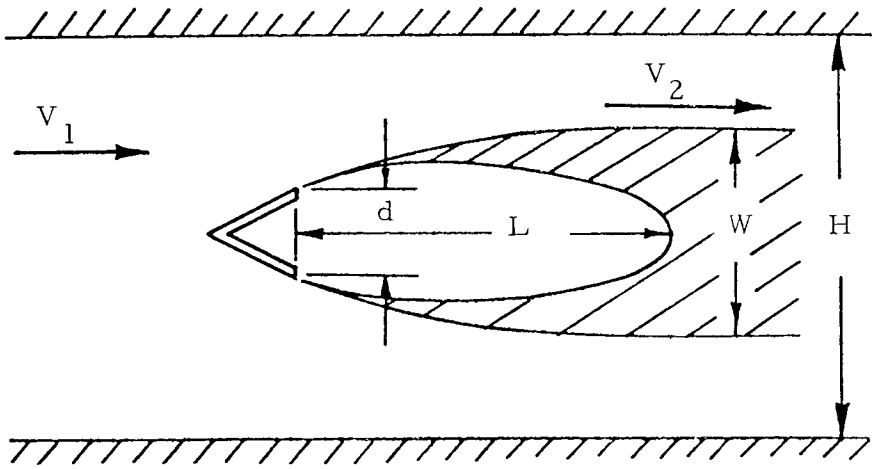

Fig. 2.10 Notation used in analysis of stabilization.

recirculation zone. Its introduction in Eq. (2.8) will lead to a useful simplification described below. Also, V_{1c} and V_{2c} are the values of velocity of the approach stream and the flow past the wake evaluated at blowoff condition.

In order to apply the criterion, V_1/V_2, L/W, and W/H as functions of the blockage ratio d/H, the flameholder geometry, and the usual parameters

of compressible and viscous flows and Reynolds and Mach numbers must be known. In addition, the flameholder temperature must be considered as it affects the boundary layer on the holder and the turbulence level in the approach stream. In the following paragraphs, the effects of changing d/H (called the blockage ratio) and the flameholder geometry will be considered first, and later the effects of Reynolds number, Mach number, flameholder temperature, and turbulence will be described. (Note that in some figures D replaces d.)

(1) Blockage and flameholder geometry. Consider again the flow described schematically in Fig. 2.10. Note that the flow separates from either side of the flameholder and that the wake continues to spread downstream of the holder and asymptotically approaches a width W. (Later it will be shown that W rather than d is the most useful characteristic scale for the holder in this problem.) The flameholder and its burning wake block an appreciable part of the cross-sectional area of the duct and causes the unburned flow to accelerate to a higher velocity, V_2.

The wake width is a critical parameter since it not only affects the ratio V_2/V_1 but also fixes the recirculation zone length L. For example, the width of the mixing zone increases almost linearly with distance along its length. This spreading rate is similar to that of many other two-dimensional turbulent shear layers and has a constant width-to-length ratio of roughly $\frac{1}{8}$. At the downstream end of the zone, the two mixing layers occupy the entire width of the wake and consequently the ratio of recirculation length to wake width L/W should be close to 4. For a wide range of flameholder shapes, experimental data lie in the range

$$3.6 \leq (L/W) \leq 4$$

Data illustrating this result are shown in Fig. 2.11 for a number of circular cylinders. Despite the strong dependence of L/d on the blockage ratio, the values of L/W are almost constant for the whole range. The dependence of L/d on blockage is shown here for circular cylinders; in general, the dependence of L/d on blockage is a strong function of flameholder geometry. However, the spreading of the mixing zones and presumably, the entrainment in the mixing zones is remarkably independent of the shape of the wake region and flameholder. This simple dependence of the recirculation zone length on the wake width indicates that in this problem (as in many fluid dynamic problems involving flows over bluff bodies), the wake width rather than flameholder scale is the most useful measure of bluff-body scale.

The ratios V_2/V_1 and W/H appearing in Eq. (2.8) depend on the flameholder geometry and the blockage ratio. A simple continuity argument for incompressible flow can be used to estimate the velocity change if entrainment in the mixing layer is neglected. Conservation of mass gives

$$\rho V_1 H = \rho V_2 (H - W)$$

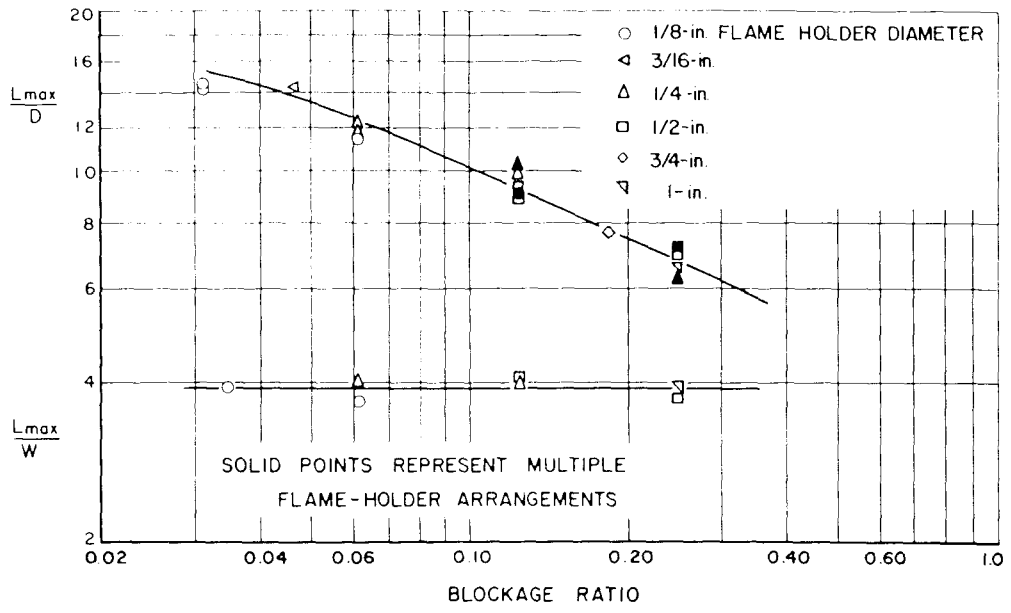

Fig. 2.11 Dependence of recirculation zone length and wake width on flameholder blockage ratio d/H.

or

$$(V_2/V_1) = 1/(1 - W/H) \tag{2.9}$$

An approximate calculation is also available that allows W/H to be calculated as a function of geometry and blockage ratio for a V-gutter or wedge flameholder geometry. Again, considering the flow shown in Fig. 2.10, examine an incompressible and inviscid flow over a wedge-shaped body of half-angle α and treat the outer boundary of the wake as a streamline that separates the unburned flow from a stagnant, constant-pressure wake. The wake spreads asymptotically to reach a width W. In the region where W is constant, the unburned flow speed reaches a value V_2 given by Eq. (2.9) and the pressure will be uniform across the wake and the unburned flow. Application of the Bernoulli equation shows that the velocity along the dividing streamline must be constant and be equal to V_2. Values of W/H can be computed from this model by a simple hodograph transformation. Calculations of this type are given by Cornell[9] for the V-gutter flameholder geometry with $0 \leq \alpha \leq 90$ deg. Values of W/H, V_2/V_1, and the parameter WV_1/HV_2 [see Eq. (2.8)] are given in Table 2.2 for wedge half-angles of 15 and 90 deg (a flat plate) and a range of blockage ratios. Note that values of W/d decrease and values of V_2/V_1 increase as the flameholder blockage is increased. The net result is that the parameter $(W/H)(V_1/V_2)$ has a rather broad maximum around blockage ratios of 0.5 for the 30 deg wedge (half-angle) and 0.3 for the 90 deg wedge or flat plate.

The wake widths and velocity ratios determined from this simple model are in reasonable agreement with values obtained experimentally for stabi-

Table 2.2 Dependence of Wake Width W, Edge Velocity V_2, and a Stability Parameter on Blockage Ratio d/H and Wedge Half-Angle α

	$\alpha = 15$ deg			$\alpha = 90$ deg		
$\frac{d}{H}$	$\frac{W}{d}$	$\frac{V_2}{V_1}$	$\left(\frac{W}{H}\right)\left(\frac{V_1}{V_2}\right)$	$\frac{W}{d}$	$\frac{V_2}{V_1}$	$\left(\frac{W}{H}\right)\left(\frac{V_1}{V_2}\right)$
0.05	2.6	1.15	0.11	4.0	1.25	0.16
0.10	1.9	1.23	0.15	3.0	1.43	0.21
0.20	1.5	1.42	0.20	2.2	1.75	0.248
0.30	1.3	1.62	0.23	1.7	2.09	0.250
0.40	1.2	1.90	0.25	1.6	2.50	0.248
0.50	1.2	2.3	0.25	1.4	3.16	0.22

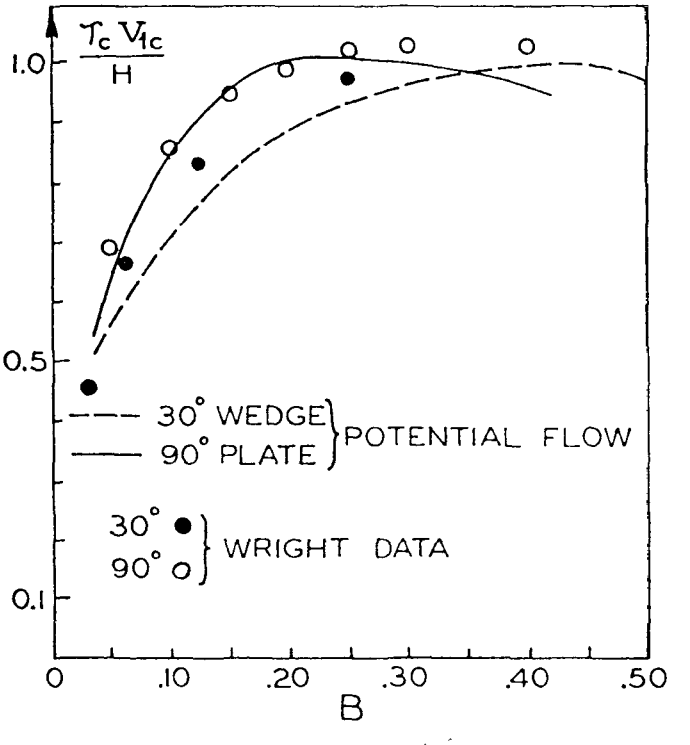

Fig. 2.12 Dependence of stability parameter on blockage ratio B and flameholder geometry for wedges with half-angles of 30 and 90 deg.

lized flames. The excellent measurements obtained by Wright[7] for flat-plate holders with $\alpha = 90$ and 30 deg are available for comparison. The differences in the values of W/H are no more than 20% and those for the ratio V_2/V_1 are less than 6%.

Given data or calculations of this type and assuming that $L/W = 4$, all of the parameters given in Eq. (2.8) can be evaluated. The experimental results of Wright and values calculated by the method described above are presented in Fig. 2.12 as a plot of $\tau_c V_{1c}/H$ vs the blockage ratio B. The

agreement between the data and calculated values is good and suggests that the model discussed here is correct.

The material presented in Table 2.2 and Fig. 2.12 shows that the maximum values of the stability parameter ($V_{1c}\tau_c/H$) are close to 1 for the 15, 30, and 90 deg half-angle wedges. This value is a reasonable estimate for all two-dimensional flameholders. For example, using the continuity argument presented above for V_1/V_2 and the rule of thumb that $L/W = 4$, Eq. (2.8) can be rewritten in terms of W/H to find the relationship for the blowoff criteria,

$$(V_{1c}\tau_c/H) = 4(W/H)(1 - W/H) \tag{2.10}$$

Note that the flameholder shape does not appear here explicitly. However, both the flameholder geometry and the blockage ratio enter in the determination of W/H. Equation (2.10) is a particularly useful and interesting result because it shows the importance of the wake width as a critical parameter (independent of flameholder-duct geometry) and because it allows a very simple starting point for the determination of the holder scale maximizing the stabilization velocity V_{1c}. The function $(W/H)(1 - W/H)$ clearly has a maximum at $W/H = \frac{1}{2}$. For small W/H, V_{1c} increases almost linearly with W. However, as W/H approaches $\frac{1}{2}$, the effect of increasing W is offset by the increase in V_2 produced by the wake-blockage effect. For $W/H > \frac{1}{2}$, the blockage effect dominates and the blowoff speed decreases.

The optimum wake width in this simple model is exactly one-half the duct height. Consequently, the maximum value of blowoff velocity that can be achieved for any flameholder geometry V_{1m} is given by

$$V_{1m}\tau_c/H = 1 \tag{2.11}$$

Note that this result is independent of the flameholder geometry and is corroborated by the experiments described above.

Flows over axisymmetric bodies can also be examined, such as the flameholder shown in the lower half of Fig. 2.8. For this geometry, the wake width W and body diameter d are equal; consequently, the recirculation zone length is $4W$ or $4d$. If this holder is placed on the axis of a circular duct of diameter D and the blockage is defined as $B = (d/D)^2$, the stabilization criterion given in Eq. (2.8) becomes

$$V_{1c}\tau_c/D = 4\sqrt{B}\,(1 - B)$$

For this example, the value of B maximizing V_1 is $\frac{1}{3}$ and

$$V_{1m}\tau_c/D = 1.54 \tag{2.12}$$

The above result holds for *any* axisymmetric flameholder-duct geometry. In the general axisymmetric case, V_{1m} is attained when the ratio of the wake width to the duct diameter W/D is $1/\sqrt{3} = 0.57$. It is interesting to note that the analysis indicates that the axisymmetric holders will allow about a

50% greater value of approach stream velocity than the two-dimensional holders.

In summary, for the two-dimensional case, the effects of blockage and flameholder geometry can be predicted from a simple model. Results obtained from the model and experimental work show that blockage effects are very important, that a maximum in blowoff velocity exists as flameholder scale is increased in a duct of fixed size, and that this maximum occurs when the flame wake width is about 50% of the duct height for all two-dimensional flameholder shapes. Similar conclusions hold for axisymmetric shapes except that for this case the optimum wake width is one-third of the duct diameter. The flameholder scale and blockage ratio required to produce the optimum wake width depend strongly on flameholder geometry.

(2) Temperature, fuel-air ratio, and vitiation. Temperature changes have little observable effects on the wake width or velocity. However, a large increase in temperature does result in a reduction in the recirculation length. For example, doubling the unburned mixture temperature can decrease recirculation zone length by 15–20%. Similar changes are observed when fuel-air mixture ratios are changed to values far from stoichiometric.

In both cases, the length of the zone decreases when the ratio of burned to unburned gas density λ increases. This trend is in agreement with trends recently observed in spreading rates of turbulent mixing regions formed between parallel flows with different velocities and densities. Experimental investigation of this simpler problem shows that if the high-speed stream is also the high-density stream, an increase in the density of the low-speed and low-density stream will increase the spreading rate. In this case, increasing spreading rates of the mixing layers will decrease the length of the recirculation zone.

For a given temperature, vitiation of the approach stream produces a reduction in the oxygen content, which results in a reduction in heat release and consequently an increase in λ. Again, the effect is qualitatively similar to an increase in the approach stream temperature.

(3) Multiple flameholder arrays. The previous discussion was restricted to a single flameholder placed on the centerline of a duct of constant height. In most practical situations, a number of flameholders must be used. When these are arranged in a single plane perpendicular to the flow direction and when they are spaced so that each holder lies on the centerline of equivalent ducts of equal height, the above analysis can be used directly to estimate the stability limits and spreading characteristics. For this case, each holder is treated as if it were in an isolated duct. For example, see Fig. 2.11 and the blowoff data of Ref. 10.

This approach gives reasonable results for laboratory-scale experiments; however, interactions do occur that may change stability limits by 5–10%. One effect results when flame stabilization fails on one holder in a multiflameholder array slightly before the others. Failure of one stream to ignite

has the effect of reducing the acceleration of the flow over the wake and hence of reducing the velocity of the flow past the wakes of the other holders. Thus, a partial blowoff can occur, leaving the remaining holders in a more stable configuration.

When the holders are spaced irregularly in either lateral dimension, or fore and aft, prediction of the wake geometry from the results of tests on isolated flameholders is no longer possible. However, these modeling ideas are still useful in a qualitative way. For example, it is expected that, if flameholders are not arranged in a plane, the disturbance produced by the flow over the downstream flameholders will pinch off the circulation zone of the upstream holder unless the spacing along the duct axis is greater than the recirculation zone length. Similarly, the burning wake of the upstream holder will increase the effective blockage of the downstream holders and hence reduce their stability limits.

(4) Reynolds number and Mach number effects. When the Reynolds number is so low that the mixing layers in the wake of the flameholder become laminar or transitional, the transport processes in the wake change drastically. Molecular diffusion becomes important and the rule of thumb for L/W is no longer applicable.

Measurements made in systems with low approach stream turbulence levels[6] have shown that the transition Reynolds number for circular cylinder flameholders is in the range $1\text{–}4 \times 10^4$. This result is for flameholders cooled to approach stream temperature and the Reynolds number is based on upstream flow properties, $R_e = \rho_1 V_1 d/\mu_1$. When the flameholder is allowed to reach temperatures hotter than the approach stream, those gas properties based on the holder temperatures should be used. Some effects of the geometrical shape of the holder on transition is expected.

Transition occurs when the separated flameholder boundary layers become turbulent very close to the separation point and upstream of the location in the mixing zone where the mixing effects or combustion can heat the gas in the separated layers. Any heating will increase the kinematic viscosity (which is roughly proportional to the temperatures to the 1.75 power) and reduce the effective Reynolds number. When the flow in the separated boundary layers remains laminar up to the point of appreciable heat addition, it remains laminar throughout the whole recirculation zone and region of flame spread. The development of a turbulent boundary layer on the flameholder upstream of separation and high levels of the approach stream turbulence will also insure that the mixing zone will be turbulent.

Transition to turbulence in the wake of a circular cylinder used as a flameholder is shown in Fig. 2.13. The schlieren photographs are taken along a line of sight looking down on the plane containing the undisturbed velocity vector and the flameholder axis. At the lowest Reynolds number (Fig. 2.13a), large-scale vortices are present, which appear as vertical lines in the left picture. However, at the highest Reynolds number, these regular features are hidden by small-scale disturbances assumed to be evidence of turbulent flow. The Reynolds numbers examined here differ by a factor of less than two and the change in the appearance is quite striking.

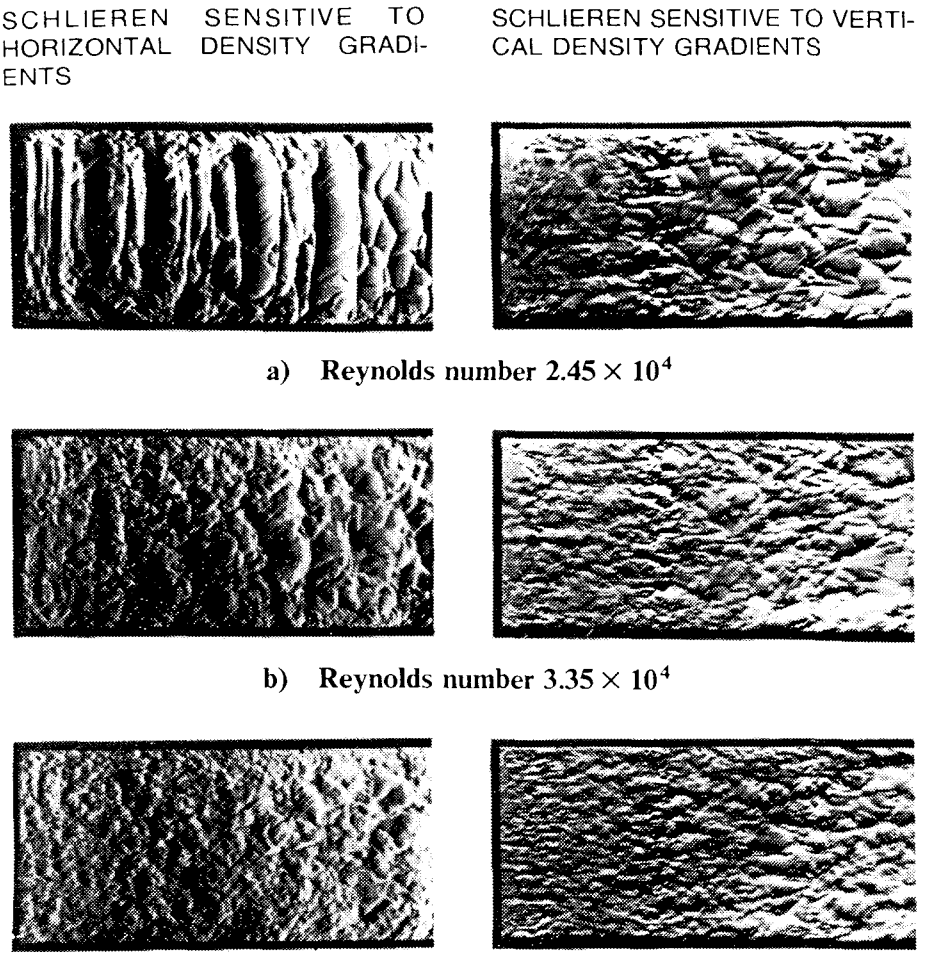

Fig. 2.13 Transition to turbulence in recirculation zone of cooled circular cylinder.

Because the Reynolds number is directly proportional to the pressure level in the engine (through the density dependence), the Reynolds number will *decrease* as the altitude increases. Hence, the Reynolds number should be evaluated at high altitudes to insure that the transition to laminar flow described here does not occur.

When appreciable heat is to be added in a burner with a constant cross-sectional area, inlet Mach numbers of about 0.15–0.25 must be used to prevent choking due to heat addition. Thus, compressibility effects usually are not important near the flameholder and recirculation zone.

However, note that the near-optimum one-half wake width (for the two-dimensional case), the flow area is reduced by a factor of two. This results in sonic speed past the recirculation zone for approach stream Mach numbers as low as $M_1 = 0.3$. Measurements made by Wright[7] bear out this prediction and further show that the W/H correlation discussed above fails when the Mach number past the recirculation zone M_2 is greater than 0.8.

(5) Freestream turbulence. The effects of freestream turbulence can be described only in a qualitative manner. As the intensity of turbulence increases, the recirculation zone shortens. However, the stabilization criterion in its most direct form, $V_{2c}\tau_c/L = 1$, remains valid even when the recirculation zone length is reduced by factors of two. Thus, turbulence appears to effect the rate of the spread of the mixing layers without changing the mechanism of stabilization.

Chemical parameters. The dependence of τ_c on chemical parameters is very strong and unfortunately much less well understood than the influence of the fluid dynamic parameters. Hence, the chief use of the scaling scheme discussed here is to predict the effect of changes in the fluid dynamic parameters for fixed chemical parameters. However, it is still interesting to list the important chemical parameters and to indicate the nature of their effects. The principal parameters are: fuel properties, fuel-air mixture ratio,

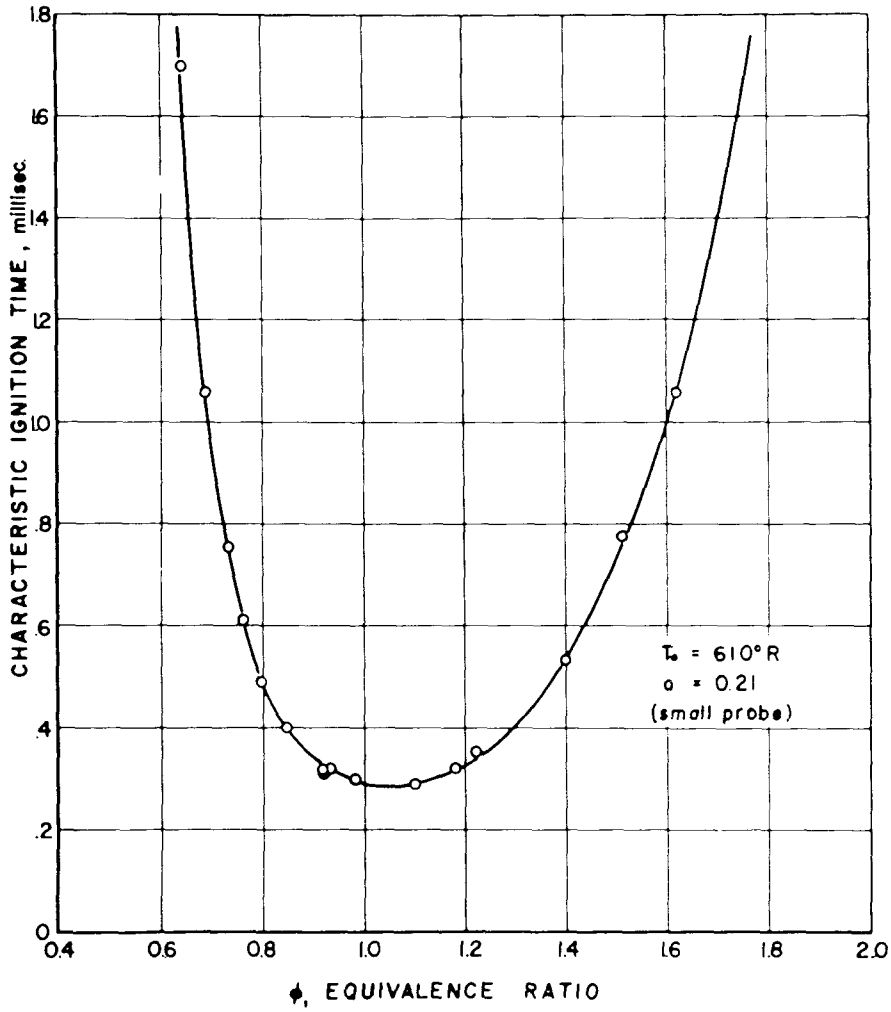

Fig. 2.14 Variation of characteristic ignition time τ_c with equivalence ratio.

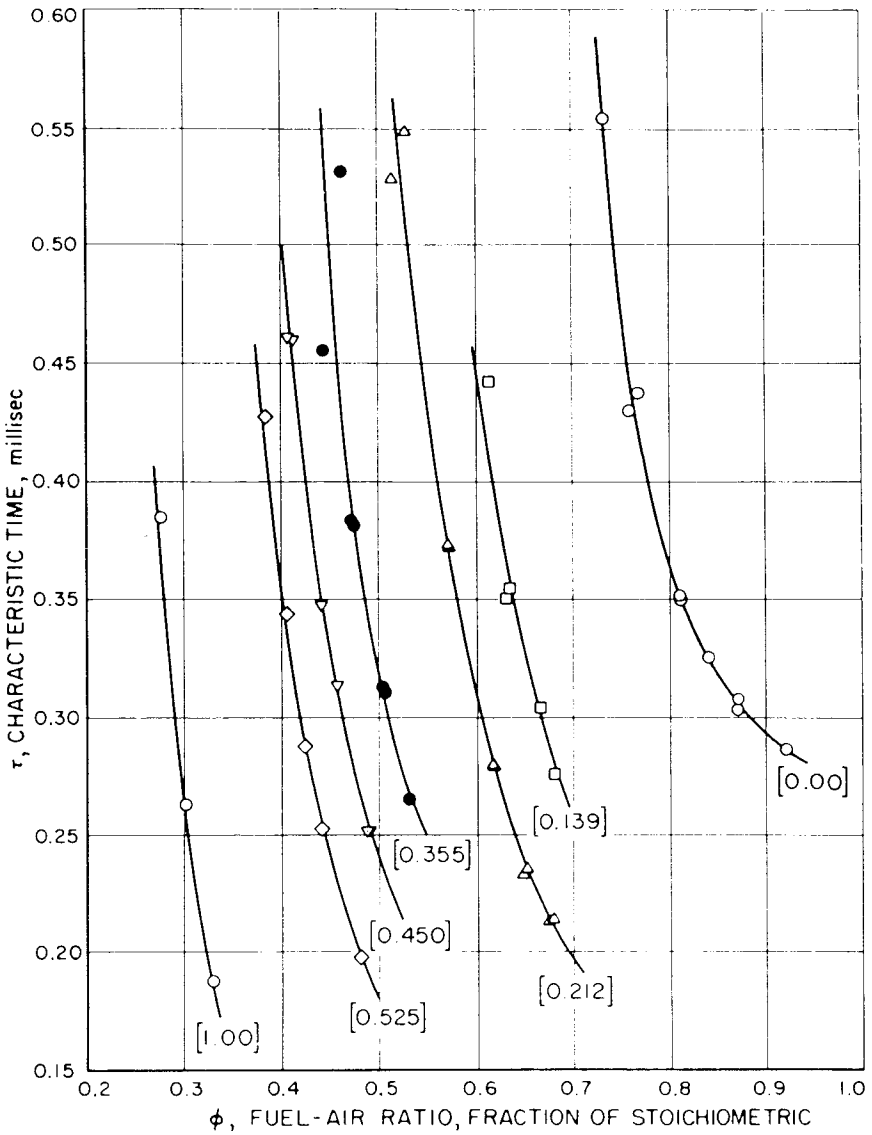

Fig. 2.15 Effect of fuel properties on characteristic time (parameter is mass fraction of hydrogen in the fuel).

approach stream temperature and oxygen concentration, and approach stream pressure.

The dependence of the critical time on fuel-air ratio and fuel type is illustrated in Figs. 2.14 and 2.15. In both, τ_c is plotted as a function of the equivalence ratio (the fuel-air ratio divided by the stoichiometric fuel-air ratio). In Fig. 2.14, values are presented for a hydrocarbon fuel vapor with a molecular weight of about 100. A number of flameholder geometries were used to obtain these data. In Fig. 2.15, a number of fuels were made up of this hydrocarbon plus various mass fractions of hydrogen. The values of τ_c decrease dramatically as the fraction of hydrogen increases. Also note that

τ_c increases very rapidly for both high and low values of the equivalence ratio.

The characteristic time is also a sensitive function of approach stream temperature and oxygen concentration. In general, τ_c decreases rapidly as the temperatures increase, even when this increase is due to vitiation (i.e., preburning at a fuel-air ratio below stoichiometric). However, for a given temperature, τ_c increases as the oxygen mass fraction decreases due to increasing vitiation.

The critical time increases as pressure decreases roughly as $\tau_c \propto 1/P$ for hydrocarbon fuels of high molecular weight (e.g., see Ref. 11). A similar result was obtained in small-scale experiments carried out with hydrogen.

In attempting to obtain an independent estimate of values of τ_c or some other experimentally determined quantity proportional to τ_c, the dependence of a time based on the ratio of the laminar flame thickness δ to laminar flame speed S has been examined. In the single case for which comparable data were available, values of $\delta/S\tau_c$ for methane were computed for stoichiometric fuel-air ratio of one and approach stream temperature between 300 and 400 K. The ratio had a value close to one for the whole range of temperatures examined. Similarly, values of the ratios of δ/S and τ_c for hydrocarbon and hydrogen fuels are about 10. Thus, δ/S may be a useful predictor for the dependence of τ_c on various chemical parameters.

Finally, there is a persistent attempt to relate the characteristic stabilization time to a thermal ignition time (e.g., Ref. 12) or a global reaction rate (e.g., Refs. 13 and 14). These efforts often lead to a representation for τ similar to the reciprocal of a reaction rate

$$\tau_c \propto T^m P^{-n} e^{-(A/RT_f)}/\phi$$

where m and n are numbers of the order of one or two, A an activation energy determined empirically, R the universal gas constant, T_f an ignition temperature or the gas temperature in the recirculation zone, and ϕ an equivalence ratio of less than 1, which is the stoichiometric value. In the works of Solokhin and Mironenko[13,14] where a more complex expression is used, the effective values of the parameters are

$$n = 1,\ m = 2.5,\ A/R = 2 \times 10^4\ \text{K}$$

Although the dependence on temperature and pressure by this approach is plausible, the use of global reaction rates and the application of this approach to processes involving chemical reactions in turbulent mixing regions does not have a sound physical basis and should be viewed as a sophisticated form of curve fitting.

Because of the lack of understanding of the chemical parameters, the stabilization criterion is useful only when τ_c values have been determined for the range of chemical parameters expected in practice. However, small-scale experiments can be used to make the required determinations and some physical feel is given by the flame speed correlation suggested above.

Alternate schemes. One popular alternate scheme for scaling stabilization phenomena is based on the arbitrary use of a dimensional parameter group of the form

$$V_{1c}/P^a d^b T^c = F\{f\}$$

to correlate a body of experimental results. Here f is the fuel-air ratio, d the flameholder scale, P and T the pressure and temperature of the approach flow, and F a function of the fuel-air ratio. (For example, see Ref. 15.) The values for the exponents selected by various authors to correlate their data have ranges of $0.8 \le a \le 2$, $\frac{1}{2} \le b \le 1$, and $\frac{1}{2} \le c \le 2.5$ and F must be determined experimentally.

At the beginning of the study of bluff-body flame stabilizers, there was great confusion concerning the exponent for d that arose because the influence on the recirculation zone region of flameholder and duct geometry, described above, was not fully appreciated. For example, when a circular cylinder held with its axis perpendicular to the gas stream is used as a flameholder, the duct walls have a large effect on the flameholder wake width, even when the ratio of holder diameter to duct height is as small as $\frac{1}{50}$. In the range $\frac{1}{20} \le d/H \le \frac{1}{4}$ and in a duct of fixed size, the wake width and hence the recirculation zone length scale approximately as $L \propto W \propto \sqrt{d}$ rather than as $L \propto d$. This square root dependence leads to a value of the exponent b of $\frac{1}{2}$. Similarly, if cylinders with their axis parallel to the flow are used as flameholders, the wake width grows linearly when d is increased in a duct of fixed size. There is an effect of blockage in this example as well, since the ratio V_2/V_1 will increase with d due to blockage changes but this increase depends on $[1-(d/D)^2]^{-1}$ and hence is hard to detect when $d/D < \frac{1}{4}$. Hence, in this example the exponent b would be close to 1. Further confusion arose because data in the laminar and turbulent regimes were used together to determine these exponents.

A value of the pressure exponent near one is a typical choice and, for the temperature, values still range between 0.5 and 2.5. Thus, a scaling parameter of the form V_{1c}/Pd is often used for fixed inlet temperature. When d is changed by scaling the entire flameholder-duct system, this parameter gives an excellent correlation—as would be expected from the previous analysis. A correlation of this type is given by Hottel et al.[15] However, note that this correlation is useful only in general if d characterizes the scale of the system; if d is changed and the duct height is held fixed, the correlation will fail because of the effect of changes in blockage on recirculation zone length and the velocity ratio V_2/V_1.

Flame Stabilization by Jets in a Homogeneous Stream

The process of flame stabilization in the wake of a gas jet is similar to the processes, described above, occurring in the wake of a bluff body. In either example, a region of strong recirculating flow is created by a physical obstacle or in the wake of interacting jets in which the hot products of combustion can be trapped. This hot gas then acts as a steady source of

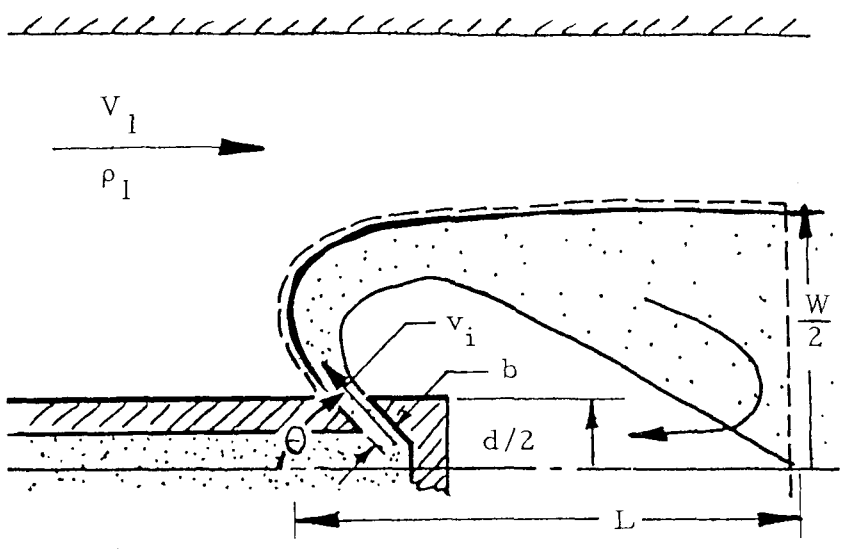

Fig. 2.16 Flame stabilization by a jet.

ignition for the oncoming stream. In the case of flame stabilization by gas jets, two new features are added: (1) the size of the recirculation zone can be changed by changing the rate of gas injection, and (2) the fuel-air ratio and hence the temperature of the gas in the recirculation zone can be changed by changing the fuel-air ratio of the injectant. Because the stabilization process is very strongly affected by changes in the temperature of the recirculation zone gas, having an independent control on this parameter will allow stabilization at fuel-air ratios far below those that could be achieved with bluff-body holders producing the same sized recirculation zone. The advantages of these two features are offset in part by the performance losses and the mechanical problems associated with supplying the gas flow required for flame stabilization and, if a fuel-air mixture is to be used, the problems involved with the production of the vaporized fuel and the preparation of a homogeneous mixture prior to injection.

A crude scaling law for one example of this type of system will be developed here, along with a few experimental results to illustrate the general features of the stabilization process.

The flowfield produced by axisymmetric injection of a jet into a cross flow is shown in Fig. 2.16. The jet is injected through an annular slot of width b in the wall of a center body of diameter d and at an angle $(\pi - \theta)$ with respect to the oncoming flow. In this model, a momentum balance is made on the injectant and the approximation that the drag of the effective body produced by injection (see dotted contour in Fig. 2.16) is balanced by the momentum change of the injectant. Thus,

$$\frac{1}{2}\rho_1 V_1^2 C_d \left(\frac{\pi W^2}{4}\right) = (\rho_i v_i \pi d b) v_i (1 + \cos\theta)$$

where the drag is characterized by a drag coefficient C_d having a value

around one, and it is assumed that the injected mass flow ($\rho_i v_i \pi d b$) enters and leaves the control volume with its velocity of injection v_i. (The assumption that the exit velocity is v_i and not a value closer to V_1, is certainly questionable.) Given this crude balance,

$$\frac{W}{b} = \left[\left(\frac{d}{b}\right)\left(\frac{8(1+\cos\theta)}{C_d}\right)q\right]^{\frac{1}{2}}$$

where $q = (\frac{1}{2}\rho_i v_i^2)/(\frac{1}{2}\rho_1 V_1^2)$.

When W is much larger than the thickness of the boundary layer on the center body and when W is much smaller than the duct diameter (so that blockage effects can be ignored), C_d should be constant. Consequently, the above equation indicates that W will scale as $q^{\frac{1}{2}}$ and when ρ_i/ρ_1 and the geometric parameters are constant, this equation reduces to

$$W \propto \rho_i v_i \propto \dot{m}_i$$

where $\dot{m}_i$ is the mass flow of the injectant.

Experiments (e.g., Ref. 16) have shown that the length of the recirculation zone formed by this injection process is between one and two times the width of the region and that the value of L/W is independent of q but does depend on the injection angle θ. Hence, $L \propto \dot{m}_i$ will hold for this system and $L \propto \sqrt{q}$ for the more general case. Combining the latter results with the scaling law for W and the blowoff criterion, $\tau_c V_{1c}/L = 1$, results in an equation for the blowoff velocity,

$$V_{1c} \propto L/\tau_c \propto (L/W)(W/\tau_c)$$

or

$$V_{1c} = \left[\left(\frac{L}{W}\right)^2 \frac{8(1+\cos\theta)}{C_d}\right]^{\frac{1}{4}}\left[\frac{v_i\sqrt{b}\,d}{\tau_c}\right]^{\frac{1}{2}}$$

when the densities of the injectant and the approaching stream are equal. The terms in the first square bracket on the right-hand side of this equation depend on the angle of injection and those in the second on the velocity and area of the injector. If the geometry and chemical parameters are held fixed, the blowoff velocity is proportional to the square root of the injector velocity and the injector mass flow rate.

As an example, the experiments of Kosterin et al.[16] indicate that flame stabilization in a stream with approach stream speeds of about 100 m/s and fuel-air ratio near $\frac{1}{2}$ of stoichiometric could be achieved with values of q near 50. Mass flows in the injector were less than 1% of the approach stream flow for this example. In addition, the data are roughly correlated by $V_{1c} \propto \sqrt{q}$, which agrees with the above analysis.

The gas entering the recirculation zone is made up from the approach stream as well as the injectant stream and the ratio of these two mass flow rates has been found to be independent of q and strongly dependent on the injectant angle. For example, Kosterin et al.[16] find that the ratio of approach stream to injectant entrainment rates E_r is about 6.5 at $\theta = 135$

Table 2.3 Effect of Injectant Equivalence Ratio on Equivalence Ratio of Mainstream at Blowoff

ϕ_i	ϕ_{1c}	ϕ_e	Flameholder characteristics, mm
0	0.60	0.52	$b = 0.5$
			$d = 15$
0.54	0.54	0.54	$q = 45$
1.0	0.43	0.51	Kerosene fuel
1.2	0.40	0.51	$\theta = 135$ deg

deg, 4.0 at 90 deg, and 2.5 at 180 and 70 deg. Thus, the mixture ratio and hence temperature of the recirculation zone can be strongly influenced by the injectant.

The magnitude of this effect is shown in Table 2.3 where equivalence ratio (the fuel-air ratio, fraction of stoichiometric), in the approaching stream at the blowoff condition ϕ_{1c} is shown as a function of the equivalence ratio in the injectant stream ϕ_i when the gas speed of the approach stream was 100 m/s. In this example, the lean blowoff limit of the approach stream was reduced from 60% of the stoichiometric fuel-air ratio to 40% when the fuel-air ratio of the injectant fluid was increased from 0 to 120% of stoichiometric. The quantity ϕ_e is the calculated value of the equivalence ratio in the recirculation zone based on a measured value of entrainment ratio E_r. Note that ϕ_e is almost constant. Hence, the recirculation zone temperature, which is presumably also almost constant, is believed to be a critical feature in the ignition process.

Note that using injectant angles with smaller values of E_r will increase the sensitivity of the equivalence ratio at the blowoff condition to changes in ϕ_i, but at the same time will change the relationship between wake width, recirculation zone length, and injectant parameter q.

Large-scale tests of a complete afterburner system using two-dimensional arrays of jets of the type discussed here as flame stabilizers are reported in Ref. 17. Good stabilization characteristics and afterburner combustion efficiency were achieved with a total injectant flow rate of 2–4% of the total flow to the afterburner. Total pressure losses associated with jet flameholder systems were found to be 3–4% lower than corresponding values for bluff-body systems when the augmentation was zero. The possibility that gains can be made in reducing the nonafterburning total pressure loss is another reason for pursuing the investigation of this system.

Flame Stabilization in a Heterogeneous Fuel-Air Mixture

In almost any afterburner configuration, the weight savings to be made by reducing all of the length scales in the system will insure that the fuel injection system will be located so close to the flame stabilizers that some of the liquid fuel will arrive at the plane of the flameholders in an unvaporized state. When afterburners are to be used in the airstream of a fan engine, the

low temperatures of these streams will greatly increase the fraction of fuel that is not evaporated. For example, in low-pressure-ratio fan engines operating at high altitudes, present-day jet fuels will be almost completely in the liquid state. In such streams, the flame stabilization system must produce some vaporization of the fuel in addition to acting as a continuous source of ignition.

In addition to these low-temperature problems, special requirements are placed on the fan stream augmentation system (often called a duct burner) by the operating characteristics of the fan. The fan is typically a low-pressure-ratio device and a relatively weak pressure disturbance propagating upstream from the augmentor can push the fan into a strong surge or stall. Hence, ignition of the fan stream augmentor must be achieved at a very low overall fuel-air ratio so that the sudden increase in total temperature (due to the start of afterburning) will not interact with the choked nozzle to produce a pressure pulse which will cause the fan to stall.

Common duct system. Under conditions such that the fuel in the fan stream is poorly vaporized, the simplest system is the engine in which afterburning takes place in a common duct with fuel injection system modulated so that combustion starts in the afterburner in the core stream where high temperatures insure good vaporization. Some of the hot gas produced by afterburning in the homogeneous core stream can then serve to support the flame stabilization process in the fan airstream and to produce vaporization in regions where the fan and core streams mix. The fan engine described in the introduction of this chapter (e.g., see Fig. 2.2) uses this system.

If fan air is to be burned in a separate duct where this support is not available, the flameholder must operate alone. In the following paragraphs, a qualitative picture of several flame stabilization schemes is given for this second and most extreme example. Few experimental data are available and because the process is complex, systematic experimental or theoretical treatment of this important problem is lacking.

Bluff-body flameholders. There is evidence that the picture of the bluff-body stabilization process described above applies in most respects to bluff-body stabilization in a heterogeneous flow. The principal difference is that in heterogeneous flows fuel vaporization must take place during the stabilization process itself. This can occur in two ways: (1) when liquid fuel drops impinge on the hot flameholder and (2) when fuel drops enter the mixing zone. In either case, the fuel-air ratio in the wake will be fixed by local conditions in a manner similar to that described above for the gas jets when a fuel-air mixture is used as the injectant. In this case, as there, the fuel-air ratio of the gas entering the wake appears to be the dominant factor and maximum blowoff velocity occurs for the injection conditions that supply the recirculation zone with a stoichiometric fuel-air mixture. Proper design and control of the fuel injection system can be used to get the best conditions for stabilization regardless of the overall fuel flow requirements.

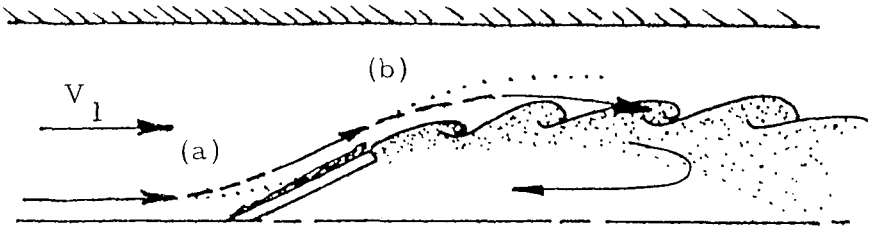

Fig. 2.17 Capture of fuel droplets.

The process of fuel vaporization by the flameholder involves a number of steps. First, the fuel droplets must be captured by the flameholder. Capture results because the droplets cannot exactly follow the gas streamlines; as the gas flows over the flameholder, the droplets will first be accelerated toward the holder (region a of Fig. 2.17) and then away from the mixing zone at region b. The drift rate across streamlines will depend strongly on particle size, the flameholder shape, and the velocity, density, and viscosity of the gas. After the fluid is captured on the holder, its residence time there will be fixed by a balance between the shear forces produced by the gas stream and the shear and surface tension forces acting between the liquid film and the flameholder. If too thick a film is formed, ablation of liquid drops from the downstream edge of the holder will result. If the vaporization rates are high, the holder may operate in a dry state. Heat transferred between the recirculation zone gas and the liquid film will depend on the usual convective parameters, and hence will increase with the speed, temperature, and pressure of the gas in the recirculation zone, and again will depend on the flameholder geometry.

Given the capture and heat-transfer processes, the properties of the fuel will then fix the rate of production of the fuel vapor at the flameholder, and the entrainment of vapor and air in the mixing zones will fix the fuel-air ratio of the recirculation zone gas. Additional vaporization of fuel droplets entrained in the mixing and recirculation zones will further increase the fuel-air ratio.

When the capture, heat-transfer, and evaporation rates are high, the fuel-air ratio in the recirculation zone can be much higher than in the stream approaching the flameholder. This difference would make possible ignition and stabilization when the overall fuel-air ratio is far below stoichiometric and hence would be advantageous during startup of the augmentation process. However, when the overall fuel-air ratio is increased toward the stoichiometric value (as it must be to achieve maximum augmentation), the fuel-air ratio in the recirculation zone could increase to values far above stoichiometric and a flame blowoff on the fuel rich side would occur. Hence, having the fuel-air ratio in the wake larger than that in the flow is not always advantageous.

It is clear from this brief qualitative description that the fuel injection system and the fuel capture and heat-transfer rates of the flameholder must be carefully controlled over a wide range of operating conditions if the

simple bluff-body flameholder is to be used successfully. In general, such control is not possible with existing injection systems over wide operating ranges.

Flame stabilization by jets. A second system that has shown promise in heterogeneous systems is the aerodynamic flameholder or gas-jet holder described in a previous section. For duct burners, this system is perhaps the best of the three discussed here as far as its flame stabilization properties are concerned. However, losses and mechanical problems associated with the system may make its use impractical. (For example, see Ref. 17.)

Pilot burner. A third system suggested for use in heterogeneous fuel-air mixtures is a piloted burner. A small part of the afterburner flow, say 5–10%, is burned in a can-like pilot burner (or a number of burners) at the stoichiometric fuel-air ratio. The hot gas from this source is then used to support the stabilization by a system of conventional flameholders. The pilot burners require separate fuel injection and control systems to maintain fuel-air ratios different from those in the main flow. Systems of this type can be ignited at very low overall fuel-air ratios (e.g., Ref. 17) and low pressure levels. However, larger total pressure losses are produced by this system both with and without augmentation.

In summary, a number of schemes are available to produce flame stabilization in heterogeneous flows under conditions suitable for fan engine applications. Although the common burner scheme is the most well developed, the aerodynamic and pilot burner schemes offer advantages that are worth further exploration.

Discussion

The model used above to describe flame stabilization in homogeneous fuel-air streams by bluff bodies has the advantage of cleanly separating aerodynamic and chemical features of the process. The influence of various aerodynamic parameters is well understood from a qualitative point of view and many features can be treated in a quantitative manner. In particular, the dependence of stability limits on the geometry and scale of the flameholder-duct system is now clear.

The influence of the various chemical parameters of the problem are much less well understood. The use of an ignition time delay as suggested by Mullins,[12] Solokhin and Mironenko,[14] and Kosterin et al.[16] to describe ignition in a turbulent mixing zone is not correct, in the opinion of the author.

In one typical version of this approach (by Solokhin and Mironenko[14]), the ignition time is calculated from a global model of the chemical reaction rate and the chemical concentrations and temperature used in the calculation are taken from a mathematical model of the mixing zone that is based on time-averaged measurements of these parameters. There are three problems here. Global models for reaction rates have been used in calculations of laminar flame speeds and have led to qualitatively useful results. How-

ever, in order to obtain quantitatively accurate predictions, it has been found necessary to consider detailed chemical analyses that usually involve a large number of reaction steps, reaction rates, and activation energies.

A second and perhaps more serious problem arises from the treatment of the mixing layer. The model used by Solokhin pictures the layer as a region in which the temperature and concentrations change smoothly from values corresponding to the unburned mixture on one side to values corresponding to the products of combustion on the other. This is the result obtained experimentally with instrumentation producing time-averaged values. However, recent experimental developments (e.g., Brown and Roshko[18]) suggest that the conditions in the shear or mixing layer are quite different. Experimental results indicate that large-scale structures predominate in the mixing layer and that consequently gas in the layer, at a given instant and at a given point, has a high probability of being either completely burned or unburned. The probability of finding gas with a temperature or concentration of an intermediate value is small even at the center of the layer. In this picture of the flow, chemical reactions will start at boundaries between fully burned and unburned masses of gas and *not* in a uniform mixture of burned and unburned material. Thus, if the new model of the mixing layer is correct, the use of the time-averaged values of temperature and composition in the calculation of chemical reaction rates is inappropriate.

Finally, flame stabilization involves more than the simple ignition process. In order to stabilize a flame, the gas ignited in the mixing layer must continue to burn after it moves past the downstream end of the recirculation zone. Thus, the heat release rate in the mixing zone gas must be high enough to overcome the quenching effects of the entrainment of unburned gas in the region downstream of the recirculation zone. A simple ignition model is probably not sufficient to describe this process.

2.6 Flame Spread in Premixed and Homogeneous Fuel-Air Mixtures

In this section, the process of heat addition after flame stabilization has been achieved is discussed. Processes occurring in a premixed and homogeneous fuel-air mixture are considered. The term homogeneous is used here to denote mixtures of fuel vapor and air, as contrasted with heterogeneous mixtures by which is meant mixtures of fuel droplets and perhaps some fuel vapor with air. The combustion in the latter fuel-air system is important in duct-burner systems for fans, but will not be discussed here. (See the supplementary reading list at the end of this chapter.)

Given the flame stabilized in a duct, it should be possible to calculate the distance downstream of the stabilizer required to achieve a selected value of the heat release or combustion efficiency. The parameters that may influence the required length are: (1) *flow properties* (such as the pressure, temperature, and oxygen concentration; the fuel-air ratio and fuel properties; and the Mach number, velocity, and turbulence level of the unburned stream); and (2) *duct parameters* (such as duct height, flameholder geometry and blockage, and cross-sectional area changes with axial distance).

Unfortunately, at the present time, the dependence of the heat release rate in a combustion changer of fixed size on any of these parameters from basic principles cannot be predicted. Indeed, the understanding is so poor that the appropriate dimensionless parameters have not been identified or agreed upon. However, several fluid dynamic parameters (the Reynolds number and Mach number) are used to characterize the flow.

Although a great deal of experience is available that can serve as a guide for a new combustion chamber design, a large and expensive development effort is usually required to produce a satisfactory configuration. Conventional wisdom is in agreement, for example, that an increase in pressure, temperature, oxygen concentration, and turbulence level will increase the heat release rate and reduce the combustion chamber length required for high combustion efficiency. However, quantitative measures of the effects to be expected, given a particular change in a parameter, are not available. The reason for this is that the combustion process is turbulent and occurs in a region of strong shear and large axial pressure gradient.

General features of the flowfield of a typical flame are shown in Fig. 2.18. In this example the flame is stabilized by a bluff body placed on the centerline of a constant-area duct. The downstream end of the recirculation zone is about one tunnel height H downstream of the flameholder. The fuel is a hydrocarbon that produces a highly visible flame and the outer boundaries, shown in Fig. 2.18a, are based on time-exposure photographs taken in the light of the flame itself.

Temperature profiles shown in the lower half of Fig. 2.18a at a number of positions exhibit a sharp initial rise from the cold-gas temperature, which is followed by a very small and more gradual further increase. The maximum values, reached at the centerline of the duct, are close to the adiabatic flame temperature. The two boundaries based on the positions at which the initial temperature rise starts and stops are also shown in the lower half of Fig. 2.18b and they contain the region of strong chemiluminescence (shown here as a dotted region).

The temperature values shown here are averaged over long periods of time. Time-resolved temperature measurements suggest that the rapid initial rise is produced by averaging in time over temperatures that fluctuate rapidly between values close to the unburned and burned gas temperatures.

Spark schlieren photographs, similar to the sketch at the top half of Fig. 2.18b, support this picture. They indicate that the edge of the flame contains distinct vortex-like structures that produce a strongly corrugated surface (see Figs. 2.9 and 2.13). Hence, a probe located in this region would alternately observe hot and cold fluid. The scale of these structures grows slowly with the increasing distance from the flameholder and typically occupies between 30–40% of the width of the flame W. That is, regions of strong temperature gradients penetrate far into the flame front.

Concentration profiles for the products of combustion are similar to the temperature profiles: regions of the strong chemiluminescence produced by combustion (the dotted region in Fig. 2.18b) and of strong ionization, concentration, and temperature gradients almost exactly coincide. This result suggests that the sharp boundaries shown in the schlieren photo-

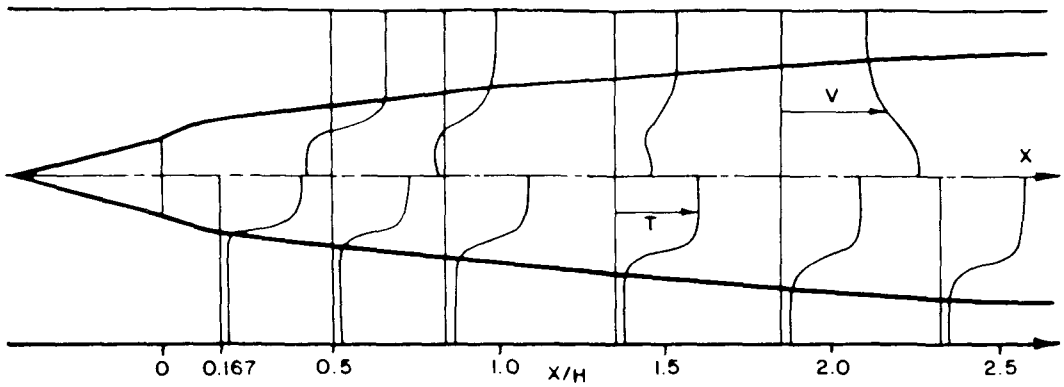

a)

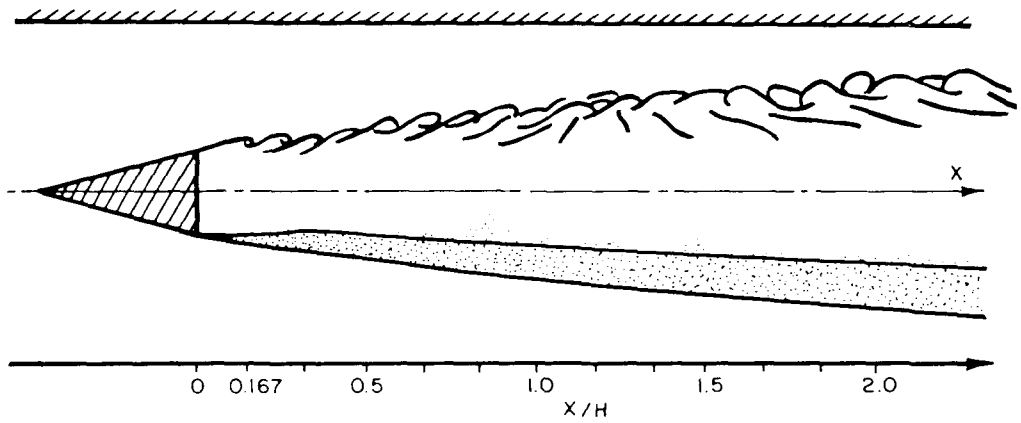

b)

Fig. 2.18 Flame stabilized on a two-dimensional wedge flameholder: a) temperature and velocity profiles; b) schlieren and chemiluminescence boundaries.

graphs are flame fronts and that their positions are restricted to the region of sharp temperature rise.

The velocity profiles (shown in Fig. 2.18a) are also averaged over long periods of time and show less steep gradients than the temperature profiles. Near the flameholder and in the recirculation zone, the time-averaged velocity is reversed. The centerline velocity increases rapidly for positions farther downstream and exceed the unburned gas speed at positions farther downstream than $1\frac{1}{2}$ duct heights. This acceleration of the burned gas is a result of the action of the axial pressure gradient, produced by heat addition, on the high-density unburned gas and the lower-density burned material. The axial gradient, which is uniform across the duct, causes the lower-density fluid to accelerate more rapidly than the high-density stream and thus produces the hat-shaped profile.

In summary, the flame front appears to be made up of thin regions of chemical reaction that are rolled up into vortex-like structures. The size of these structures grows slowly as the axial distance increases and they occupy between 30–40% of the "flame" width. Strong chemical reaction and large heat release occur in the shear layers forming the boundaries between streams with large density and velocity differences.

The vortex-like structures lie in the region with a strong average velocity gradient. This suggests that they are related to the large-scale structures observed in two-dimensional shear layers. However, the vortex pairing observed without combustion has not been observed in spreading flames.

This picture of the spreading flame suggests that the rate of consumption of unburned fluid in the spreading flame is fixed by an entrainment process, rather than by a simple flame propagation process that might be expected to depend at least weakly on molecular transport properties. Much of the experimental data presented later support this view. The primary problem concerned with the prediction of flame spreading rates is the determination of this entrainment process. At the present time, no satisfactory physical model has been developed to describe it.

The remainder of this section reviews experimental information concerning flame spreading rates and discusses the implications of these data for turbulent entrainment rates or flame speed. Several simple models are described that allow a reasonable description of the dependence of some of the fluid dynamic parameters on the heat addition from the flame. However, even these restricted models remain incomplete because the entrainment rate of the turbulent flame cannot yet be prescribed.

Spreading Rates of Turbulent Flames

The quantity that the afterburner designer needs to know is the manner in which the combustion efficiency of a burner varies with the parameters described in the previous paragraphs. Unfortunately, combustion efficiency is difficult to measure accurately and has not been the subject of detailed investigations under conditions in which the effects of changing combustion chamber parameters were clearly isolated. Instead, a number of investigations have been made of the spreading rate of the flame front and then conclusions regarding the more applied problem of combustion efficiency have been drawn based on these results. See, for example, Williams et al.,[19] Wright and Zukoski,[20] and Solntsev.[21]

There are a number of problems with this approach. First, the flame is observed to have a finite thickness, which may be as great as 20% of the duct height (e.g., see Fig. 2.18). The spreading rate and conclusions drawn from it will depend strongly upon which surface is defined as the flame front. Further, since the combustion process presumably takes place within this thickness, any interpretation of combustion efficiency based on a single boundary will be suspect.

Second, there is a strong interaction of the flow with the heat addition process. The strong axial pressure gradient produced by heat addition produces acceleration in the unburned fluid that, in turn, produces an

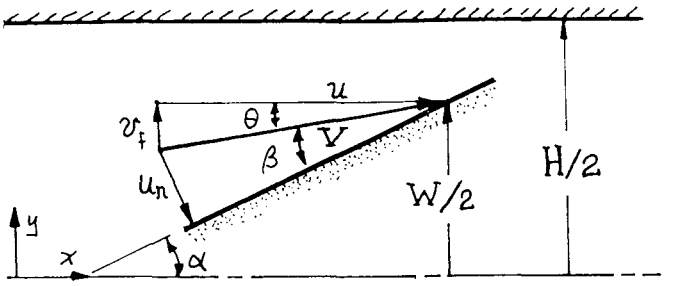

Fig. 2.19 Calculation of streamline angle at flame front.

appreciable curvature of streamlines near the flame front. The acceleration and curvature can have important effects on the interpretation of the flame width data.

This process is illustrated by the two-dimensional flow shown in Fig. 2.19. The problem is simplified by assuming that the unburned flow is isentropic, incompressible, and has a velocity vector which is almost axial and almost uniform. Under these assumptions the continuity and axial momentum equations can be written for the unburned flow as

$$\frac{\partial u}{\partial x}+\frac{\partial v}{\partial y}=0 \quad \text{and} \quad \rho u\frac{\partial u}{\partial x}+\frac{\partial P}{\partial x}=0$$

Combining these and making use of the approximation that ρ, u, $\partial u/\partial x$, and P are independent of vertical position y leads to the small angle that the velocity vector V makes with respect to the axis at the flame front,

$$\theta \approx \frac{v_f}{V}=\left(\frac{V_1}{V}\right)^2\left(\frac{H-W}{4}\right)\left(\frac{\partial C_p}{\partial x}\right) \tag{2.13}$$

where V_1 is the gas speed far upstream of the flameholder, v_f the y component of the velocity at the flame front, and C_p the pressure coefficient defined as

$$C_p=(P_1-P)/\tfrac{1}{2}\rho_1 V_1^2$$

The ratio V/V_1 is different from 1 because of the velocity change produced by acceleration of the flow around the flameholder and then by heat addition.

The angle α is one made between the flame front at the point of interest and the axis of the duct. It can be obtained from the shape of the flame front and is just

$$\alpha=\frac{1}{2}\frac{dW}{dx} \tag{2.14}$$

The velocity of the gas normal to the flame front u_n, sometimes called the turbulent entrainment velocity or flame speed, is given by $V \sin \beta$. β can be obtained from the difference between angles θ and α, that is,

$$u_n/V = \sin(\alpha - \theta) \tag{2.15}$$

Thus, to calculate u_n consistent with any choice of the flame front, V/V_1 and both angles α and θ must be known. In many situations in which turbulent flame spreading is considered, the ratio V/V_1 can be as large as 2 to 3 and the angles α and θ are often nearly equal. Hence, neither of these effects can be ignored a priori.

This section outlines the dependence of the wake width on a number of parameters that describe the combustion chamber and the implications of these results with regard to the combustion efficiency and turbulent entrainment velocity.

Flame spreading. The spreading rate of the flame is a very strong function of the condition of the flame. When the flame is laminar, the flame width is a strong function of laminar flame speed and turbulence level in the approach stream.[22,23] However, at higher speeds and Reynolds numbers, the flame becomes turbulent under the same conditions that the mixing layers become turbulent and the dependence of the flame shape upon the molecular transport processes becomes negligible.

This transition is illustrated by the schlieren photographs of Fig. 2.13 and by the data shown in Table 2.4, taken from Thurston.[24] He examined flame spreading in a rectangular duct (about 15×7.5 cm in cross section) and used several cooled circular cylinders as flameholders. The data of this table show the wake width and velocity ratios measured near the downstream end of the recirculation zone (subscript 2) at about 4 cm and at a station 37 cm downstream of the holder (subscript 37). The outer edge of the flame defined in schlieren photographs and averaged through its bumpy surface

Table 2.4 Variation with Approach Speed of Velocity Ratio and Wake Width at the Downstream End of Recirculation Zone (sub 2) and 37 cm (sub 37) from Flameholder[a]

V_1 (m/s)	$\frac{V_2}{V_1}$	$\frac{W_2}{H}$	$\frac{V_{37}}{V_1}$	$\frac{W_{37}}{H}$
30	1.09	0.23	1.55	0.40
60	1.06	0.22	1.34	0.34
80	1.06	0.21	1.31	0.33
100	1.05	0.21	1.29	0.33
120	1.04	0.21	1.27	0.33
140	1.04	0.21	1.27	0.33

[a] Duct about 15×7.5 cm with 0.32 cm diam cylinder spanning the 7.5 cm dimension; stoichiometric fuel-air ratio.

was used to determine the wake width. Total and static pressure measurements were made as a function of axial position and the velocity in the unburned flow was determined from the pressure measurements.

Note in Table 2.4 that as the approach speed V_1 is increased from 30 m/s (at the beginning of the transition to turbulence) to 60 m/s, the wake width at the 37 cm station decreases by about 15%. A similar doubling of speeds to 120 m/s produces a much smaller change. Similarly, at $x = 37$ cm, the ratio of the velocity to the approach stream speed decreases rapidly at first and then approaches a constant value. Further, of the 6% velocity reduction occurring as the approach speed is changed from 60 to 120 m/s, 2% is evidently caused by changes occurring in the neighborhood of the recirculation zone, e.g., see the V_2/V_1 column. The small changes in the wake width and velocity ratio observed here for the turbulent flow condition are typical of measurements obtained in the turbulent regime for holder sizes in the range of 0.32–2.54 cm. A similar transition was also reported in Ref. 19.

The spreading rates of flames stabilized on bluff-body flameholders operating in constant-area ducts and in the turbulent regime have been determined by Wright and Zukoski[20] as a function of the approach stream speed, fuel-air ratio, temperature, fuel type, and flameholder-duct geometry. Fortunately for the designer of afterburners, the observed spreading rates have been found to be almost independent of these parameters. Typical results are shown in Fig. 2.20 taken from Ref. 20.

In Fig. 2.20a, the dependence of the wake width on the fuel-air ratio is shown. In this range of equivalence ratios, the laminar flame speed for a typical hydrocarbon fuel has a maximum near an equivalence ratio of 1.10 and would decrease to about 60% of the maximum value for $\phi \approx 0.75$. Similarly for the temperature increase shown in Fig. 2.20b, the laminar flame speed would increase by factors of about two or more. Finally, the laminar flame speed for hydrogen-air mixtures is of the order of 10 times that of the hydrocarbon fuel used in these tests. Despite these changes in parameters, which produce large changes in laminar flame speed, little change is observed in the flame geometry. The lack of change in Fig. 2.20c is particularly interesting.

Similar results concerning the very weak dependence of the flame geometry on the approach stream speed and fuel-air ratio are reported by Williams et al.[19] and also by Solntsev[21] who carried out experiments in much larger-scale apparatus. The former measurements were made from schlieren photographs and Solntsev used photographs, as well as temperature, oxygen concentration, and ion density profiles to determine the widths. Thus, it is clear that the measurements described above are general and that the laminar flame speed and presumably other molecular transport processes are *not* important in fixing the geometry of the spreading turbulent flame.

The dependence of flame geometry on the turbulence level of the unburned mixture is less clear. The experiments of Williams et al. showed a very weak dependence in small-scale experiments, whereas Solntsev found a somewhat larger dependence. The latter suggested that the entrainment rate of the turbulent flame is proportional to the turbulence level in the unburned flow.

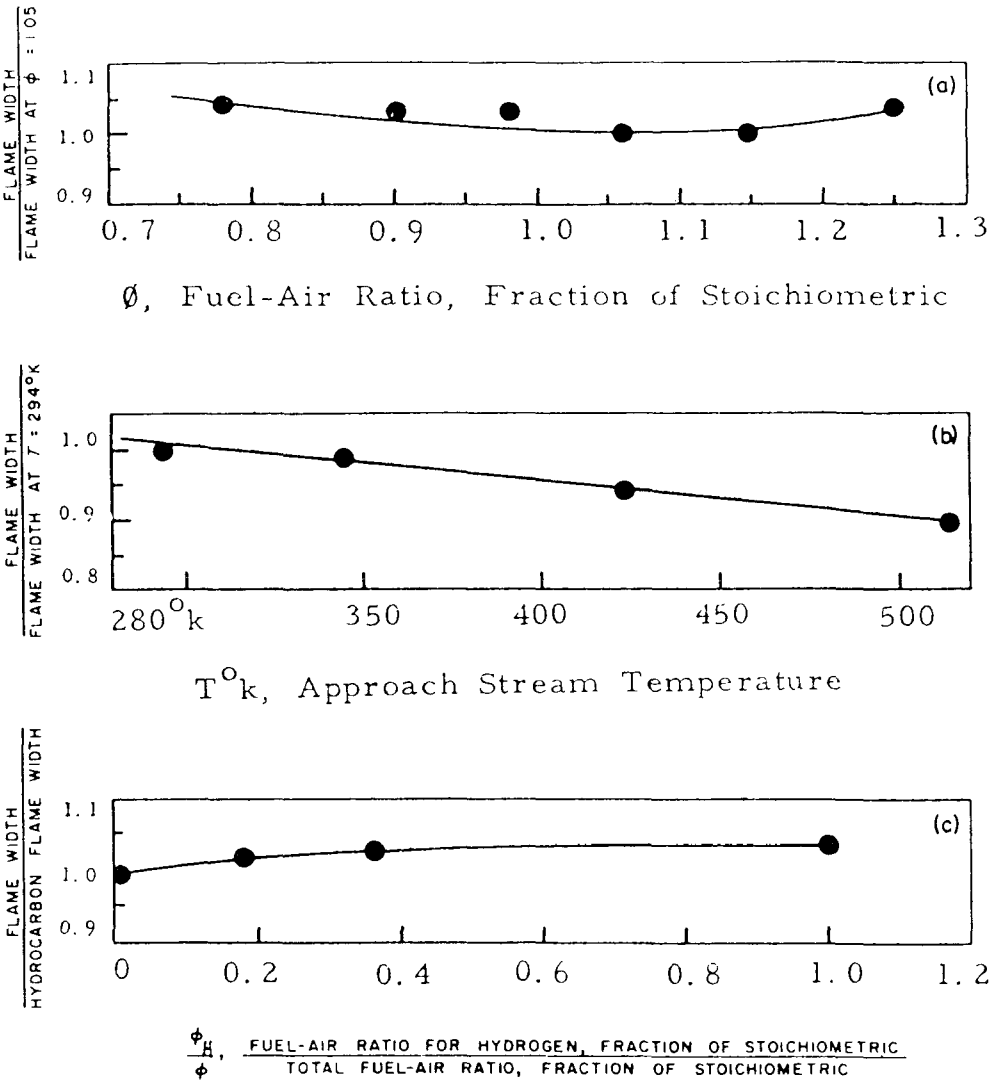

Fig. 2.20 Dependence of flame width on fuel-air ratio, approach stream temperatures, and fuel type (holder is a $\frac{1}{8}$ in. circular cylinder and width is measured 15 in. from holder).

Experiments carried out by Wright[7] in which high subsonic speeds were observed in the flow past the wake indicate that the Mach number does not have a large effect on flame geometry as long as the local Mach number is below 0.8.

No experiments dealing directly with the pressure dependence of the flame spreading phenomena have been reported. A number of experiments have been made of complete afterburner systems in which the pressure effects were examined and were found to have strong effects on combustion efficiency when the pressure fell below a limiting value.[15] However, since the complete system was involved, it is not clear which process (injection, flame stabilization, or flame spreading) was responsible for the drop in efficiency

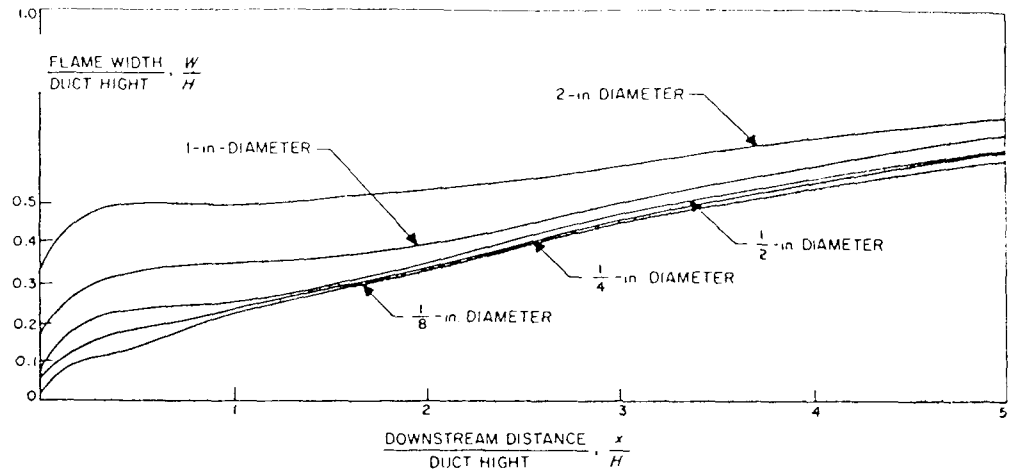

Fig. 2.21 Flame shapes for flameholders of several sizes in a duct of fixed size, $V = 300$ ft/s, $\phi = 1.0$, $H = 15$ cm.

as the pressure was reduced. The Reynolds number is reduced when the pressure falls and the velocity is held fixed. Such a reduction could cause a transition from turbulent to laminar flow, which would have a very adverse effect on flame spreading and combustion efficiency as well as on the flame stabilization process. In addition, Hottel et al.[15] suggest that a pressure reduction would also reduce the turbulence level of the approach stream and that this will result in a reduction of the flame spreading rate.

The dependence of flame geometry on flameholder-duct geometry is weak and complicated. The wake width at a given distance downstream from the flameholder in a duct of fixed size does increase slowly as the flameholder scale is increased. However, at distances greater than several recirculation zone lengths of the larger holder, wake widths are almost independent of holder scale. Thus, an increase in blockage for a flameholder of fixed size will cause a slight decrease in the flame spreading rate.

Data illustrating this result are shown in Fig. 2.21 and are taken from Ref. 20. Flame boundaries are shown for flames stabilized in a rectangular duct (15 cm high by 7.5 cm wide) for five cooled circular cylinders with diameters of 0.32, 0.63, 1.27, 2.54, and 5 cm. The outer edge of the flame, determined from schlieren photographs and normalized by the duct height H of 15 cm, is given as a function of the axial position, which is also normalized by the duct height. The large initial differences are due to differences in the width of the recirculation zone, discussed earlier. However, farther downstream, the boundaries begin to merge. At $x/H = 5$, the differences in the wake width are small despite the change in the blockage ratio from $1/48$ to $\frac{1}{3}$.

If the flame geometry of a single flameholder in a duct is compared with the flames produced by two holders of the same scale located in the same duct, each flame width of the latter configuration will be slightly smaller than that of the single holder. However, the fraction burned will be greatly

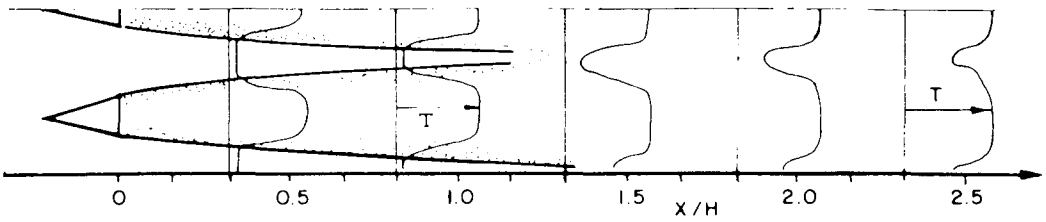

Fig. 2.22 Flame edge and temperature profiles for a three-flameholder array (from Ref. 21).

Table 2.5 Comparison of Flame Widths for 30 deg Half-Angle Wedge Holders in a Duct of 300 mm Height

x (cm)	$\frac{x}{H}$	$\frac{W_1}{H}$	$\frac{W_3}{\frac{1}{3}H}$	$\frac{x}{\frac{1}{3}H}$
100	0.33	0.31	0.68	1.0
250	0.83	0.48	0.89	2.5
400	1.33	0.60	1.00	4.0
850	2.83	0.71	1.00	8.5

Subscript 1: one single 70 mm holder; subscript 3: three 30 mm holders.

increased at a given distance downstream of the holder. Hence, if stabilization problems are not a limiting constraint, increasing the number of holders will always improve combustion efficiency.

This situation is illustrated by the data of Solntsev[21] shown in Figs. 2.18 and 2.22 and in Table 2.5. The sketches show flame boundaries and temperature profiles for two flameholder configurations placed in the same 300 cm high duct. In Fig. 2.18, the holder is a 30 deg half-angle wedge with a 70 mm base height; in Fig. 2.22, three 30 deg half-angle wedges are used. Wake widths are presented as a fraction of the duct height and for a number of axial positions in Table 2.5. The duct height used in presenting the three-flameholder data is divided by three so that each holder is charged with its equivalent duct height. The flame fronts for the three-holder configurations begin to merge near $x/H = 1.3$ and combustion is complete before the $x/H = 2.8$ station at which the flame width of the single holder configuration is less than 75% of the duct height. If the wakes widths and axial positions are normalized by the height of the duct occupied by each holder, i.e., by 300 mm for the single holder and 100 mm for the three-holder configuration, the systems look more similar. Thus, the flames occupy about 65% of their ducts at a station one equivalent duct height downstream of the holder.

Entrainment rates. The entrainment rate of the flame can be determined from knowledge of the flame geometry and the pressure and

Table 2.6 Parameters Used in the Calculation of Entrainment Velocity u_n for Stoichiometric Fuel-Air Ratio[a]

D (cm)	V_1 (m/s)	C_{p37}	$\partial C_p/\partial x$ (l/cm)	$(H-W)/2$ (cm)
0.32	30	1.40	0.040	4.6
0.32	60	0.80	0.020	5.0
0.32	120	0.62	0.016	5.1
0.32	140	0.62	0.016	5.1
0.64	60	0.87	0.015	4.9
0.64	120	0.70	0.013	5.0
1.27	60	1.10	0.014	4.6
1.27	120	0.96	0.010	4.6

$\partial W/\partial x$	α	θ	β, u_n/V	u_n (m/s)
0.140	0.070	0.040	0.030	1.4
0.086	0.043	0.028	0.015	1.2
0.090	0.045	0.025	0.020	3.1
0.090	0.045	0.025	0.020	3.6
0.076	0.038	0.019	0.019	1.6
0.062	0.031	0.011	0.020	3.1
0.066	0.033	0.015	0.018	1.6
0.065	0.033	0.012	0.021	3.5

[a] Data from Thurston.[24] (Note: no boundary-layer correction has been made for β.)

velocity field produced by the flame. However, the entrainment rates determined by this method are very strongly dependent on the definition used for selection of the flame front position and on a number of corrections. A set of calculations made from the data of Thurston[24] illustrates the process.

Consider Fig. 2.19 and the data presented in Table 2.6. Values of experimental parameters and the angles α, β, and θ calculated from Eqs. (2.13) and (2.14) are presented in the table for three flameholders of diameter D and a range of approach stream speeds V_1. Calculated values of the entrainment speed are given in the last column.

The entrainment rate per unit area of the flame is ρu_n, which in Eq. (2.15) was given by

$$\text{Entrainment rate} = \rho u_n = \rho V \sin \beta$$

and when β is small

$$\text{Entrainment rate} = \rho V \cdot \beta$$

One interesting result shown in Table 2.6 is that the entrainment angle β is almost independent of approach stream speed and flameholder blockage when the flame is turbulent. The values of β lie around 0.02 with a scatter of at least 0.005 or 25%. Some of the data used to calculate values of $\beta = \alpha - \theta$ are also shown in the table. Examination of the quantities shows that β is constant despite substantial changes in these quantities resulting from changes in flameholder diameter D. Note also that β changes only slightly when the speed of the approaching stream V_1 is increased by a factor of two.

The large scatter is due to the rather arbitrary definition of the flame width W and uncertainties in the estimation of the slopes for W and C_p that appear in calculation of α and θ. Notice that in most cases the velocity vector V is turned away from the axis through an angle θ that is roughly half of α, the angle between the spreading flame front and the axis of the duct. Because θ is greater than the angle β for many of the conditions presented here, large errors in β must be expected from this source. In addition, the boundary layers growing on the walls of the combustion chamber will also produce an acceleration of the flow by reducing the effective cross-sectional area of the duct and hence must be taken into account in calculating the angle θ. For the data presented in Table 2.5, the growth of the displacement thickness on the top wall of the duct would decrease θ and hence increase β by about 0.002 rad. Side wall boundary layers will have a similar effect. Hence, the entrainment velocity for those experiments is about 0.025 ± 0.007 of the local unburned gas speed.

The entrainment rate can also be obtained directly from the flame width and velocity data by a different mass balance technique. The idea here is to measure the mass flow of the unburned gas outside the flame as a function of axial position. The rate of change of this flow rate $\dot{m}_c$ with the axial position can then be used to determine the entrainment rate. When α is small, the entrainment rate per unit area at one side of the flame is $(-\frac{1}{2})(\mathrm{d}\dot{m}_c/\mathrm{d}x)$ and can be expressed in terms of the total mass flow $\dot{m}_1 = \rho_1 V_1 H$ as

$$\beta = \frac{u_n}{V} = -\frac{H}{2}\left[\frac{\mathrm{d}}{\mathrm{d}x}\left(\frac{\dot{m}_c}{\dot{m}_1}\right)\right]\left(\frac{V_1}{V}\right)$$

Measurements of $\dot{m}_c$ of the type required were carried out by Thurston[24] for one of the experiments reported in Table 2.5. An estimate of β based on the above equation and Thurston's data was 0.027 for the 0.32 cm flameholder. The agreement of the two methods is close considering all the uncertainties.

The entrainment rate of a turbulent flame will certainly depend on a number of parameters not changed in the experiments described here and hence this value for β cannot be viewed as having any general applicability. However, the small rate of entrainment is of general interest and probably represents the lower bound of values for entrainment in a low-turbulence experiment.

One-Dimensional Heat Release

As a first crude approximation for the processes occurring in the combustion chamber of an afterburner, it is convenient to investigate the process of heat addition in simple, one-dimensional channel flow. The calculation will be carried out with the assumption that the heat is added uniformally across the channel.

Differential relations. The aim of the calculations is to illustrate the variation of the variables as heat is added; of particular interest are the dependence of the stagnation pressure and Mach number on the stagnation enthalpy or temperature. The process when the assumption of constant-channel area is made will be considered first and later the expressions including the variation of area will be derived.

Referring to Fig. 2.23, a quantity of heat dH is added between two control planes separated by a distance dx. It is assumed that no change in the initial conditions (u, ρ, p, T, M) is invoked by this addition of heat. Therefore, the flow process may be described by the laws of continuity, momentum, and energy transport

$$d(\rho u) = 0$$

$$(\rho u)\,du + dp = 0$$

$$C_p\,dT + u\,du = dH = C_p\,dT_t \tag{2.16}$$

and the equation of state for a perfect gas

$$p = \rho RT$$

The change of gas velocity accompanying an addition of heat may be found

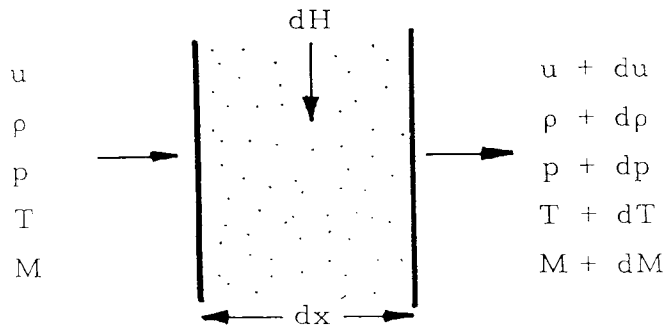

Fig. 2.23 One-dimensional flow of gas with infinitesimal heat addition.

by eliminating the temperature variation from the energy equation, using the equation of state

$$u\,\mathrm{d}u + C_p T\left(\frac{\mathrm{d}p}{p} + \frac{\mathrm{d}\rho}{\rho}\right) = \mathrm{d}H \tag{2.17}$$

Now computing $\mathrm{d}p/p = -u\,\mathrm{d}u/RT$ and $\mathrm{d}\rho/\rho = -\mathrm{d}u/u$ from the momentum and continuity equations, respectively, it follows, upon collecting and rearranging terms, that

$$\frac{\mathrm{d}u}{u} = -\left(\frac{1}{M^2 - 1}\right)\frac{\mathrm{d}H}{C_p T} \tag{2.18}$$

The result indicates that the variation of the gas velocity with heat addition depends critically upon the Mach number of the flow at the point of heat addition. The velocity increases with heat addition for subsonic flow and decreases with heat addition for supersonic flow. This distinction between the behavior of flow at subsonic and supersonic velocities is somewhat reminiscent of that occurring in the behavior of the velocity during a contraction of the channel cross section in isentropic flow.

The pressure variation may be computed directly from the momentum relation as

$$u\,\mathrm{d}u = -\frac{1}{\gamma}a^2\frac{\mathrm{d}p}{p} \tag{2.19}$$

and employing Eq. (2.18) for the velocity variation,

$$\frac{\mathrm{d}p}{p} = +\left(\frac{\gamma M^2}{M^2 - 1}\right)\left(\frac{\mathrm{d}H}{C_p T}\right) \tag{2.20}$$

The addition of heat causes a drop in the gas pressure for subsonic velocities, which becomes progressively more severe as the Mach number approaches unity.

The static temperature is found by writing the logarithmic derivative of the equation of state as

$$\frac{\mathrm{d}T}{T} = \frac{\mathrm{d}p}{p} - \frac{\mathrm{d}\rho}{\rho}$$

Substituting for the terms on the right from the continuity and momentum equations, this gives

$$\frac{\mathrm{d}T}{T} = 1 - \left(\frac{u^2}{RT}\right)\frac{\mathrm{d}u}{u}$$

or, substituting from Eq. (2.18) for the velocity variation,

$$\frac{dT}{T} = \left(\frac{\gamma M^2 - 1}{M^2 - 1}\right)\left(\frac{dH}{C_p T}\right) \tag{2.21}$$

The factor $(\gamma M^2 - 1)/(M^2 - 1)$ exhibits two changes of sign because the numerator and denominator pass through zero at $M^2 = 1/\gamma$ and $M^2 = 1$, respectively. So long as $M^2 < 1/\gamma$, the temperature rises with the addition of heat, which is the trend naturally to be expected. However, as the Mach number increases, but remains in the range $1/\gamma < M^2 < 1$, the temperature decreases as heat is added to the gas, a result that is not at all obvious physically and requires a bit closer investigation. Finally, when $M > 1$, the static temperature again increases with dH, as would be expected.

The energy equation (2.16) indicates the proportion of a heat increment dH appearing as gas enthalpy $C_p dT$ and appearing as kinetic energy of mean motion $u\,du$. Expressing the differentials du and dT in terms of dH and simplifying the result, it is found that

$$\underbrace{\left[\frac{(\gamma - 1)M^2}{1 - M^2}\right]\frac{dH}{C_p T}}_{\substack{\text{increment of} \\ \text{kinetic energy}}} + \underbrace{\left(\frac{1 - \gamma M^2}{1 - M^2}\right)\frac{dH}{C_p T}}_{\substack{\text{increment of} \\ \text{gas enthalpy}}} = \frac{dH}{C_p T} \tag{2.22}$$

so that a portion $[(\gamma - 1)M^2]/(1 - M^2)$ of the added energy dH is devoted to increasing the kinetic energy of the gas, while a portion $(1 - \gamma M^2)/(1 - M^2)$ appears as the enthalpy of the gas. Now clearly, as the Mach number increases, the amount of heat required to supply the kinetic energy increases until, at $M^2 = 1/\gamma$, the entire heat addition is required to supply the kinetic energy alone, with the result that the gas enthalpy cannot change. Further increase of the Mach number increases the kinetic energy requirement even more, so that a portion of it must be furnished by the gas enthalpy itself. As a consequence, the gas temperature decreases.

The situation is clear for supersonic flow. Here, the gas velocity decreases as heat is added, with the result that all of the heat added, plus that resulting from kinetic energy reduction, is available to increase the gas enthalpy. The enthalpy increase is

$$\left[1 + \frac{(\gamma - 1)M^2}{M^2 - 1}\right]dH$$

and hence is in excess of the amount supplied. Note that the ratio of the quantity of heat passing to kinetic energy, to that passing to gas enthalpy, is given by

$$\frac{\text{Kinetic energy increment}}{\text{Gas enthalpy increment}} = \left[\frac{(\gamma - 1)M^2}{1 - \gamma M^2}\right] \tag{2.23}$$

and hence is a function of the Mach number alone.

It is a simple matter now to compute the change of Mach number with heat addition; logarithmic differentiation indicates that

$$\frac{dM}{M} = \frac{du}{u} - \frac{1}{2}\frac{dT}{T}$$

Combining the known values of du/u and dT/T from Eqs. (2.18) and (2.21) the formula for dM/M is simply

$$\frac{dM}{M} = \frac{1}{2}\left(\frac{1+\gamma M^2}{1-M^2}\right)\frac{dH}{C_pT} \tag{2.24}$$

It is clear from Eq. (2.24) that heat addition always brings the flow toward a Mach number of unity, that is, heat addition results in a Mach number increase for subsonic flow and a Mach number decrease for supersonic flow.

The variation of stagnation pressure can now be simply determined by taking the logarithmic derivative of

$$p_t = p\left(1 + \frac{\gamma-1}{2}M^2\right)^{\gamma/(\gamma-1)}$$

and substituting for the appropriate results given above. Then it is found that

$$\frac{dp_t}{p_t} = \left[\frac{(1-\gamma/2)M^2}{1+[(\gamma-1)/2]M^2}\right]\frac{dH}{C_pT}$$

or, more simply,

$$\frac{dp_t}{p_t} = -\left(\frac{\gamma}{2}M^2\right)\left(\frac{dH}{C_pT_t}\right) \tag{2.25}$$

It is evident that the stagnation pressure drops with the heat addition and that the rate depends very strongly on the Mach number at which the heat is added.

The results derived in the previous paragraphs concern heat addition in a constant-area channel. The effect of simultaneous changes in area and total gas enthalpy are also of interest and may be simply derived on the basis of the following considerations. For example, consider the Mach number to be a function of both area and stagnation temperature. Then,

$$dM = \left(\frac{\partial M}{\partial T_t}\right)_A dT_t + \left(\frac{\partial M}{\partial A}\right)_{T_t} dA$$

However, the quantity $(\partial M/\partial T_t)$ is obtained from Eq. (2.24) since the derivative given in the above equation was obtained with the area held fixed.

Thus,

$$\left(\frac{\partial M}{\partial T_t}\right)_A = \left(\frac{M}{T}\right)\left(\frac{1}{2}\right)\left(\frac{1+\gamma M^2}{1-M^2}\right)$$

Similarly, the quantity $(\partial M/\partial A)_{T_t}$ was previously obtained during study of isentropic channel flow, and is given by

$$\left(\frac{\partial M}{\partial A}\right)_{T_t} = \left(\frac{M}{A}\right)\left(-\frac{1-[(\gamma-1)/2]M^2}{1-M^2}\right)$$

Therefore,

$$\frac{dM}{M} = \left(\frac{1}{2}\frac{(1+\gamma M^2)}{(1-M^2)}\right)\left(\frac{dH}{C_pT}\right) + \left(-\frac{1+(\gamma-1)M^2}{1-M^2}\right)\frac{dA}{A}$$

The results for other parameters of interest are

$$\frac{du}{u} = \left(\frac{1}{1-M^2}\right)\frac{dH}{C_pT} + \left(-\frac{1}{1-M^2}\right)\frac{dA}{A}$$

$$\frac{dp}{p} = \left(\frac{-\gamma M^2}{1-M^2}\right)\frac{dH}{C_pT} + \left(\frac{\gamma M^2}{1-M^2}\right)\frac{dA}{A}$$

$$\frac{dT}{T} = \left(\frac{1-\gamma M^2}{1-M^2}\right)\frac{dH}{C_pT} + \left(\frac{(\gamma-1)M^2}{1-M^2}\right)\frac{dA}{A}$$

$$\frac{d\rho}{\rho} = \left(\frac{-1}{1-M^2}\right)\frac{dH}{C_pT} + \left(\frac{M^2}{1-M^2}\right)\frac{dA}{A}$$

$$\frac{dp_t}{p_t} = \left(\frac{-(\gamma/2)M^2}{1+[(\gamma-1)/2]M^2}\right)\frac{dH}{C_pT} = \left(-\frac{\gamma}{2}M^2\right)\frac{dH}{C_pT_t}$$

$$\frac{dT_t}{T_t} = \left(\frac{1}{1+[(\gamma-1)/2]M^2}\right)\frac{dH}{C_pT} = \frac{dH}{C_pT_t} \tag{2.26}$$

Use of these equations makes possible a determination of the local rate of the changes in the various parameters when both heat addition dH and area change dA are made. Note, although, that dM/M, dp/p, dT/T, $d\rho/\rho$ may be held constant by appropriate matching of the variation of dH/C_pT and dA/A. For example, if $dH/C_pT = dA/A$, then the static pressure and velocity remain constant. However, the ratio dp_t/p_t is always finite and negative.

The equations cannot be used in general to obtain algebraic solutions for the flowfield in a duct of specified area variation and heat addition. However, they can be used in numerical calculations.

Integrated relations. The equations for heat addition in *constant-area channel flows* can be integrated to give the changes in the variables of interest occurring when heat is added or the equations for conservation of energy, momentum, and mass can be applied directly across the heat addition zone. The results are

$$\frac{T_{t_2}}{T_{t_1}} = \left(1 + \frac{\Delta H}{C_p T_{t_1}}\right) = \left(\frac{1+\gamma M_1^2}{1+\gamma M_2^2}\right)^2 \left(\frac{1+[(\gamma-1)/2]\,M_2^2}{1+[(\gamma-1)/2]\,M_1^2}\right)\left(\frac{M_2^2}{M_1^2}\right)$$

$$\frac{p_{t_2}}{p_{t_1}} = \left(\frac{1+\gamma M_1^2}{1+\gamma M_2^2}\right)\left(\frac{1+[(\gamma-1)/2]\,M_2^2}{1+[(\gamma-1)/2]\,M_1^2}\right)^{\gamma/(\gamma-1)}$$

$$\frac{u_2}{u_1} = \frac{\rho_1}{\rho_2} = \left(\frac{1+\gamma M_1^2}{1+\gamma M_2^2}\right)\left(\frac{M_2}{M_1}\right)^2$$

$$\frac{p_2}{p_1} = \left(\frac{1+\gamma M_1^2}{1+\gamma M_2^2}\right)$$

$$\frac{T_2}{T_1} = \left(\frac{1+\gamma M_1^2}{1+\gamma M_2^2}\right)^2 \left(\frac{M_2}{M_1}\right)^2 \tag{2.27}$$

These equations are given in terms of M_1 and M_2, whereas in most problems of interest, the heat addition $\Delta H/C_p T_{t_1}$ and M_1 will be the specified quantities. Since elimination of M_2 from the above equations is algebraically complicated, the results will be expressed numerically in order to obtain a directly useful form.

Pick state 1 as the initial condition corresponding to a Mach number M at the start of heat addition in a constant-area duct. Define a second state, denoted by a super *, at which heat addition has been sufficient to drive the Mach number to 1. This state is to be used as a reference condition in a manner analogous to the A^* state (of Sec. 2.19 of *Aerothermodynamics of Gas Turbine and Rocket Propulsion*) of one-dimensional, isentropic, channel flow.

In the above equations, P_{t_1}, for example, becomes P_t, P_{t_2} becomes P_t^*, and M_1 becomes M and M_2 becomes 1.0. Values of p_t/p_t^*, p/p^*, T/T^*, and T_t/T_t^* are given in Table 2.7 as a function of the initial Mach number M and for $\gamma = 1.40$. The variation with γ is small in subsonic regions, but becomes important when $M > 1.5$. Also note the rapid increase in p_t/p_t^* for supersonic speeds.

Table 2.7 or a plot may be used to obtain solutions of problems involving uniform heat addition in a channel of constant cross section. Note that the

Table 2.7 Frictionless, Constant-Area Flow with Change in Stagnation Temperature (perfect gas, $\gamma = 1.4$ exactly)

M	T_t/T_t^*	T/T^*	p/p^*	p_t/p_t^*	M	T_t/T_t^*	T/T^*	p/p^*	p_t/p_t^*
0.02	0.00192	0.00230	2.3987	1.2675	0.62	0.83982	0.93585	1.5603	1.06821
0.04	0.00765	0.00917	2.3946	1.2665	0.64	0.86920	0.95298	1.5253	1.06146
0.06	0.01712	0.02053	2.3880	1.2647	0.66	0.87709	0.96816	1.4908	1.05502
0.08	0.03021	0.03621	2.3787	1.2623	0.68	0.89350	0.98144	1.4569	1.04890
0.10	0.04678	0.05602	2.3669	1.2591	0.70	0.90850	0.99289	1.4235	1.04310
0.12	0.06661	0.07970	2.3526	1.2554	0.72	0.92212	1.00260	1.3907	1.03764
0.14	0.08947	0.10695	2.3359	1.2510	0.74	0.93442	1.01062	1.3585	1.03253
0.16	0.11511	0.13843	2.3170	1.2461	0.76	0.94546	1.01706	1.3270	1.02776
0.18	0.14324	0.17078	2.2959	1.2406	0.78	0.95528	1.02198	1.2961	1.02337
0.20	0.17355	0.20661	2.2727	1.2346	0.80	0.96394	1.02548	1.2658	1.01934
0.22	0.20574	0.24452	2.2477	1.2281	0.82	0.97152	1.02763	1.2362	1.01569
0.24	0.23948	0.28411	2.2209	1.2213	0.84	0.97807	1.02853	1.2073	1.01240
0.26	0.27446	0.32496	2.1925	1.2140	0.86	0.98363	1.02826	1.1791	1.00951
0.28	0.31035	0.36667	2.1626	1.2064	0.88	0.98828	1.02690	1.1515	1.00698
0.30	0.34686	0.40887	2.1314	1.1985	0.90	0.99207	1.02451	1.1246	1.00485
0.32	0.38369	0.45119	2.0991	1.1904	0.92	0.99506	1.02120	1.09842	1.00310
0.34	0.42057	0.49327	2.0647	1.1821	0.94	0.99729	1.01702	1.07285	1.00174
0.36	0.45723	0.53482	2.0314	1.1737	0.96	0.99883	1.01205	1.04792	1.00077
0.38	0.49346	0.57553	1.9964	1.1652	0.98	0.99972	1.00636	1.02364	1.00019
0.40	0.52903	0.61515	1.9608	1.1566	1.00	1.00000	1.00000	1.00000	1.00000
0.42	0.56376	0.65345	1.9247	1.1480	1.10	0.99392	0.96031	0.89086	1.00486
0.44	0.59748	0.69025	1.8882	1.1394	1.20	0.97872	0.91185	0.79576	1.01941
0.46	0.63007	0.72538	1.8515	1.1308	1.30	0.95798	0.85917	0.71301	1.04365
0.48	0.66139	0.75871	1.8147	1.1224	1.40	0.93425	0.80540	0.64102	1.07765
0.50	0.69136	0.79012	1.7778	1.1140	1.50	0.90928	0.75250	0.57831	1.1215
0.52	0.71990	0.81955	1.7410	1.1059	2.00	0.79339	0.52893	0.36364	1.5031
0.54	0.74695	0.84695	1.7043	1.0979	2.50	0.71005	0.37870	0.24616	2.2218
0.56	0.77248	0.87227	1.6678	1.09010	3.00	0.65398	0.28028	0.17647	3.4244
0.58	0.79647	0.89552	1.6316	1.08255	3.50	0.61580	0.21419	0.13223	5.3280
0.60	0.81892	0.91670	1.5957	1.07525	4.00	0.58909	0.16831	0.10256	8.2268
					4.50	0.56983	0.13540	0.08277	12.502
					5.00	0.55555	0.11111	0.06667	18.634

starred quantities are functions of the initial conditions, e.g., $T_t^* = T_t^*\{M_0, T_{t_0}, \gamma\}$, and hence vary in magnitude as M_0 and T_{t_0} are changed. The tabulated values can be used in the following manner. Assume the conditions at the inlet and total temperature ratio across the burner τ_b are given. Then,

$$\tau_b = \frac{T_{t_3}}{T_{t_2}} = \frac{T_{t_3}}{T_{t_3}^*}\frac{T_{t_3}^*}{T_{t_2}^*}\frac{T_{t_2}^*}{T_{t_2}}$$

Since a constant-area burner with constant mass flow is used,

$$T_{t_3}^* = T_{t_2}^* = T_t^*$$

and

$$\frac{T_{t_3}}{T_t^*} = \tau_b \frac{T_{t_2}}{T_t^*}$$

But if M_2 is specified, T_{t_2}/T_t^* can be found from the table and consequently T_{t_3}/T_t^* can be evaluated. Given this result, the other properties at state 3 can be determined. Consider a few examples.

Example 2.1

Letting $M_1 = 0.2$, how much heat can be added to the flow if heat addition is limited by choking the flow? Since the final Mach number is 1, $T_{t_{\max}} = T_t^*$, and from Table 2.4,

$$T_t^*/T_t = (1/0.17355) = 5.8$$

Thus, the total temperature of the flow may be increased by a factor of 5.8. The total pressure ratio across the area of heat addition is

$$(p_t^*/p_t) = (1/1.2346) = 0.81$$

Example 2.2

To determine the Mach number change and stagnation pressure ratio across a combustion chamber when $M_2 = 0.2$ and $T_{t_3}/T_{t_2} = 4$, let

$$\frac{T_{t_3}}{T_{t_2}} = \left(\frac{T_{t_3}}{T_t^*}\right)\left(\frac{T_t^*}{T_{t_2}}\right) = 4$$

and

$$\frac{T_{t_3}}{T_t^*} = \frac{T_{t_2}}{T_t^*} \times 4 = 0.17355 \times 4 = 0.695$$

The Mach number corresponding to this value of T_t/T_t^* is 0.50. Consequently, $M_3 = 0.50$, and

$$\frac{p_{t_3}}{p_{t_2}} = \left(\frac{p_{t_3}}{p_t^*}\right)\left(\frac{p_t^*}{p_{t_2}}\right) = \frac{1.114}{1.235} = 0.90$$

Example 2.3

The total temperature of a stream is to be increased by 50% and the total pressure loss compared if the heat is added at Mach 3.0 and 0.3. For the high Mach number case,

$$T_{t_3}/T_{t_2} = 1.5$$

therefore,

$$T_{t_3}/T_t^* = 1.5 \times 0.654 = 0.98 \quad \text{and} \quad M_3 = 1.15$$

Then,

$$\frac{p_{t_3}}{p_{t_2}} = \frac{p_{t_3}/p_t^*}{p_{t_2}/p_t^*} = \frac{1.01}{3.42} = 0.296$$

For the low Mach number case,

$$M_3 = 0.40 \quad \text{and} \quad \frac{p_{t_3}}{p_{t_2}} = \frac{1.16}{1.20} = 0.97$$

Obviously, supersonic heat addition causes a much greater reduction in total pressure.

Thermal choking. If the heat addition for example 2.1 had been greater than $(4.8T_{t_1})$, the tables give no solution. This is a result of the fact that as heat is added to a subsonic flow of constant cross-sectional area, the Mach number approaches unity. If more heat is added, the Mach number at the channel exit will remain at the value unity, but the upstream boundary condition must change so that the ratio $[T_{t_1}/T_t^*\{M_1\}]$ corresponds to the actual head addition. For example, if heat addition in example 2.1 had been $(5.32)T_{t_1}$, then $T_t^* = T_{t_1} + (5.32)T_{t_1}$, or $T_{t_1}/T_t^* = 1/6.32 = 0.158$, and the value of M_1 would drop from 0.2 to 0.19.

Two-Dimensional Heat Addition Calculations

The effect on the flow parameters of the heat addition from a spreading flame in a constant-cross-section duct will be calculated in this section. Although the calculations are idealized, they give a more realistic picture of

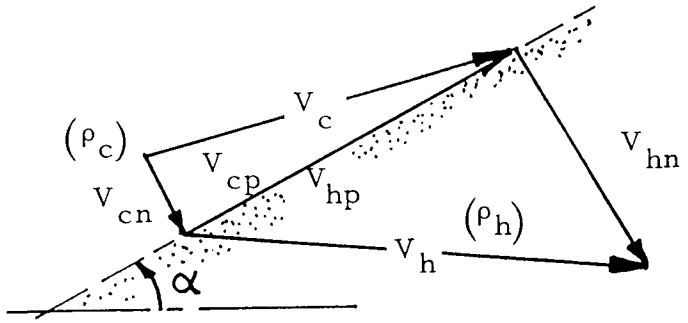

Fig. 2.24 Velocity change across an infinitely thin flame.

heat addition than the one-dimensional calculation described above. After a brief description of the flow across a flame sheet, the heat addition at a thin flame spreading across a constant-area duct will be analyzed, along with the effects of the flameholder and the compressibility. Finally, problems involved with the calculation of the flame geometry are outlined briefly.

Flow across a flame sheet. Before examining the geometric spreading of a flame in a duct, it is interesting to examine the processes occurring at a flame front. Consider Fig. 2.24. Unburned gas with velocity V_c approaches the flame front, making a small angle α with respect to the axis of the combustion chamber. After passing through the flame, the velocity is V_h and the density ρ_h. Subscripts n and p denote components of velocity normal and parallel to the flame. The continuity equation and the two momentum equations can be applied to determine the relationship of the vector components and the static pressure. Consider an incompressible flow and replace the energy equation with the statement that the density ratio $\lambda = \rho_h/\rho_c$ is a given quantity. The three equations are

$$\rho_c V_{cn} = \rho_h V_{hn}$$

$$\rho_c V_{cn}^2 + P_c = \rho_h V_{hn}^2 + P_h$$

$$(\rho_c V_{cn}) V_{cp} = (\rho_h V_{hn}) V_{hp}$$

These equations can be manipulated to give

$$V_{hn}/V_{cn} = \rho_c/\rho_h = 1/\lambda$$

$$V_{cp} = V_{hp}$$

$$(P_c - P_h)/\rho_c V_c^2 = (V_{cn}/V_c)^2[(1/\lambda) - 1] \qquad (2.28)$$

The total pressure loss can be written as

$$\frac{P_{ct} - P_{ht}}{\frac{1}{2}\rho_c V_c^2} = \left(\frac{V_p}{V_c}\right)^2 (1 - \lambda) + \left(\frac{V_{cn}}{V_c}\right)^2 \left(\frac{1}{\lambda} - 1\right) \tag{2.29}$$

The major problem arising in computing flame spreading is that the values of the normal velocity of the cold stream cannot be predicted accurately. However, some idea of the order of magnitude of the static pressure difference can be obtained by selecting a value for λ, say 0.25, and using the value of 0.025 for V_{cn}/V_c. (The latter value is that determined from experimental data in the above subsection on spreading rates, where the velocity ratio was called β or u_n/V.) With these assumptions, the pressure jump is less than 2×10^{-3} of the dynamic pressure in the cold gas. If a laminar flame speed were used, V_{cn}/V_c would be even smaller for conditions of interest. Hence, it is justified to ignore the effects of the pressure rise on the flowfield and to assume that the static pressure across the entire duct is constant for the afterburner flowfield. [However, if one is interested in laminar flame shapes, $(V_{cn}/V_c)^2$ may be made as large as necessary and the pressure difference clearly cannot be ignored.]

In addition, when $V_{cn} \ll V_c$, the magnitudes of the velocity vectors V_c and V_h will be approximately equal to the parallel velocity component and hence they will be equal. That is, $V_c \approx V_{cp} \equiv V_{ch} \approx V_h$. The total pressure change [see Eq. (2.29)] reduces to $(1 - \lambda)$ or $(1 - \rho_h/\rho_c)$ and is produced by the change in the density due to heat addition. Hence, the velocity and pressure jumps that occur at the flame front are often negligibly small. Given these results, the velocity profile chosen for the following study and the assumption that pressure depends only on axial position are reasonable.

Idealized flame spread. The effects of adding heat to a one-dimensional compressible flow in a constant-area duct have been discussed above. Here, the effect on the flow of heat addition by a flame spreading from the center of a constant-area duct will be investigated.

To simplify the analysis, first consider a flame developing in a two-dimensional flow of an incompressible gas. Because the entrainment rate of a turbulent flame is not known, the pressure drop, velocity profile, and width between flame fronts must be described as functions of the fraction of the gas that has been burned. Even though the distance required to obtain complete combustion cannot be obtained from this analysis, the total pressure loss, flow acceleration, and a rough idea of the resulting velocity profile can be obtained. The approach used here is taken from that of Tsien[25] whose work was based on profiles suggested by the experiments and calculations of Williams et al.[19]

Tsien proceeded by using an integral approach. He specified the shape of the velocity profile in terms of the width of the burned region W and two velocity parameters. These unknown parameters and a pressure parameter were found as functions of the fraction of the mass flow that is burned at

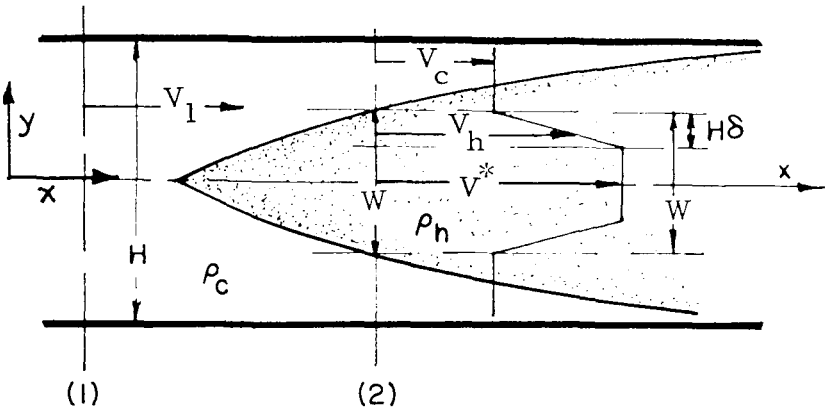

Fig. 2.25 Notation for ideal flame spread calculation.

any station by use of integrated forms of the continuity equation and the Bernoulli relationship applied to the burned and unburned streams. A similar approach is used here, but a momentum equation is applied in place of the Bernoulli equations for the burned gas and the velocity distribution is slightly more complex. Since the burned gas flow is rotational, this appears to be a more satisfactory approximation. The notation and velocity distribution are identified in Fig. 2.25.

A trapezoidal velocity profile is shown in this figure. The axial velocity V_c in the unburned gas is constant at any x station; the velocity in the burned gas rises linearly from V_c to V^* over a distance $H\delta$ at the edge of the flame and is constant with a value V^* over the central region of the burned gas. The static pressure P is assumed to be a function of axial position x alone and the heat addition at the flame is taken into account by specifying that the burned stream density ρ_h is constant and is given by $\lambda\rho_c$. The y component of velocity is ignored.

Continuity and momentum equations are

$$\rho_c V_1 H = 2\left(\int_0^{H/2} (\rho V \mathrm{d}y)\right) = \dot{m}_1 \tag{2.30}$$

$$(P_1 - P)H = 2\left(\int_0^{H/2} \rho V^2 \mathrm{d}y\right) - \dot{m}_1 V_1 \tag{2.31}$$

Here subscript 1 refers to conditions for upstream of the flame. The Bernoulli equation for the unburned stream is

$$\tfrac{1}{2}\rho_c V_1^2 + P_1 = \tfrac{1}{2}\rho_c V^2 + P \tag{2.32}$$

The fraction burned is

$$f \equiv \left(2\int_0^{W/2} \rho V \mathrm{d}y\right) / \dot{m}_1 \tag{2.33}$$

where $\dot{m}$ is total mass flow rate, $\rho_1 V_1 H$. The trapezoidal velocity profile is

$$V = V_c,\ W/2 \le y \le H/2$$

$$V = \left[V_c + (V^* - V_c)\left(\frac{W}{2} - y \right) \Big/ H\delta \right]$$

$$(W/2 - H\delta) \le y \le (W/2)$$

$$V = V^*,\ 0 \le y \le (W/2 - H\delta) \tag{2.34}$$

The unknowns are f, W, V_c, V^*, and P. Since there are four equations, it is possible to solve for four of them, say V_c, V^*, f, and P, as a function of the fifth, the width W. The parameter δ is treated as a fixed fraction of duct height H and must be specified. It is included here so that the effect of the velocity profile shape on the other parameters can be examined.

The solution of the four algebraic equations resulting from the substitution of the velocity profiles assumed here in Eqs. (2.30–2.33) is straightforward and can be expressed in terms of dimensionless parameters defined as

$$\psi \equiv (P_1 - P)/\tfrac{1}{2}\rho_c V_1^2$$

$$\bar{u} \equiv V_c/V_1$$

$$\bar{u}^* \equiv V^*/V_1$$

$$\eta = W/H$$

$$\lambda = \rho_h/\rho_c$$

$$f = \text{fraction burned} \tag{2.35}$$

The solutions are

$$\psi = (\bar{u}^2 - 1)$$

$$f = [1 - \bar{u}(1 - \eta)]$$

and a pair of equations for $\bar{u}$ and $\bar{u}^*$,

$$\bar{u}(1 + \lambda\delta - \eta) + \bar{u}^*(\eta - \delta)\lambda - 1 = 0$$

$$\bar{u}^2\left(\tfrac{1}{2} + \tfrac{2}{3}\lambda\delta - \eta\right) + \bar{u}^*\left[\eta - \left(\tfrac{4}{3}\right)\delta\right]\lambda$$

$$+ \left(\tfrac{2}{3}\right)\bar{u}^*\bar{u}(\delta\lambda) - \tfrac{1}{2} = 0$$

Numerical solutions are found by specifying values for δ and λ and calculating values of $\bar{u}$, $\bar{u}^*$, and f from the above equations for various

Table 2.8 Dependence of Flame Spread Parameters on Dimensionless Flame Width η for $\lambda = 0.25$ and $\delta = 0.1$

η	f	ψ	$\bar{u}$	$\bar{u}^*$
0.2	0.07	0.36	1.17	1.55
0.3	0.12	0.59	1.26	1.69
0.4	0.18	0.89	1.37	1.88
0.5	0.25	1.3	1.50	2.11
0.6	0.34	1.7	1.65	2.38
0.7	0.45	2.4	1.83	2.70
0.8	0.59	3.2	2.05	3.08
0.9	0.76	4.4	2.31	3.55
1.0	1.0	6.1	2.66	4.15

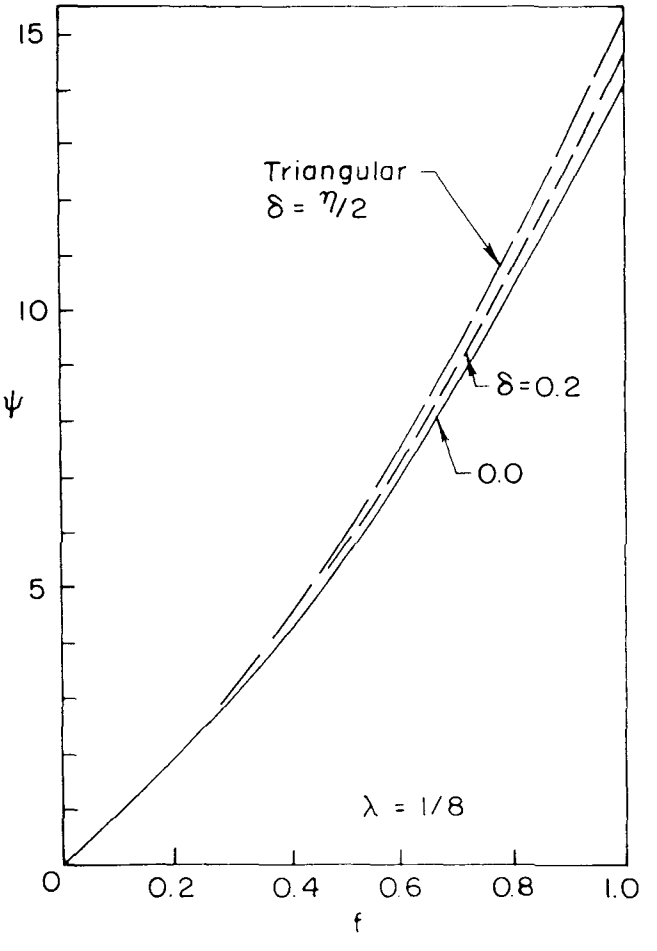

Fig. 2.26 Dependence of normalized pressure ψ on fraction burned and hot steam profile parameter.

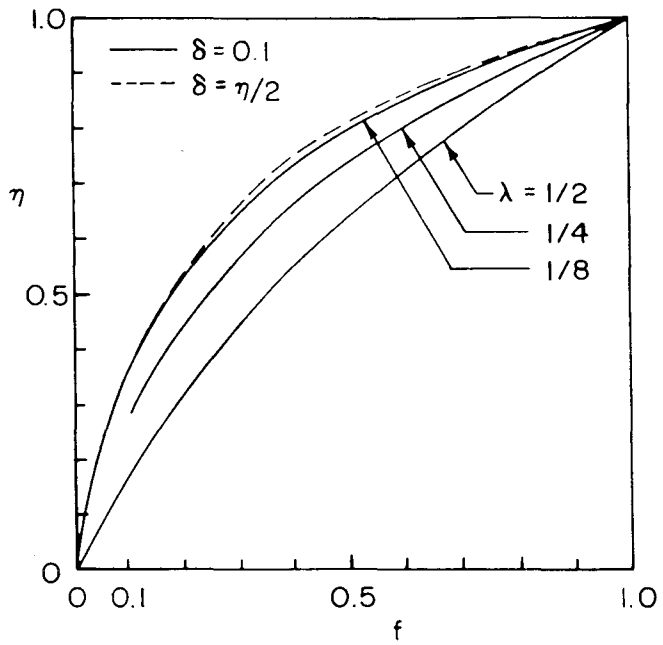

Fig. 2.27 Dependence of normalized width of flame on fraction burned with density ratio as a parameter.

values of η. Table 2.8 presents numerical examples to illustrate the variation of the parameters for the conditions that $\rho_h/\rho_c = 0.25$ and $\delta = 0.1$.

Note that the fraction burned does not reach 50% until the flame width is about 75% of the duct height and that both the cold and hot streams have large velocity changes. The velocity increase for the simple one-dimensional case is just $1/\lambda$ or 4.0 for the incompressible when $\delta = 0$. The total pressure change along the central streamline for this incompressible case is

$$\Delta P_t / \tfrac{1}{2}\rho_c V_1^2 = -\left(1 + \psi - \lambda(\bar{u}^*)^2\right)$$

The dependence of the parameters on f is shown in Figs. 2.26–2.30 with λ and δ as parameters. Consider first the effect of changing the profile parameter δ. Remember that $\delta = 0$ corresponds to a square velocity profile with all the burned fluid moving with speed V^* and that the $\delta = \eta/2$ corresponds to a triangular profile with a linear change from velocity V_c at the flame front to V^* on the axis.

The dependence of the pressure drop on fraction burned is shown in Fig. 2.26 with δ as a parameter. The pressure drop is almost independent of δ for this example and similar results were obtained for values of the density ratio λ between $\frac{1}{8}$ and $\frac{1}{2}$. A similar result is obtained for the cold stream velocity $\bar{u}$ and wake width η; the examples shown in Figs. 2.27 and 2.28 for $\delta = 0.1$ are representative for all δ values. The velocity profile shape factor δ was found to have very little effect on these parameters, so it can be concluded that the predicted relationships between burned gas wake width ηH, the cold stream velocity V_c/V_1, and the fraction burned f will be reasonably accurate regardless of the real velocity profile in the burned

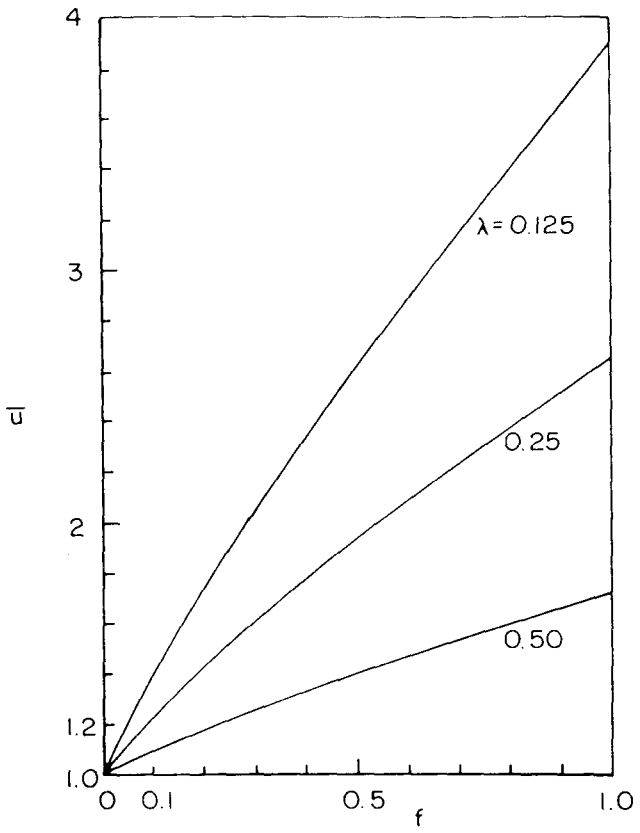

Fig. 2.28 Dependence of cold stream velocity ratio on fraction burned with density ratio as a parameter.

stream. Of course, the choice of profile parameter will have a large effect on the value of the maximum velocity in the hot stream. An example of this dependence is shown in Fig. 2.29 for $\lambda = \frac{1}{8}$ and in Fig. 2.30 for all λs and small δ values.

The strong dependence of ψ and $\bar{u}$ on density ratio is to be expected because the density change fixes the fluid acceleration. The weak dependence of $\eta\{f\}$ on λ is more surprising. An appreciable change in λ (see Fig. 2.27) would produce only a few percent change in the fraction burned. For example, when λ is changed from $\frac{1}{8}$ to $\frac{1}{6}$, values of f corresponding to $\eta = 0.4$ change from 0.12 to 0.15 and values of f corresponding to $\eta = 0.7$ change from 0.37 to 0.39.

Comparison of Figs. 2.28 and 2.29 for $\lambda = 8$ and $\delta = 0.1$ shows the rapid acceleration of the hot gas as compared with the unburned stream. The gas speed on the centerline is always greater than the cold flow.

Effect of flameholder. This type of calculation can be easily extended to include the effects of the flameholder and recirculation zone on the flame spreading calculation. For example, consider the flow shown schematically in Fig. 2.31. The simple triangular velocity profile will be used with the

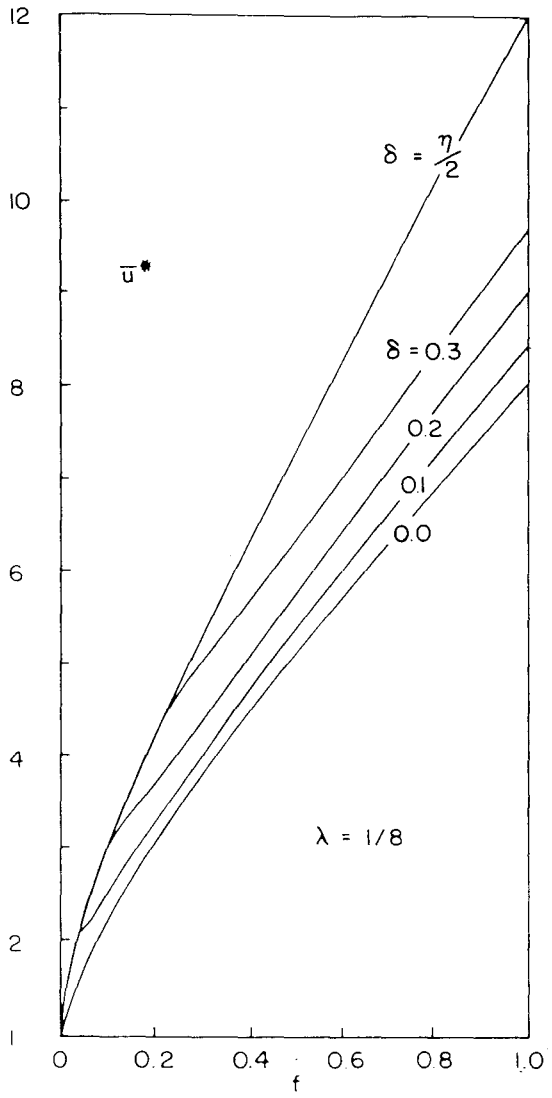

Fig. 2.29 Dependence of hot stream central velocity on fraction burned and velocity profile parameter.

additional assumption that the velocity on the centerline of the flow and at the downstream end of the recirculation zone (station 2) is zero. This approximation is a reasonable one since this point corresponds to the rear stagnation point of the recirculation zone.

Conditions at station 2 are specified when the wake width there, $\eta_2 H$, and density ratio λ are chosen. Combining the continuity and Bernoulli equations for the unburned flow results in

$$\bar{u}_2 = 1/[1 - \eta_2(1 - \lambda/2)]$$

$$f_2 = (\tfrac{1}{2}\lambda)\eta_2 \bar{u}_2$$

$$(P_1 - P_2)/\tfrac{1}{2}\rho_c V_1^2 = (\bar{u}_2)^2 - 1 = \psi_2$$

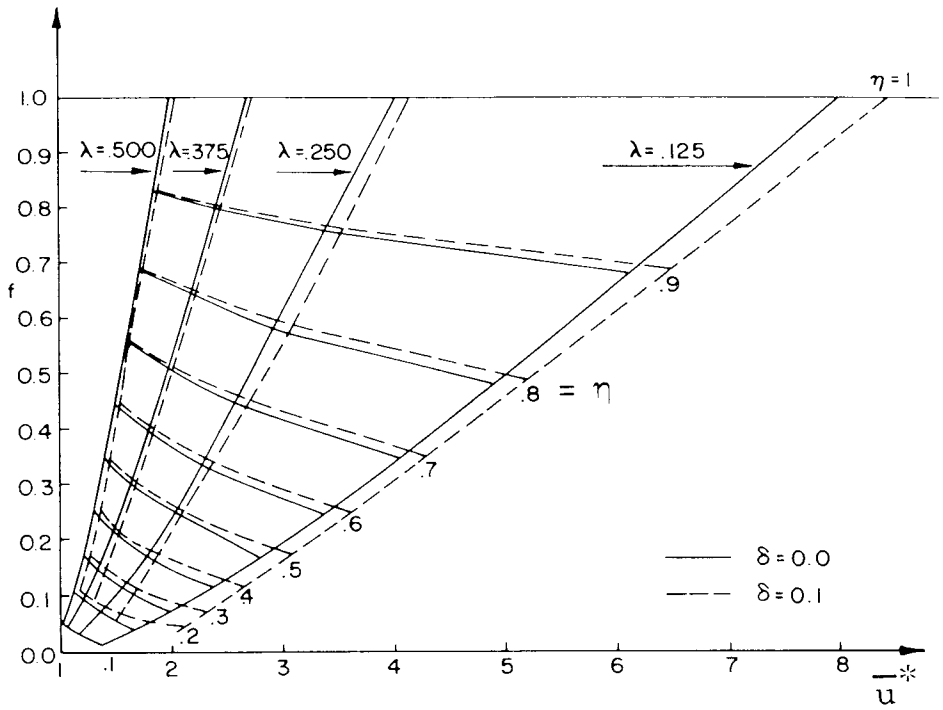

Fig. 2.30 Dependence of hot stream central velocity on fraction burned with density ratio λ and velocity profile factor δ as parameters.

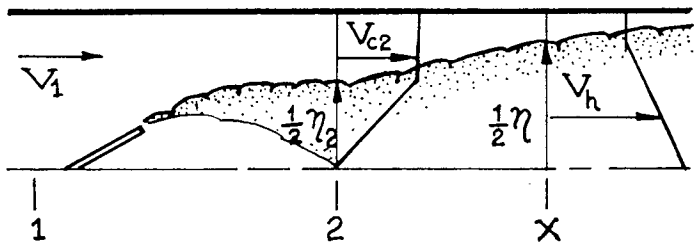

Fig. 2.31 Spreading flame with flameholding region.

Conditions at an arbitrary point downstream of station 2 can be calculated by an analysis identical to that described above. Tabulated values are shown in Table 2.9 for $\lambda = 0.25$ and as a function of η_2, the flame width at station 2. Here f_2, $\bar{u}_2$, and ψ_2 are the fraction burned, cold stream velocity ratio, and normalized pressure difference at station 2, respectively, and $\bar{u}_3$ and $\bar{u}_3^*$ are the cold stream and centerline values of the gas speeds at station 3 where the fraction burned is 1. When $\eta_2 \equiv 0$, this solution reduces to that described above for the triangular velocity profile. Values of $\bar{u}$ and η are presented in Figs. 2.32 and 2.33 as functions of the fraction burned with $\lambda = 0.25$.

Table 2.9 Dependence of Conditions at Station 3, Where $f = 1$ on Recirculation Zone Width η_2 for $\delta = \eta/2$ and $\lambda = \frac{1}{4}$

η_2	f_2	$\bar{u}_2$	ψ_2	$\bar{u}_3$	$\bar{u}_3^*$	ψ_3
0.0	0.0	1.00	0.0	2.69	5.30	6.28
0.2	0.04	1.21	0.46	2.70	5.28	6.32
0.4	0.08	1.54	1.37	2.75	5.24	6.64
0.5	0.11	1.78	2.17	2.82	5.18	6.99

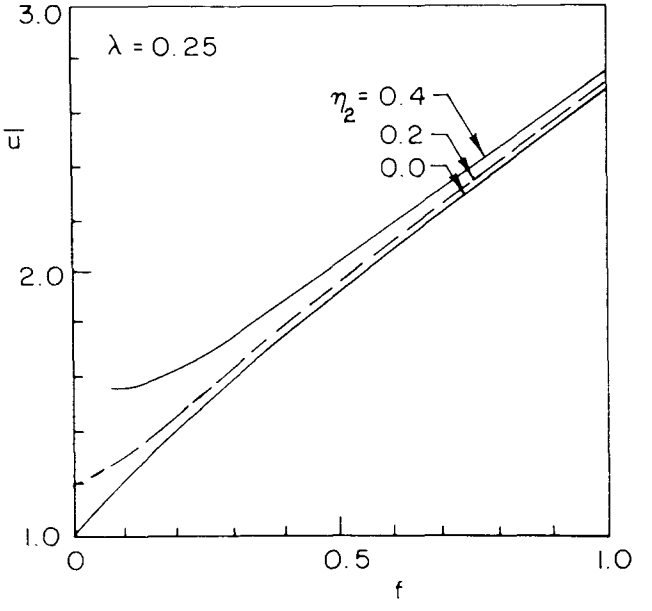

Fig. 2.32 Dependence of $\bar{u} \equiv V_c/V_1$ on fraction burned f and flame width at recirculation zone.

At low values of f, the present solutions differ appreciably from the simple $\eta_2 = 0$ case. However, for values of the fraction burned greater than about $\frac{1}{3}$, the solutions are insensitive to η_2. Hence, the overall pressure drop and acceleration of the burned stream at station 3, where the flow is completely burned, can be estimated with reasonable accuracy from the simple $\eta_2 = 0$ case. Changing η_2 in this example corresponds to changing the wake width and, hence, to increasing the flameholder size in a duct of constant height. This calculation suggests that flameholder size or blockage effects will not be very strong when η is greater than $(1.5\ \eta_2)$. Also note in Table 2.9 that, despite very large differences in the pressure coefficient ψ_2 at station 2, differences in values of ψ_3 are no more than 10%. The dependence in $\eta\{f\}$ on η_2 is even weaker.

This analysis indicates that flameholder blockage effects will not be large.

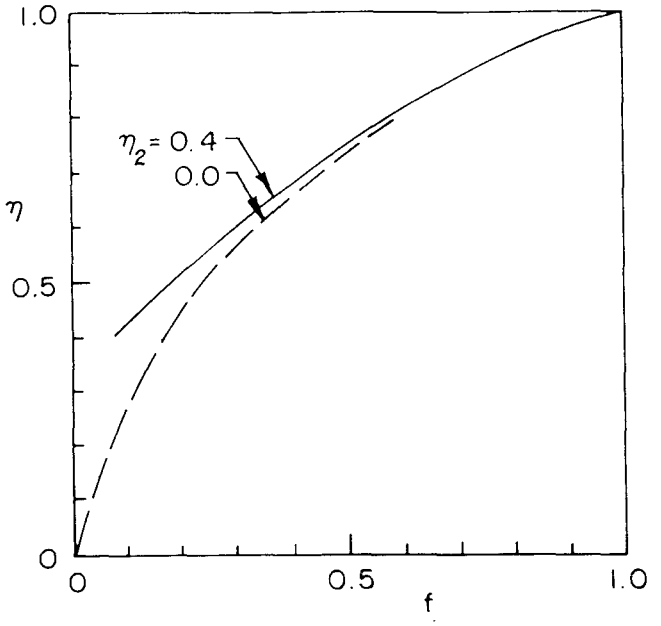

Fig. 2.33 Dependence of flame width η on fraction burned f and flame width at recirculation zone η_2.

Effect of compressibility. Tsien[25] carried out the calculation for the triangular velocity profile discussed above. He also extended the calculation to include compressible flows in which density changes in the unburned flow must be considered. The assumption is made that the density $\rho_h\{x\}$ in the burned region at position x is uniform and equal to $\lambda(\rho_c\{x\})$, where λ is a constant.

Values of the parameters for the spreading flame discussed above were calculated for the triangular velocity profile. The dependence of the width of the burned region η on the fraction burned f is almost identical to that obtained here for the incompressible case as long as no choking occurs.

For large enough values of the approach stream Mach number M_1, Tsien's solutions do not reach $\eta = f = 1$, but reverse themselves. These solutions are inadmissible and it is assumed that the smallest value of M_1 at which this behavior is observed corresponds to the "choking" limit. Values of the critical inlet Mach number for the "choked" flow, M_{1c}, were calculated by this technique and are compared in Table 2.10 with values found in the above subsection for the inlet Mach number required to choke the flow for one-dimensional heat addition.

The density ratio λ in the two-dimensional treatment presented here is the density ratio across the flame (or the temperature ratio since the static pressure change across the flame front is small). Critical Mach numbers are given in Table 2.10 for both the static and total temperature ratios across the one-dimensional heat addition region described earlier. There is little difference between these two nor between the one- and two-dimensional

Table 2.10 Comparison of Critical Mach Numbers Calculated by One- and Two-Dimensional Techniques[a]

$1/\lambda$	$(M_{1c})_{2D}$ $(\lambda \equiv T_1/T_2)$	$(M_{1c})_{1D}$ $(\lambda \equiv T_1/T_2)$	$(M_{1c})_{1D}$ $(\lambda \equiv T_{t_1}/T_{t_2})$
2	0.36	0.34	0.38
2.67	0.29	0.29	0.32
4	0.22	0.22	0.25
8	0.13	0.15	0.17

[a]Air with $\gamma = 1.40$.

results. Hence, the one-dimensional calculation gives as good an approximation of choking as the more complex two-dimensional one.

A number of other calculations of this type have been made (e.g., Fabri et al.[26]) and they also lead to predicted values of the critical Mach numbers that are close to the one-dimensional values.

Another parameter of interest is the total pressure loss associated with the heat addition. Calculations based on the two-dimensional incompressible model discussed above predict mass-averaged values of the total pressure ratio across the burner that are a few percent higher than the one-dimensional values when the triangular velocity profile was used in the calculation. Again, the simple one-dimensional heat addition calculation appears to give satisfactory estimates.

Burning rate. The ideas developed in several of the preceding paragraphs can be used to illustrate the problems associated with calculating the position of the flame front in a duct. Consider the flow shown in Fig. 2.24 to be a small part of the spreading flame shown in Fig. 2.25. Let the mass flux in the burned flow be $\dot{m}_b$ and total mass flux be $m_1 = \rho_c V_1 H$. Then, the continuity of mass requires that

$$\frac{d(\dot{m}_b)}{dx} = 2\left(\frac{\rho_c V_{cn}}{\cos\alpha}\right)$$

where the $(1/\cos\alpha)$ term enters because the flame front length corresponding to the length dx is $dx/\cos\alpha$ and the factor 2 because there are two flame fronts. The fraction burned f has been defined as $\dot{m}_b/\dot{m}_1$ [see Eq. (2.35)] and thus the above equation becomes

$$\frac{df}{dx} = \left(\frac{V_{cn}}{V_1}\right)\left(\frac{2}{\cos\alpha}\right)\left(\frac{1}{H}\right) \tag{2.36}$$

In order to proceed further in a simple way, some other approximations must be used. One reasonable one is that α is small enough so that $\cos\alpha$ is approximately 1. With this approximation, the effects of flame shape on f are removed from the calculation.

In addition, information concerning the normal velocity component must be supplied. If the flow is laminar (an unlikely event for afterburners), then V_{cn} = laminar flame speed = S is a reasonable supposition. Then

$$\frac{df}{dx} = \frac{2S}{V_1 H}$$

and integration with the assumption that S is constant gives

$$f = (2S/V_1 H)x\{f\}$$

Defining the position at which the combustion is complete, i.e., at $f = 1$, as $x\{1\}$ results in

$$x\{1\}/H = V_1/2S$$

Thus, as the initial velocity V_1 increases or the flame speed S decreases, the length required for complete combustion will increase. Also, the fraction burned at any station x will decrease under these same circumstances.

If the flow is turbulent, other approaches to describe V_{cn} must be developed. As an illustrative example, consider the combustion region at the edge of the flame as a turbulent mixing layer with unburned gas of density ρ_c and velocity V_c on one side and hot combustion products of density ρ_h and velocity V_h on the other. Entrainment rates in shear layers have been the subject of considerable study and the conventional wisdom is that entrainment rates scale as the velocity difference or as $(V_h - V_c)$ in this example. Studies by Brown[27] and Brown and Roshko[18] of shear layers with large density differences (e.g., large differences in ρ_h and ρ_c) have led to an appreciation of the importance of large-scale structures in the mixing region and the influence of the density ratio in fixing the entrainment rates. Brown suggests that the entrainment velocity from the cold stream could be expressed as

$$V_{cn}/V_c \approx 0.18\left[(\bar{u}^*/\bar{u}) - 1\right]\left[1 + (1/\lambda)^{1/2}\right]$$

Direct use of Brown's suggestion leads to entrainment rates that are within a factor of two to three of those presented above in Table 2.10 for mixing layer experiments in which the density and velocity ratios are similar to those in the combustion experiments discussed above.

The axial pressure gradients and the complicated flow at the duct centerline are certainly not anticipated by Brown's model and may be responsible for the differences. Errors in determining the experimental values for entrainment rates may also be responsible.

Finally, part of this difference may also be associated with the definition used to determine the flame front and with the effects of combustion on the mixing process. The similarities of the processes of entrainment with and without combustion appear to be large and indicate that approaching the determination of turbulent flame speeds or entrainment rates from this point of view will be useful.

Despite differences, it is interesting to calculate spreading rates when entrainment rates are given by an ad hoc expression of the form

$$\beta = V_{cn}/V_c = (0.03)\left[(\bar{u}^*/\bar{u}) - 1\right] \tag{2.37}$$

where

$$\bar{u}^* = (V_h^*/V_1) \quad \text{and} \quad \bar{u} = (V_c/V_1)$$

The dependence on density is ignored here and the constant 0.03 was picked to give values of β of 0.025 that were observed experimentally for $\lambda = \frac{1}{8}$. If this suggestion is followed, Eq. (2.36) can be usefully rewritten as

$$\frac{df}{dx} = 2\left(\frac{V_{cn}}{V_c}\right)\left(\frac{V_c}{V_1}\right)\left(\frac{1}{H}\right) = 2\left(\frac{V_{cn}}{V_c}\right)\frac{\bar{u}}{H}$$

where $\bar{u} = (V_c/V_1)$ is the function of f and the density parameter λ determined in preceding paragraphs. Integration gives

$$\frac{2x\{f\}}{H} = \int_0^f \frac{df}{\left(\beta\{\bar{u}^*/\bar{u}\}\right)\bar{u}\{f,\lambda\}} \tag{2.38}$$

This form is convenient since the ratio $\bar{u}^*/\bar{u}$ appearing in the expression for β is a very weak function of f.

The results of carrying out the integration are presented in Table 2.11, where the changes in several parameters are shown as $\eta = W/H$ increases from 0.2 to 1.0 for $\lambda = \frac{1}{8}$ and $\delta = 0.10$. The orders of magnitude for values of x determined here agree roughly with experimental values for $0 \leq \eta \leq 0.4$. Solutions of this type show a strong dependence on the density ratio. This dependence arises because both $\bar{u}^*/\bar{u}$ and $\bar{u}$ decrease as the density ratio

Table 2.11 Variation of Spreading Parameters with Dimensionless Flame Width

η for $\lambda = \frac{1}{8}$ and $\delta = 0.1$

η	f	$\bar{u}^*/\bar{u}$	β	x/H
0.2	0.04	1.73	0.022	0.9
0.4	0.12	1.80	0.023	2.2
0.6	0.25	1.93	0.024	2.7
0.8	0.49	2.05	0.027	5.4
1.0	1.00	2.16	0.029	7.8

increases. It can be seen from Eqs. (2.37) and (2.38) that these changes cause $x\{f\}/H$ and $x\{W/H\}/H$ to increase. However, experimental results indicate that, for the range of values of W/H and f examined experimentally, the dependence of the flame geometry on the density ratio is very small.

This discrepancy can be eliminated by replacing the constant 0.03 appearing in the definition for β [Eq. (2.37)] by a function of λ. However, currently there is no rational explanation for this dependence, although the work of Brown[27] indicates that β does depend on λ in a mixing layer.

The preceding calculation is indicative of the types of simple approaches used in calculating the geometric features of turbulent flames. Calculations of this type cannot be taken very seriously until the dependence of V_{cn} or β on the density ratio, turbulence level, flame width, etc., has been established.

Other more ambitious schemes have been developed to calculate the complete flowfield. For example, the calculations of Spalding[28] are based on a general model for computing turbulent flows. A set of differential equations is developed in an ad hoc manner from which turbulent transport parameters can be determined as part of the general solution of the equations of motion. Combustion phenomena are included by assuming infinitely fast reaction rates when the premixed fuel-air gas is mixed with the burned gas at the flame front. The results of one set of calculations made by Spalding agree with the picture reported here of the dependence of flame spreading rates on approach stream parameters. However, the infinite reaction rate assumption and the ad hoc nature of the treatment of the turbulent transport phenomena suggest that great care must be exercised in using the results of this type of calculation outside of the range of the parameters which fixed the constants in the model and which were used in checking the accuracy of the results.

Combustion efficiency in full-scale tests. The previous discussion concerned flame spreading rather than combustion efficiency. A large number of experiments have been carried out on full-scale systems in which the combustion efficiency has been measured as a function of parameters such as the inlet temperature, pressure, velocity, fuel-air ratio, the flameholder geometry, and, in at least one case, the combustion chamber length. Typical results are presented in Refs. 29–31. Because both the injection and vaporization processes and the stabilization and spreading processes are affected by changing the inlet conditions, the process affected by the changes cannot be distinguished.

However, Useller[30] has measured the effects of changing the combustor length while holding the other parameters constant. Some of his results are shown in Fig. 2.34, where combustion efficiency η_{AB} is plotted as a function of combustion chamber length downstream of the plane of the flameholder. The flameholders were 1.5 in. high V-gutters arranged in two concentric rings and with two crossed gutters on diameters serving as supports. Each flameholder occupied a part of duct with an equivalent duct height of very roughly 10 cm. The actual duct diameter was 62 cm and the inlet velocity

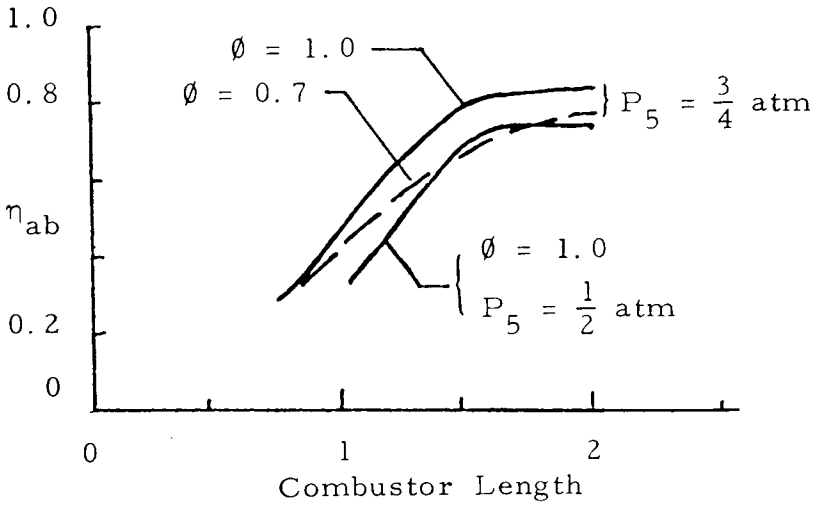

Fig. 2.34 Dependence of combustion efficiency on combustion chamber length (data from Ref. 30).

was 170 m/s. Note that all three curves of Figure 2.34 have a well-defined knee for chamber lengths of about 150 cm and that a further increase in combustor length has little effect on efficiency. Thus, the length-to-height ratios of roughly 15 are required to approach the maximum efficiency, a ratio that is unchanged as the pressure is dropped. This length ratio is slightly larger than one would expect from the smaller-scale flame spreading experiments discussed above. However, the complex flameholder shape makes direct comparison impossible. As noted above, the effects of pressure and fuel-air ratio may not be due to the influence of these parameters on the spreading process.

Summary. Simple one- and two-dimensional calculations are available that allow reasonably accurate predictions for the changes in the static and total pressure and the velocity across a region of heat addition in a constant-area duct. The inlet conditions leading to "choking" can also be predicted with reasonable accuracy. However, predictions cannot be made of the combustion chamber length required to produce a given level of combustion efficiency because the entrainment rate at a turbulent flame front is presently not understood.

A number of full-scale tests are available. However, because all components are subject to the same changes in operating parameters, it is not possible to determine whether or not changes in the spreading process produce the observed performance changes.

2.7 Nozzle and Fuel Control Systems

The afterburner control system has the primary function of controlling the flow of fuel to the afterburner and of keeping the pressure level in the afterburner at the desired value by controlling the nozzle throat area. The

control system is also responsible for carrying out the ignition process and supplying the various zones of the afterburner injection system with fuel in the proper sequence and at the proper rate during the starting sequence and, later, during steady operation and termination of thrust. The control must be able to receive data from the core engine control system from which it can determine the airflow rate to the afterburner and then set the required fuel flow rate to each injector zone. Although inlet temperature and velocity do not change a great deal, pressure levels may vary by factors of 10 and thus a wide range of fuel injection rates must be accommodated.

In addition to this control function, the control system must carry out a number of other functions. For example, the fuel lines and injector rings within the afterburner are heated to high temperatures when the afterburner is turned off by convective heat transfer from the high-temperature flow from the engine. If any jet fuel is left in these tubes, the high wall temperatures may cause the fuel to decompose and produce tar-like deposits. These deposits can clog the tubes and the small-diameter injector ports in the tube walls. This problem is usually avoided by venting the lines to a region at lower pressure than the combustion chamber when afterburner thrust is terminated. The resultant flow of gas cleans out the lines and leaves them empty. However, during the afterburner startup process, these lines must be filled again before the ignition process is initiated. The problem here is that in order to reduce the pressure pulse associated with ignition, the initial fuel flow rate is usually set at a value far below that required to fill the injector rings and supply lines in a reasonable length of time, i.e., in several seconds. Thus, the control system must be designed to fill the lines at a high flow rate and then to stop the flow so that no fuel is allowed to spill into the combustion chamber where the high temperatures in the core stream could cause autoignition.

Another important function of the afterburner control system is to maintain conditions at the turbine and fan outlets in an unchanged state so that the operation of these components will not be affected by the afterburner. This control function is particularly difficult to perform during the starting and stopping transients. To understand this problem, examine the mass flux equation for the afterburner nozzle under steady-state conditions and for a simple turbojet cycle. The mass flux at the throat of the nozzle throat can be written in terms of the total pressure and temperature P_{t_7} and T_{t_7}, the nozzle throat area A_n, the gas constant R, and specific heat ratio γ (e.g., see Secs. 2.19 and 5.11 of *Aerothermodynamics of Gas Turbine and Rocket Propulsion*). The result is

$$\dot{m}_7 = \frac{P_{t_7}}{\sqrt{T_{t_7}}} A_n \left[\sqrt{\frac{\gamma}{R}} \left(\frac{2}{\gamma + 1} \right)^{(\gamma+1)/2(\gamma-1)} \right] \tag{2.39}$$

Designating the fuel-air ratio f_{AB}, the mass flow at the inlet (station 5) can be related to that at the nozzle (station 7) by

$$\dot{m}_7 = \dot{m}_5 + \dot{m}_{\text{fuel}} = (1 + f_{AB})(\dot{m}_5) \tag{2.40}$$

Rewriting Eq. (2.39) in terms of the conditions at station 5 and using the definitions $\pi_{AB} = P_{t_7}/P_{t_5}$ and $\tau_{AB} = T_{t_7}/T_{t_5}$, Eq. (2.39) can be stated as

$$\dot{m}_7 = \left(\frac{\pi_{AB}}{\sqrt{\tau_{AB}}} A_n\right)\left\{\frac{P_{t_5}}{\sqrt{T_{t_5}}}\left[\sqrt{\frac{\gamma}{R}}\left(\frac{2}{\gamma+1}\right)^{(\gamma+1)/2(\gamma-1)}\right]\right\} \tag{2.41}$$

Let the condition for which the afterburner fuel-air ratio is zero be designated by a subzero suffix. Then, if conditions at station 5 are held fixed by the control system, $\dot{m}_5$ will be a constant and it can be shown from Eqs. (2.40) and (2.41) that

$$\frac{\dot{m}_7}{\dot{m}_{7_0}} = \frac{\dot{m}_7}{\dot{m}_5} = (1 + f_{AB}) = \frac{\left(\pi_{AB}/\sqrt{\tau_{AB}}\right) A_n}{\left(\pi_{AB_0}/\sqrt{\tau_{AB_0}}\right) A_{n_0}}$$

Consequently,

$$\frac{A_n}{A_{n_0}} \approx \left(\frac{\pi_{AB_0}}{\pi_{AB}}\right)\left(\sqrt{\tau_{AB}}\right)(1 + f_{AB}) \tag{2.42}$$

where $\tau_{AB_0} \equiv 1.0$ since the fuel flow and consequently the heat addition are zero when the afterburner is turned off. However, π_{AB_0} is not 1 since flameholder drag and wall losses will always reduce the total pressure. The nozzle throat area required to keep conditions at station 5 unchanged, when f_{AB}, π_{AB}, and τ_{AB} are changed due to afterburning, can be obtained from Eq. (2.42). This equation is only approximate because changes in γ and R due to heat addition, nonuniform velocity, etc., have been ignored.

A similar analysis can be used for a fan engine, but account must be taken of the differing conditions in the fan and core streams. To illustrate the changes required in nozzle throat area, data[29] are shown in Table 2.12 for a TF30-P-3 afterburner with an inlet pressure of about 1 atm. Equation (2.42) is applied to this fan cycle and averaged values of π_{AB} and τ_{AB} are used to evaluate the area changes. For an afterburner fuel-air ratio of 0.005 (typical of values used for ignition), the nozzle area must still be increased by about 13% and for $f = 0.04$ the increase is nearly 80%. The change is almost totally the result of large changes in τ_{AB}. Nozzle area changes of this magnitude must be effected within 5–10 s to keep the duration of the starting transient within reasonable limits. The nozzle actuation rate is usually the slowest and hence the limiting rate in the control process.

This example shows that large changes in the nozzle area must be controlled in order to maintain unchanged flow conditions at the turbine and fan exit stations. High precision is also required. For example, it is clear from Eq. (2.39) that under steady conditions, a 10% error in area A_n must be balanced by a 10% error of opposite sign in P_{t_7} when $\dot{m}_7$ and T_{t_7} are held fixed. A 10% increase in P_{t_7} and P_{t_5} would often be sufficient to stall

Table 2.12 Variation of Nozzle Throat Area A_{nt} and Afterburner Total Pressure and Temperature Ratios with Afterburner Fuel-Air Ratio f_{AB}

f_{AB}	τ_{AB}	$(\pi_{AB}/\pi_{AB})_0$	$(A_{nt}/A_{nt})_0$
0.0	1.0	1.0	1.0
0.01	1.5	0.98	1.26
0.02	1.90	0.96	1.46
0.03	2.30	0.94	1.57
0.04	2.50	0.93	1.77

Data from the TF30-P-3 afterburner (Ref. 29).

the fan stages and later the core compressor of the TF30 engine examined here. Hence, control of the exit area must be precise during both the starting transients and steady-state operation of the afterburner.

The afterburner control system can be organized in a number of ways concerning the primary functions of the fuel flow rate and nozzle throat area. One common technique is the double open-loop system. In this system, movement of the power lever by the pilot produces a demand in the control unit for a fuel flow rate and nozzle exit area. The control system changes the fuel flow rates and nozzle area according to specified schedules that must be very accurately matched and timed to avoid an excursion into burner pressure levels far from the desired values. As the term "open loop" implies, no feedback control is used, thus eliminating the dynamic interaction between the two control functions and any chance for control system instabilities.

A large number of alternate schemes are possible, including systems involving feedback. A number of existing systems are based on hydraulic control systems and digital systems are currently being studied. The use of closed-loop systems have been delayed by the lack of fast-response transducers that can perform well in the high-temperature environment of the afterburner.

In the selection of a control system, the designer must choose a device from a range bounded on one side by the very complicated systems that attempt to get the highest possible performance with the shortest delay times in all engine operating modes, and on the other by very simple systems with reduced average performance and longer delay times. See Ref. 31 for a detailed discussion of control systems and control system hardware.

A detailed design of the afterburner or any variable-area jet engine exhaust nozzle for supersonic flight is also beyond the scope of this chapter. A general discussion of this subject is given in Refs. 32 and 33. However, a few general remarks are made here concerning several important nozzle design problems.

The afterburner is often used during takeoff and at supersonic speeds. In the first regime, a high subsonic or sonic exit velocity may be desired and, in the second, a supersonic exhaust velocity will be necessary. Thus, the exhaust nozzle must be capable of operating both as a convergent and a convergent-divergent nozzle. This can be achieved in a simple design by several techniques. Consider first the system illustrated in Fig. 2.35 and described in detail in the caption. The nozzle consists of two basically coaxial convergent nozzles designed to have variable exit areas. The primary nozzle (e.g., No. 3) is made up of a large number of overlapping leaves hinged at their upstream end and sealed against each other to prevent leaks. Exit area variations by factors of 1.5–2 can be accomplished with this type of nozzle. The secondary nozzle (Nos. 5, 10, or 16) is a variable-area design of the same type. In the example shown here, it has a contoured inner surface. In other designs, it may be the same type as the primary nozzle.

The primary nozzle is responsible for fixing the throat area that controls the primary or afterburner mass flow rate and the secondary nozzle is used to fix the expansion ratio for the nozzle. The primary flow separates from the downstream lip of the primary nozzle and usually reattaches to the secondary nozzle. Reattachment is not necessary in the subsonic case (Fig. 2.35b), but is necessary in the supersonic case (Fig. 2.35a) if the secondary nozzle is to be effective in fixing the exit area.

A supersonic nozzle configuration with maximum primary throat area is shown in Fig. 2.35a and a sonic jet with minimum throat area is shown in Fig. 2.35b. The primary nozzle area changes between examples a and b by a factor of about two and the expansion ratio for example a is about 1.5.

In both Figs. 2.35a and 2.35b, a secondary gas stream (1) flows between the outer and inner cases of the engine. This flow serves several purposes in the nozzle. First, the secondary gas is usually much cooler than the primary and hence this stream can act as a film coolant for the secondary nozzle. Second, the secondary flow occupies a coaxial region about the primary flow and hence can be used to determine and control the exit area of the primary flow. For example, if the secondary flow of Fig. 2.35b were turned off, the effective exit area of the primary stream would be increased. Finally, the entrainment of fluid by the shear layer (e.g., see No. 6) removes fluid from the cavity between the secondary and primary nozzles. If no secondary flow were supplied to compensate for this effect, a strong recirculating flow would be set up to supply this entrainment material. This flow would reduce the nozzle thrust coefficient, increase heat-transfer rates, and contribute to the unsteadiness of the exhaust flow.

The motion required by the secondary nozzle flaps (Nos. 5 and 10) to accommodate the area changes necessary to produce optimum expansion ratios are large when both afterburning and supersonic flight speeds are contemplated. Some of this motion can be avoided by use of the "blow-in" doors shown in Fig. 2.35c as No. 14. When doors of this type are opened, a tertiary flow of ambient gas can enter the nozzle and form a stream coaxial with the secondary and primary flows. Control of the secondary and tertiary streams can again change the throat area of the primary stream and hence

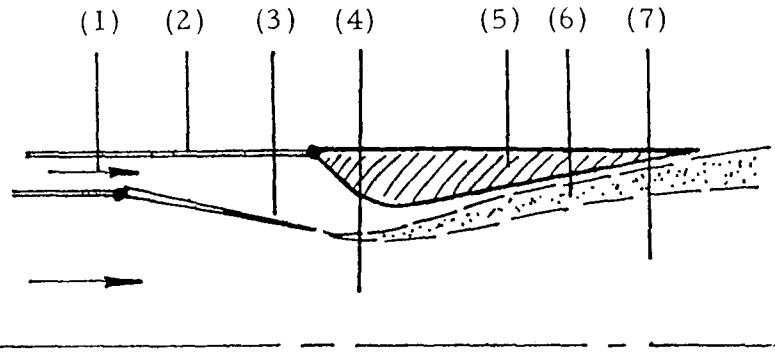

a) Supersonic nozzle configuration with afterburning: (1) secondary flow, (2) outer case of engine, (3) movable primary nozzle shown at maximum area, (4) primary flow, effective throat, (5) movable secondary nozzle shown at maximum exit area, (6) mixing layer between primary and secondary streams, and (7) supersonic primary flow.

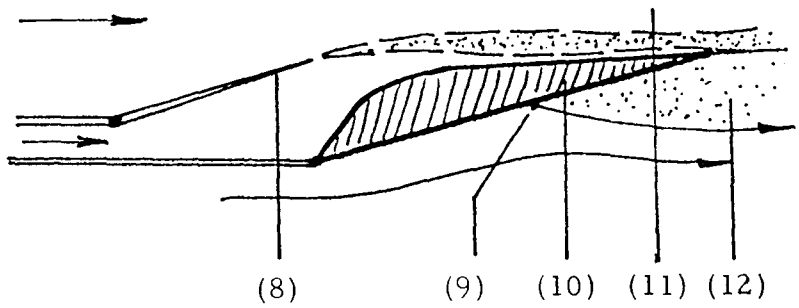

b) Subsonic nozzle configuration with no afterburning: (8) primary nozzle at minimum area, (9) separation point of external flow, (10) secondary nozzle at minimum area, (11) sonic primary stream, and (12) region of separated flow in external flow.

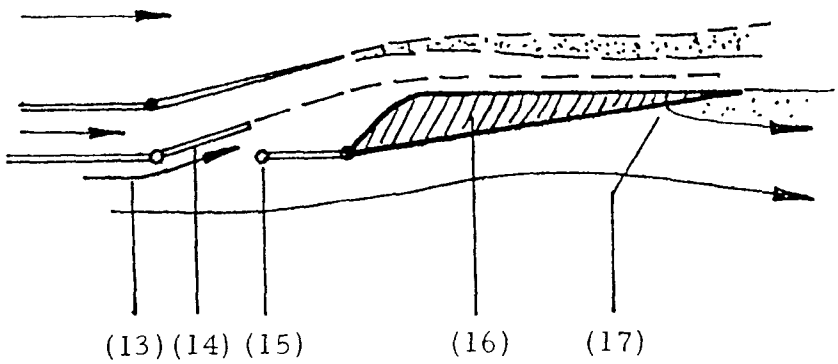

c) Subsonic nozzle configuration, not afterburning, and blow-in door in use: (13) tertiary flow of ambient gas into nozzle, (14) blow-in door and inflow configuration, (15) reversible hinge/latch, (16) movable secondary nozzle, and (17) separation point of external flow.

Fig. 2.35 Ejector nozzle configuration.

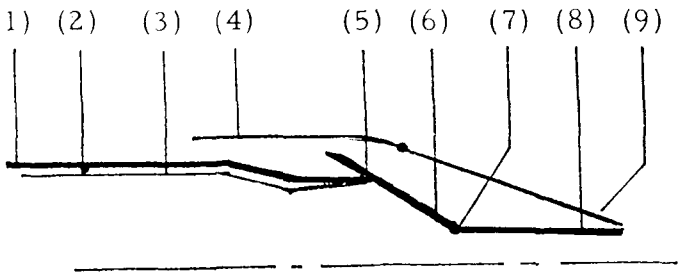

a) Subsonic nozzle configuration: (1) engine case, (2) cooling passage, (3) perforated cooling liner, (4) fixed outer cowl, (5) hinge for nozzle contraction, (6) nozzle contraction member, (7) hinge for nozzle expansion, (8) nozzle expansion member, and (9) movable outer cowl.

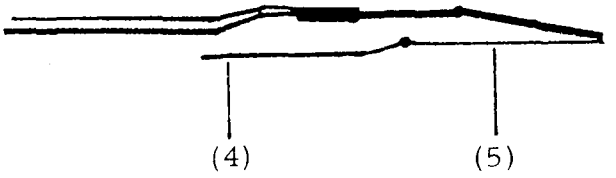

b) Supersonic nozzle configuration.

Fig. 2.36 Nozzle for Pratt & Whitney F100-PW-100 augmented turbofan engine.

reduce the motion required of the secondary nozzle flaps. The "blow-in" doors can also be used as blow-out doors, i.e., can be used as part of the control system to dump some of the secondary flow around the nozzle.

The secondary flow is usually made up of air used to cool the afterburner walls and it may also be drawn from the combustion chamber inlet flow or as far forward as the engine inlet. This nozzle is called an ejector nozzle because the primary stream can be used to pump a low-total-pressure secondary stream, just as the primary stream of an ejector pump is used to actuate a secondary flow.

A second nozzle type, shown in Fig. 2.36, does not use the ejector to minimize the motion of the secondary nozzle. In this case, a single flap (6 and 8) with two hinged joints (5 and 7) forms the nozzle contour. In Fig. 2.36a, a subsonic outlet is formed by maximum inward rotation of both members; in Fig. 2.36b, the outward rotation of both produces a larger throat area and a diverging nozzle at the exit. The nozzle is again constructed of overlapping leaves that must be sealed against each other. The throat area for this example changes by a factor of about two and the exit area ratio for the supersonic nozzle is about 1.5.

Another major area of concern for nozzle designers is the external drag of the nozzle and aft end of the propulsion pod or vehicle. Large changes in the nozzle exit area are required to accommodate the afterburner operation; consequently, it is difficult to make an aerodynamic design for the aft end of the engine that will not result in excessive drag during either afterburning or nonafterburning operation. For example, if the external surface is fixed to

accommodate the maximum nozzle exit area (see Fig. 2.35a), a large base drag will occur because of the flow separation on the "boat tail" of the nozzle when a smaller exit area is actually used (see Fig. 2.35b). The flow separation shown in Fig. 2.35b produces a significant increase in drag. Use of "blow-in" doors of Fig. 2.35c reduce the required motion of the secondary nozzle and hence decrease the boat-tail angle and the size and importance of the separated region (compare Figs. 2.35b and 2.35c). A similar problem arises with the nozzle shown in Fig. 2.36. Drag from this and other sources associated with the installation of the engines in vehicles or pods is an important problem for the nozzle designer.

Ejector nozzles are used on a number of engines in current operational use. Examples are the General Electric TF30-P-3 augmented turbofan engine used in the U.S. Air Force F111 airplane and the Olympus engine used in the Concord. In the latter case, the secondary nozzle flaps are also used as part of the thrust reverser system.[34]

The system illustrated in Fig. 2.36 is used on the Pratt & Whitney F100-PW-100 augmented turbofan engine used in the U.S. Air Force F-15 and F-16 fighter airplanes.

2.8 Complete Afterburner Systems

In this section the design details and performance for a typical afterburner system will be described. The afterburner selected for examination, the standard TF30-P-3 afterburner, is shown in Figs. 2.37 and 2.38. (The material discussed here is taken directly from Ref. 29.) This is the same system that was described briefly in the introduction. Conditions in the fan stream at the afterburner inlet were a velocity of about 95 m/s, a temperature of about 390 K, with conditions in the core or gas generator stream of about 220 m/s and 875 K, respectively. The bypass ratio was about 1 for these tests.

The flameholder system consists of three rings of V-gutters and a number of short radial segments of V-gutters. The gutters all have an included angle of 45 deg; the outer gutter ring and the radial gutters attached to it have a height of 5.1 cm and the inner two gutter rings have a height of 3.6 cm. The outer ring is held in place by a rod assembly, shown in Fig. 2.38, and the ring supports 18 radial V-gutters (which have their axis lying along a radius). The inner two rings are supported by six V-gutters, which are attached to the diffuser cone and are visible in Fig. 2.37. The projected area of all the flameholders was about 38% of the duct cross-sectional area, although the holders do not lie in a single plane. The combustion chamber is made up of an outer shell (the pressure vessel) and an inner shell (part of the cooling system). The inner shell is perforated at its upstream end and louvered at its downstream end. The narrow space between the shells acts as a cooling passage; the pressure at the upstream end of this passage is high enough compared to that in the combustion chamber to produce a flow of cool fan air through the passage and out into the combustion chamber through the holes and louvers. Flow in the passage cools by forced convection, and flow through the holes and louvers cools by a film-cooling effect. The holes in the upstream section have also been designed to produce

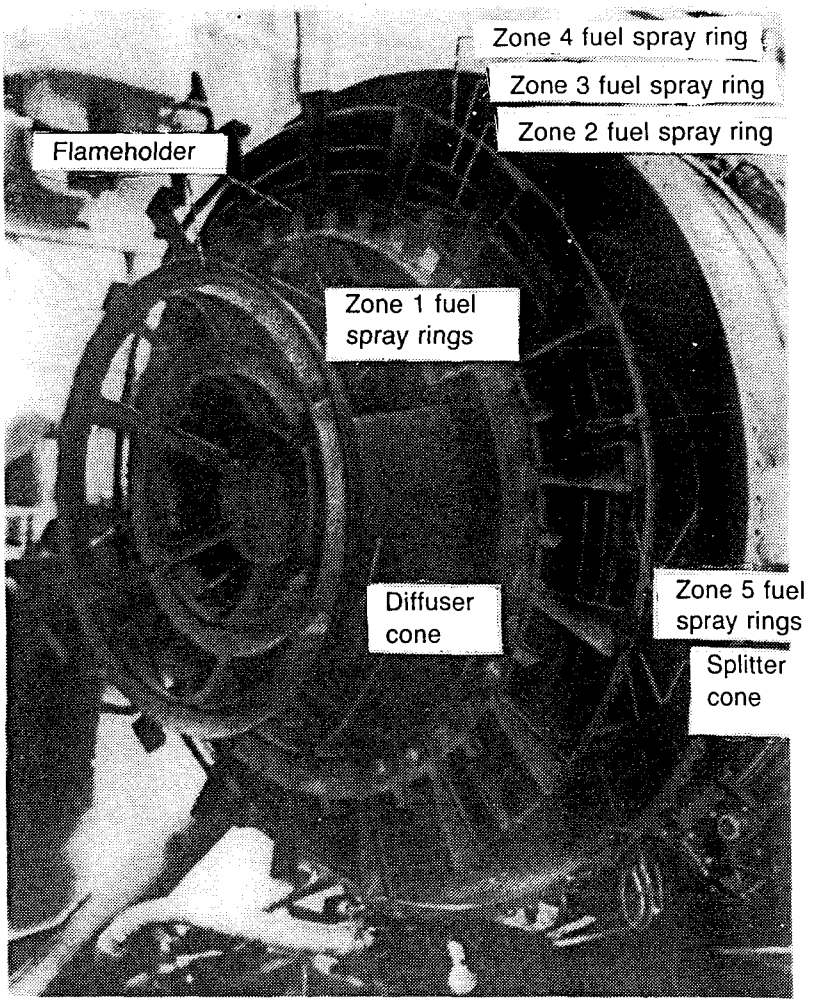

Fig. 2.37 Afterburner flameholders and fuel spray rings (from Ref. 29).

maximum damping of the acoustic disturbances at frequencies for which combustion instabilities have been observed in the chamber.

Fuel is injected into the flow through seven fuel spray rings arranged in five zones (see Figs. 2.37 and 2.38). Modulation of the fuel injection system is accomplished by an integrated afterburner/nozzle control system that simultaneously opens the nozzle and increases the fuel flow. These two operations are controlled by an open-loop hydraulic control mechanism that has no feedback information concerning the afterburner ignition or pressure level. In the present engine, fuel is first introduced to zone 1. Under low-pressure (i.e., high-altitude) operation, fuel is injected through one of the rings and, when the pressure level is above 124 kPa, the second ring is also used. These fuel spray rings lie close to the interface between the fan and the core gas streams and the fuel is primarily injected into the core or gas generator stream. If maximum power is required, the control system will start the fuel flowing to the other four zones at intervals of about 1.5 s.

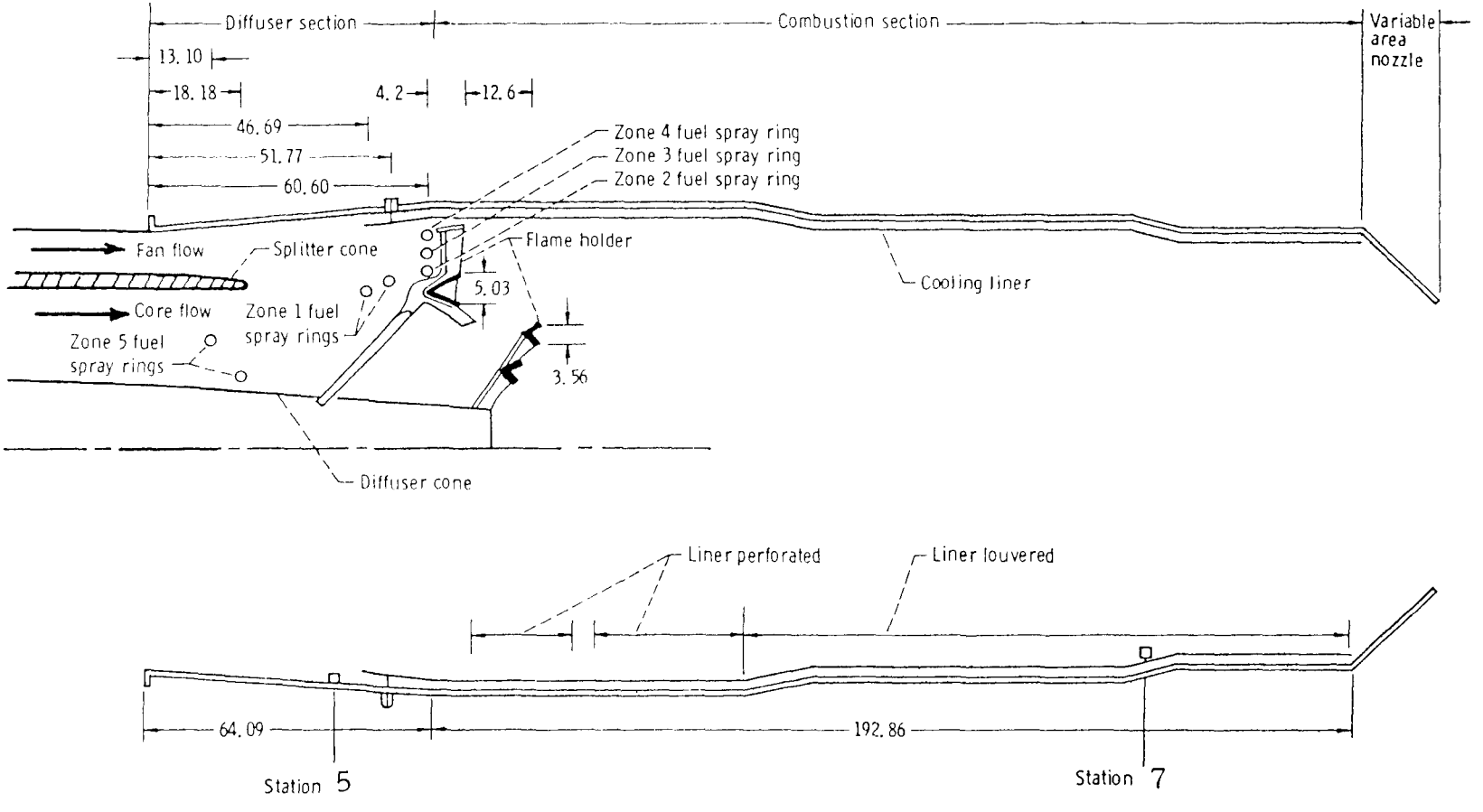

Fig. 2.38 Afterburner for TF30-P-3 augmented turbofan engine [all dimensions are in centimeters (from Ref. 29)].

Zones 2–4 are single-ring injectors that feed fuel to the fan stream. They are placed close to the radial flameholders to insure a supply of liquid fuel to the flameholders, which is then evaporated and fed to the recirculation in the manner suggested in Sec. 2.5.

Zone 5 is a double ring that supplies the core engine exhaust stream. These rings are placed about 65 cm upstream of the flameholders to give the fuel time (about 3 m/s) to vaporize before reaching the flame stabilization region.

Each of the three flameholder rings occupies an equivalent duct with a height of about 15 cm and a length of about 175 cm. Thus, the length-to-height ratio is very roughly 12, but this interpretation is complicated by the presence of numerous radial gutters. Thus, in the outer region (which has many radial holders), this ratio is much larger.

The transient processes that occur during a rapid advance of the throttle from a military power setting to a maximum power setting are shown in Fig. 2.39, which is taken directly from Fig. 9 of Ref. 29. The position of the power level controlled by the pilot is shown in Fig. 2.39a as a function of the time. It is moved forward from a military power level at time zero to maximum power at about 1.4 s. The nozzle control system opens the nozzle throat area according to the schedule shown in Fig. 2.39b.

The total fuel flow rate to the afterburner system is shown in Fig. 2.39c. Fuel flow starts at about 0.3 s after the power lever is moved to maximum power and ignition of the zone 1 system occurs at about 1.6 s. The time for ignition is deduced from the first rapid increase in static pressure at the nozzle exit (P_7) shown in Fig. 2.39d. As the fuel injection into each zone is started, the overall injection rate increases (Fig. 2.39c). The particularly large excursion in flow that peaks at about 2.6 s is an artifact of the measuring system and does not represent an increase in fuel delivered to the combustion chamber. It is caused by a change in fuel pumps from the afterburner hydraulic pump, used at very low fuel flow rates, to the main afterburner fuel pump. Note that the maximum fuel flow of the afterburner system is about 6000 kg/h, whereas that of the core engine is only about 1200 kg/h at the condition discussed here. The ignition of each zone is indicated by the pressure cusps appearing in the nozzle inlet pressure (Fig. 2.39d). The schedule for nozzle area changes (Fig. 2.39b) lags these ignition events by about 0.2 s, a mismatch producing the observed pressure disturbances.

For this particular throttle excursion, the only pressure pulse that can cause any trouble at the fan or compressor is the first pulse starting at 1.6 s. The large rise in nozzle inlet pressure (Fig. 2.39d) also appears at the fan exit station (Fig. 2.39e). This excursion increases the fan exit pressure above the steady-state stall line for the fan. In this example, the transient nature of the disturbance kept the fan from stalling. However, the disturbance was observed throughout the complete compressor system as a 5–10% excursion in pressure.

The steady-state characteristics for this afterburner are shown in Fig. 2.40 as a function of the afterburner fuel-air ratio and with the inlet pressure as a parameter. Afterburner total temperature τ_{AB} and pressure π_{AB} ratios are

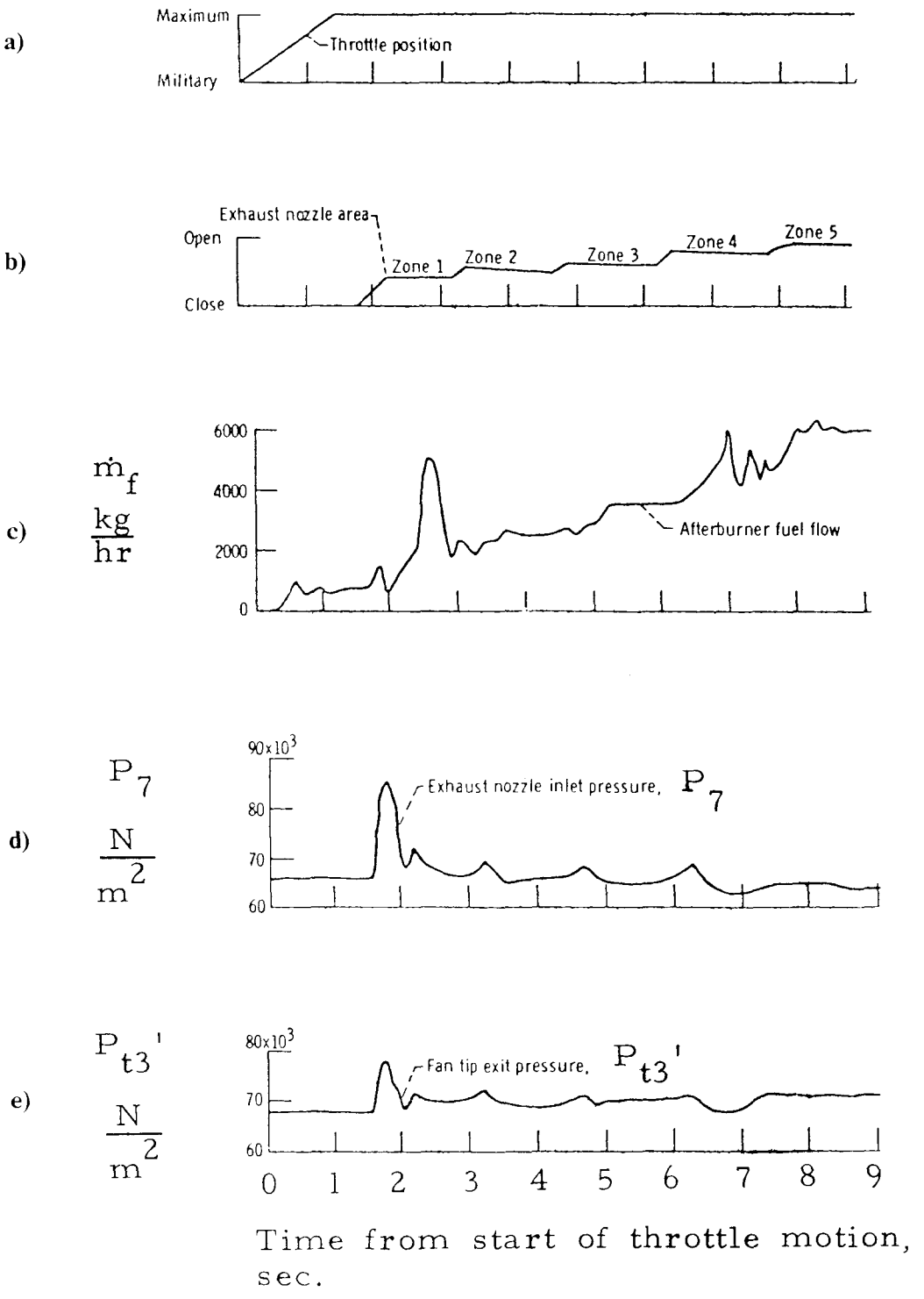

Fig. 2.39 Time history of engine and afterburner parameters during afterburner starting transient (data from Ref. 29).

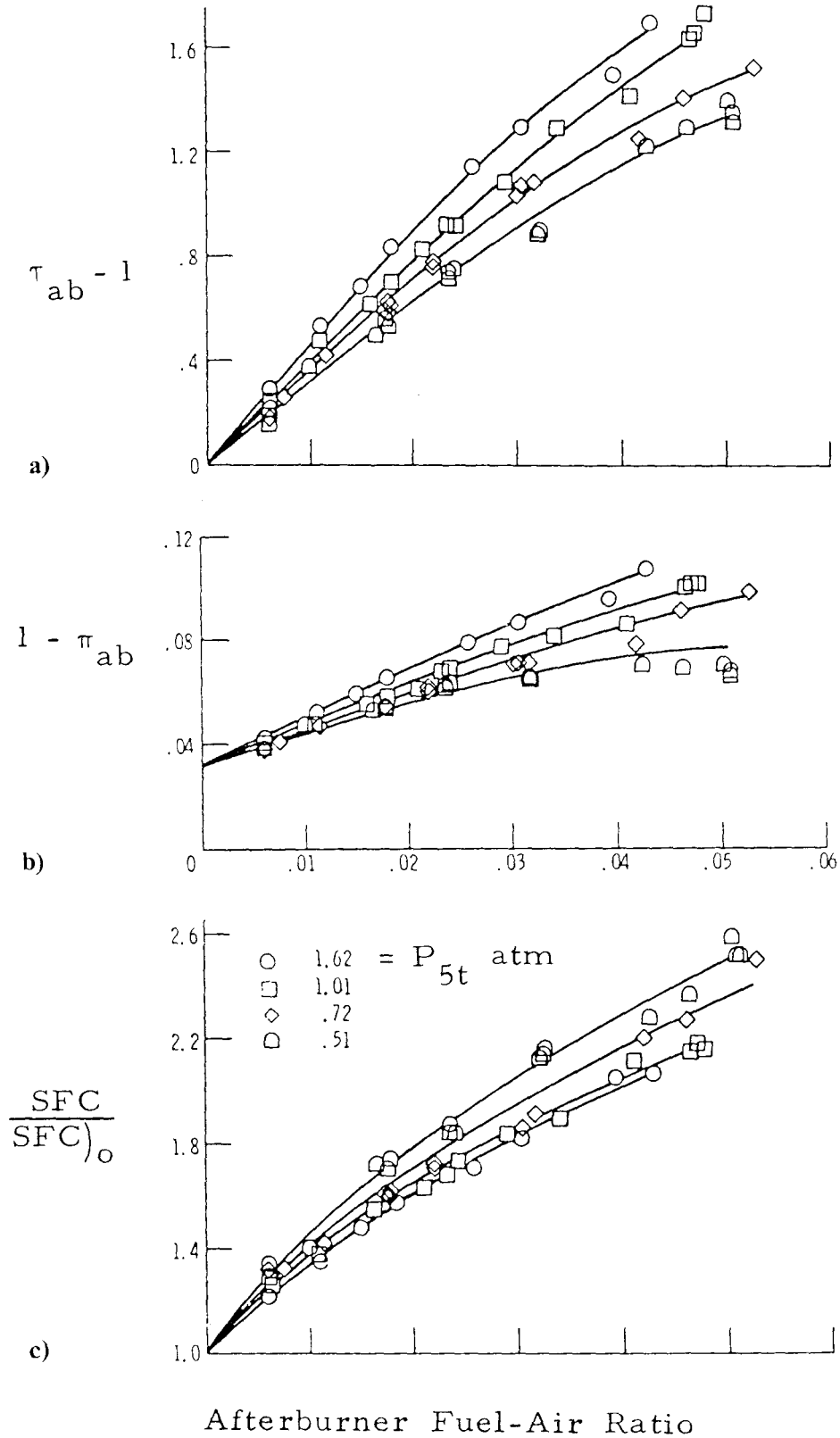

Fig. 2.40 Effect of fuel-air ratio and pressure on steady-state performance parameters (from Ref. 29).

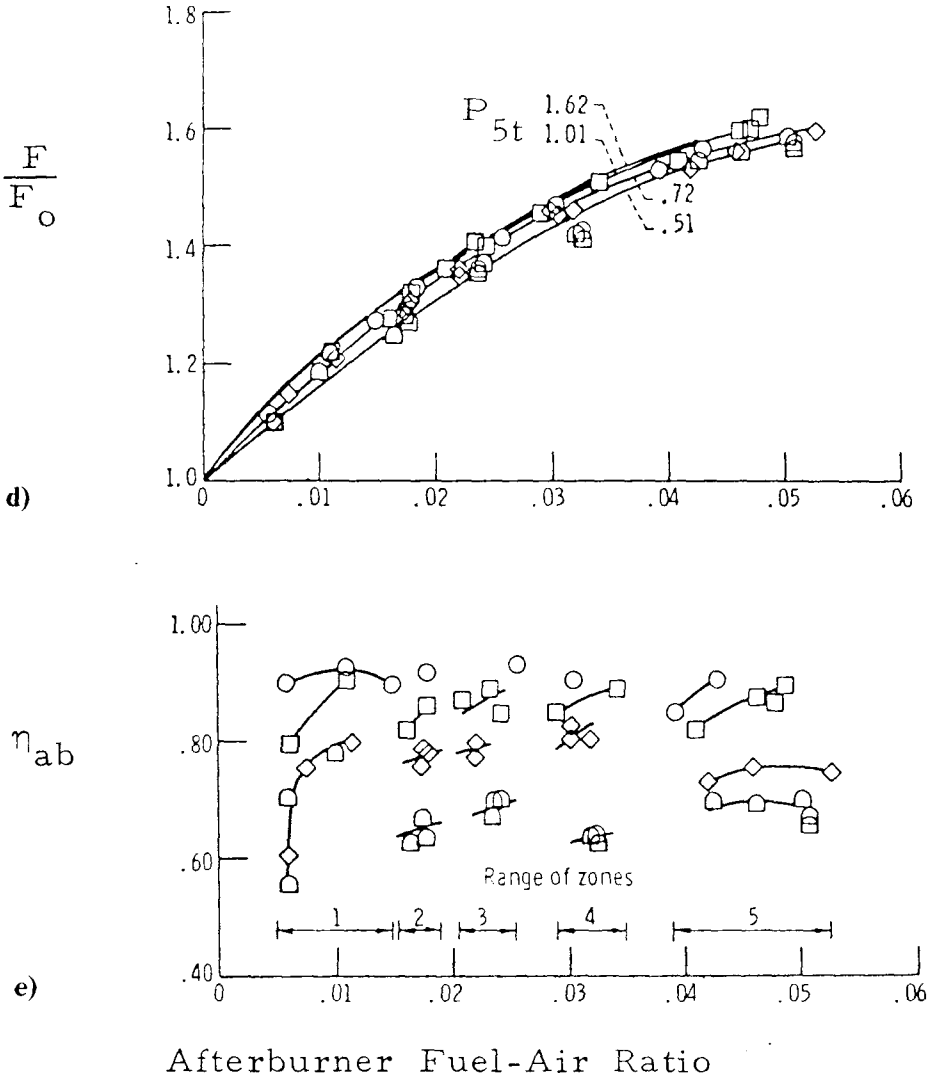

Fig. 2.40 (cont.) Effect of fuel-air ratio and pressure on steady-state performance parameters (from Ref. 29).

shown in Figs. 2.40a and 2.40b, and the specific fuel consumption (SFC) and thrust F are shown as ratios of their values with and without afterburning in Figs. 2.40c and 2.40d. Finally, the combustion efficiency is shown in Fig. 2.40e. The values presented here are based on measurements of the static pressure at stations 8 and 9 of Fig. 2.36, the total temperatures at station 8, and the measured thrust of the engine. Hence, the values are reasonable estimates, but they are not the result of detailed measurements made in the flow.

Figure 2.40 also shows the relationship between the five zones and the afterburner fuel-air ratios that can be achieved when each is activated. Thus, when zones 1–3 are operating, fuel-air ratios of 0.020–0.026 can be used. However, the value $\eta_{AB} = 0.80$ obtained for an inlet total pressure of 0.72

atm and a fuel-air ratio of 0.022 is the *overall* efficiency and is not associated with any particular zone. For inlet pressures greater than 1 atm, the combustion efficiency is uniform and greater than 85%.

Note that all of the steady-state parameters except the thrust drop off rapidly when the inlet pressure falls below about 1 atm.

It is comforting to find that relatively effective augmentation systems can be developed despite the lack of understanding of many very important features in the fuel preparation, stabilization, and flame spreading processes. However, the cost of developing these systems is greatly increased by such ignorance.

2.9 Combustion Instabilities

One of the principal problems associated with the development of high-performance augmentation systems is the suppression of the large-amplitude pressure oscillations often accompanying the combustion process. Disturbances of this type are called combustion instabilities and most appear to be driven by a coupling between an acoustic oscillation at one of the many resonant modes of the system and some step in the heat addition process.

The range of frequencies is very wide. Longitudinal modes with frequencies as low as 50–100 Hz have been identified and frequencies for radial or tangential modes can be as high as 5000 Hz. The frequency spectra of strong oscillations often exhibit 5–10 harmonics with amplitudes within 10 dB of the fundamental frequency. Also, peak-to-peak amplitudes of oscillations as large as 50% of the average pressure are observed and many systems regularly operate with oscillations with an amplitude of 5–10% of the average pressure.

In a typical situation, the amplitude of the oscillation at low fuel-air ratios is small and grows slowly as the fuel-air ratio is increased. Finally, near some critical fuel-air ratio, the amplitude grows very rapidly to a much larger value. The fuel-air ratio at the critical threshold and the rapidity with which the amplitude of the disturbance grows after the threshold has been passed often depend on the combustor inlet velocity, pressure, and temperature.

The oscillations reduce the life of combustion chamber apparatus or force an increase in weight to obtain a given life expectancy. The life of the components is decreased because of the fatigue produced by high-frequency oscillating forces and by the increased heat transfer that often accompanies the oscillations.

In analyzing problems of this type, it is helpful to consider the energy stored in a mode of oscillation of the gas in the afterburner system. This energy can be increased by a number of driving mechanisms and it can be decreased by a number of damping or attenuation mechanisms. In order to tune the driving processes to the natural resonant frequencies for acoustic disturbances, a feedback or coupling mechanism is required. A steady amplitude is reached when the attenuation and driving processes are in balance. In the following discussion, several of these damping, driving, and

coupling processes will be described, but no attempt will be made to give an overall description of a stability calculation.

Damping

There are a number of damping terms that arise at the inlet or inlets and outlet to the cavity. For example, when a traveling acoustic wave impinges on a nozzle, reflected and transmitted waves are generated. The energy carried through the nozzle by the transmitted wave is lost from the cavity and represents a loss. Similar losses can occur at the inlet. However, interactions at the inlet to the afterburner occur at interfaces defined by the turbine blades (in the case of the core stream) and by compressor blades (in the case of the fan stream). Interaction between the gas flowing through these components and the acoustic disturbances can produce either a loss or gain for the disturbance.

Additional sources of acoustic damping arise due to viscous interactions involving the boundary layers on the walls and the drag forces on bluff bodies such as flame stabilizers, fuel injection rings, and support struts.

In addition, resonators built into the combustion chamber walls can be used to greatly increase the damping rates. The cooling liner shown in Fig. 2.38 is an example of the application of this technique and it will be described briefly here because this technique is commonly used to control high-frequency disturbances. The liner has been perforated in the region close to the flame stabilizers. When there is no mean flow across these holes, a pressure oscillation in the combustor and close to the liner will produce a pressure difference across the holes that will drive gas from the combustion chamber into the cooling passage when the combustor pressure is high and suck gas back into the combustion chamber when the pressure is low. This process feeds energy from the acoustic mode into the kinetic energy of the gas that flows through the openings and is subsequently dissipated. This process removes energy from the acoustic mode and hence represents a damping of the oscillation.

The rate at which energy is removed from a particular mode of oscillation can be maximized by selecting the proper hole size and volume for the cooling passage associated with each hole, so that the natural frequency for the cavity is close to that of the acoustic mode. For example, Helmholtz showed that a cavity with a narrow neck had a natural frequency that could be analyzed approximately by treating the compressible gas in the cavity as the spring and the mass of gas in the narrow throat as the mass in a spring-mass system. The natural frequency for the cavity is approximately $a\sqrt{A/L_eV_e}$ where a is the speed of sound, A the cross-sectional area of the neck, L_e the effective length of the narrow neck (which in this thin-wall case is roughly the hole diameter), and V_e the volume of the cavity associated with each hole. By proper selection of A, L_e, and V_e the cavity can be designed so that its natural frequency is close to the frequency of the combustion instability and thus maximize the energy loss rate or the damping. Damping can be further increased by allowing fluid to flow from

the liner cooling passage into the combustion chamber. Fortunately, this flow direction is in agreement with that required to produce the best cooling effect.

Perforated cooling liners are often used successfully to suppress high-frequency oscillations. However, the effectiveness decreases for frequencies below 1000 Hz and devices of this type are almost impossible to implement for the lowest frequencies encountered in augmented turbofan systems because of constraints on the allowable volume of the cavity.

A number of numerical computer codes have been developed to analyze acoustic fields inside arbitrarily shaped cavities. Resonant frequencies and damping due to wall friction effects can be calculated by these codes. However, the effects of regions with large temperature differences and high Mach numbers have not yet been included in the codes. A discussion of calculations of this type is given in Ref. 35, which deals primarily with combustion instabilities in solid- and liquid-propellant rockets.

The physical principals required to formulate the description of the acoustic field in a cavity, which contains a gas with large temperature and mean flow variations, are well understood and the properties of the acoustic field can be calculated as accurately as required (given sufficient effort and funds). Most of the damping characteristics can also be treated with reasonable accuracy for simple modes and combustor configurations, the physical processes of which are well understood. The same statement cannot be made for the driving and coupling mechanisms discussed in the following paragraphs.

Driving Mechanisms

Consider a one-dimensional compressible gas stream flowing in a constant area duct and let heat be added uniformly at a rate $\dot{Q}$ over some finite length of the duct. The heat addition process will produce an acceleration of the gas and a drop in the pressure according to the relationships derived in Sec. 2.6. However, as long as $\dot{Q}$ is independent of time, no acoustic field will be produced.

When $\dot{Q}$ has a periodic component, say $\dot{Q} = (\dot{Q}_0 + \varepsilon \sin \omega t)$ and $\varepsilon \ll \dot{Q}_0$, a pair of traveling acoustic waves will be generated, one propagating upstream and the other downstream. The strength of the waves will depend on ε, $\dot{Q}_0$, and the Mach number at the heat addition station. If these waves are in phase with an acoustic disturbance already present in the duct, the fluctuating heat addition will drive the disturbance, i.e., will put energy into the acoustic mode.

The fluctuating heat input rate also produces a fluctuating entropy or total temperature in the gas flowing through the heater that is convected downstream with the flow. Marble and Candel[36] have pointed out that acoustic disturbances are created when a flow containing periodic entropy variations of this type passes through a region containing pressure gradients. Thus, if a nozzle is placed at the downstream end of the duct discussed above, acoustic disturbances will be generated at the nozzle by the entropy

fluctuations produced farther upstream by the periodic variations in heat input. In the present example, the nozzle will generate a second pair of traveling waves, one moving upstream and the other downstream. The nozzle will also act as a partial reflector of the traveling waves produced directly in the heat addition process and the reflected wave will also move back upstream. The acoustic disturbances travel downstream to the nozzle at a velocity that is the sum of the local speed of sound a and the flow speed u [i.e., $(u + a)$], whereas the entropy fluctuations are carried by the flowing gas and travel at a speed u. Hence, the phase difference in the two traveling waves moving upstream from the nozzle will depend on the distance between the heat addition region and the nozzle and also on the Mach number of the flow. If the phase difference is close to a multiple of 2π, the waves originating at the nozzle will reinforce each other.

In summary, any fluctuation in the heat input rate to a gas flow will directly produce acoustic disturbances and variations in the entropy of the flowing gas. When these entropy variations are convected through a pressure gradient, a second acoustic disturbance is produced. The interaction of the traveling waves produced in this process will depend on the geometry and Mach number of the flow.

Coupling

The most difficult step in the stability calculations or afterburner systems is the description of the process by which acoustic disturbances interact with the combustion process to produce fluctuations in the heat input rate. This coupling process must be understood before any meaningful stability calculations can be made.

A large number of coupling mechanisms are present in the afterburner system. These may be conveniently grouped under the heading of fuel preparation, flame stabilization, and flame spreading mechanisms.

Acoustic disturbances can interact with each step in the fuel preparation process. Thus, the rates of fuel injection, atomization, and vaporization processes can each be affected by local pressure and velocity fluctuations. For example, the rate of fuel flow at the injector orifice is proportional to the square root of the pressure drop across the orifice and hence will be affected by fluctuations in the gas pressure at the injector due to an acoustic disturbance in the duct. The fluctuations in mass flow and pressure at the upstream side of the orifice produced by this interaction must be treated as matching conditions that will specify the nonsteady operation of the whole fuel feed system (a system that will also have a set of resonant frequencies). For simplicity, consider a system with perfect atomization and vaporization. The resulting fluctuation in fuel injection rate at the injector will produce a fluctuation in the fuel-air ratio at the flame front after a time delay, which is fixed by the time required for the fuel to be carried from the injector to the flame front. The variation in fuel-air ratio will produce a fluctuation in the heat release rate at the flame front and when the acoustic disturbance in the duct is in phase with this variation of heat release, it will be driven by

this process. If the two disturbances are sufficiently out of phase, the disturbance in the duct will be damped. Analysis of the reaction of feed systems to pressure oscillations of the type described here are presented in detail in Ref. 35.

Several coupling mechanisms associated with the flame stabilization region have been suggested, one of which is described here in some detail to illustrate this class of coupling processes. This discussion is drawn from the work of Marble and Rogers[37] and Barker.[38] Consider the two-dimensional flow shown in Fig. 2.41 and assume that a strong transverse oscillation is present downstream of the flameholder. The smallest resonant frequency for a transverse mode is that corresponding to a plane wave moving vertically and having a pressure node at the axis and a maximum pressure amplitude at the walls (e.g., Fig. 2.41c). The corresponding fluctuation amplitude for the vertical velocity is also shown in this figure. The frequency f of this oscillation will be $f = \bar{a}/2H$, where H is the height of the channel and $\bar{a}$ an average speed of sound in the gas.

In this flow, the strong transverse wave interacts with the shear layers on either side of the flameholder to produce a regular train of vortices that are shed alternately from each lip of the flameholder in the manner suggested in Fig. 2.41a. Vortices are shed in an antisymmetric mode, in keeping with the antisymmetric shape of the velocity and pressure perturbations, and they grow rapidly as they convect downstream.

The coupling mechanism in this example appears to be the triggering of these vortices, which in turn are responsible for the unsteady heat addition that drives the oscillations. Rogers and Marble[37] suggested that the vortices sweep unburned gas deep within the recirculation zone and that this combustible material will burn rapidly after a short time delay. In this situation, the time delay associated with the entrainment of combustible fluid is short and the delay is primarily fixed by the chemical reaction. The entrained material will start to react τ_d s after the vortex is shed and the heat addition rate will receive a sharp pulse at that time. When τ_d is close to an integral multiple of the period of the resonant frequency for the acoustic disturbance, $2H/\bar{a} = 1/f$, the oscillation will be driven. In the present case, driving at the frequency of the first mode was strong enough to produce a large-amplitude oscillation. However, oscillations at higher harmonics were not observed.

In this example, the instability was not present at low values of the fuel-air ratio and started at a well-defined value when the fuel-air ratio was increased. This threshold value ϕ_s was found to vary with mixture temperature and fuel type. In both instances, the authors were able to predict the observed variations in ϕ_s by using the model suggested above. In making these predictions, values of the delay time τ_d were found by using the assumption that τ_d scaled with τ_c, the characteristic time described in the flame stabilization discussion in Sec. 2.5. Some of the experimental values of τ_c used in this process are shown in Fig. 2.15. The sharp boundary for ϕ_s is a result of the very rapid change of τ_d with the fuel-air ratio, which is inferred from the variation of τ_c shown by the data of this figure. In their

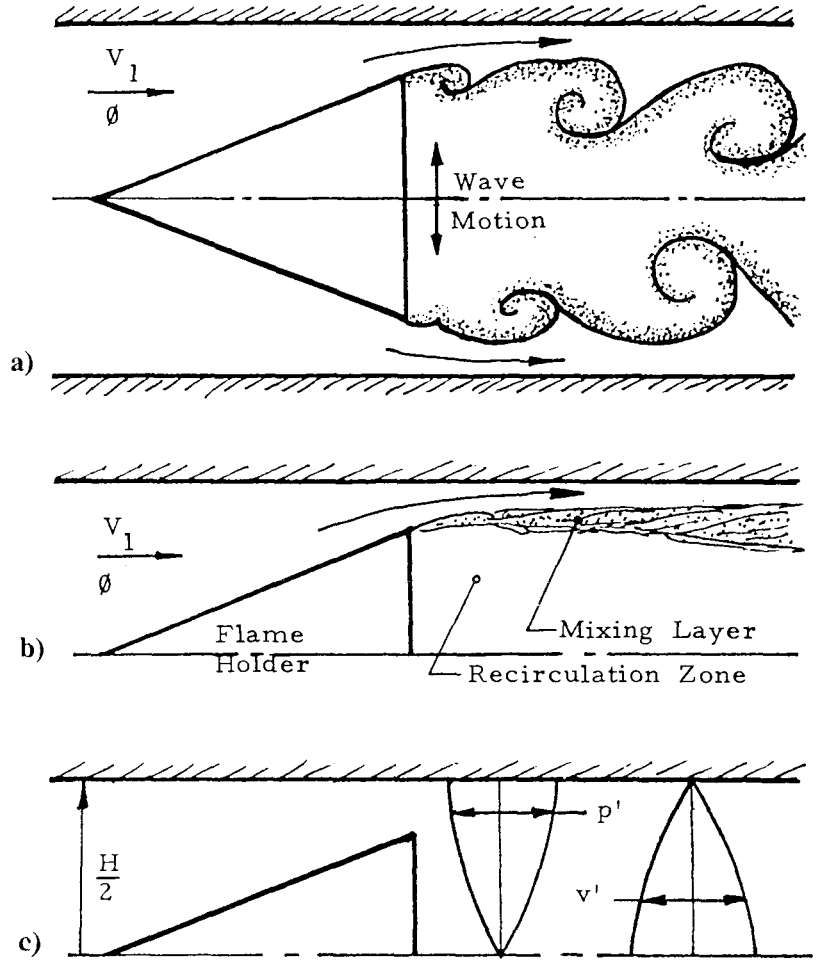

Fig. 2.41 Flame front geometry during unstable (a) and stable (b) combustion; mode shapes for perturbations in pressure p' and transverse velocity v'.

example, the resonant frequency was about 4000 Hz, which suggests that τ_d should be close to 0.25 ms (if the heat release rate rises after the first cycle of the oscillation). Thus, values of τ_d and of τ_c are almost equal (see Fig. 2.15).

The successful application of perforated liners for the suppression of high-frequency combustion instabilities has very often involved the use of liner perforations in the immediate neighborhood of the flame stabilization region. This suggests that the flame stabilization region is very important in coupling high-frequency disturbances to the heat addition process and that one important mechanism is the one described above.

Because of the large-scale inhomogeneities present in the flame spreading region, one would expect that coupling between the heat release and acoustic disturbances would be possible in this region too. However, no experimental evidence for such processes has yet been developed.

Finally, any nonsteady heat release occurring in the combustor will react with the nozzle to produce longitudinal disturbances. Note that the ampli-

tude of these disturbances can be very large. For example, for wavelengths that are long compared to the nozzle inlet length and an inlet Mach number of 0.8, a total temperature fluctuation with an amplitude of 10% will produce an upstream propagating wave with an amplitude of about 5% of the mean pressure.

In summary, some of the aspects of the combustion instability problem and a few of the many possible driving, damping, and coupling mechanisms have been described. Given the many resonant acoustic modes, the many possibilities for coupling, the high rate of heat release per unit volume, and the small amount of energy required to drive a large-amplitude oscillation, it is surprising that any afterburner system operates without acoustic disturbances.

Supplementary Reading

The purpose of this section is to call attention to a few reference works that will give the reader a different perspective on some of the material covered in this chapter and, in several cases, provide a source of more detailed information.

A number of general reviews of jet propulsion systems appeared in the late 1950s and early 1960s. The material presented in these volumes is dated, but in many cases is still of interest today and still covers many topics as adequately as they can be covered now. Two volumes from the *High Speed Aerodynamics and Jet Propulsion* series are of interest. Volume XII, edited by Lancaster contains information on augmentation systems and also ramjet systems which are pertinent. Volume XI, edited by Hawthorne and Olson, contains a series of articles covering all the engine components and includes a discussion of flame stabilization in heterogeneous flows. A brief introduction to the Soviet work on combustion problems in gas turbines is given in the translation of the book by Zuyev and Skubachevskii. Material relevant to afterburners is discussed in the chapters on ramjet engines and reheat combustion chambers.

A good report on current diffuser research work is that of Dolan and Runstadler. They present a large body of data on conical diffusers covering the effects of inlet Mach number for the whole subsonic range, a wide range of inlet boundary-layer thicknesses, and diffuser geometry including area ratio, length, and divergence angle.

The specific problems concerning ignition in afterburner systems are not treated in detail in any combustion texts. A detailed treatment of a number of experiments concerned with ignition are presented by Lewis and von Elbe, who also discuss other material concerning flame stabilization and flame spreading.

The generation of fuel sprays and their vaporization and combustion is still a topic of vigorous research. Analytic treatments are available in the text by Williams and the *Fourteenth and Fifteenth Symposia (International) on Combustion* contain interesting collections of papers given at sessions on heterogeneous combustion. Beer and Chigier also discuss relevant material,

although their chief interest is in industrial furnaces rather than aircraft engines.

Alternate views of the flame stabilization process are presented by Lewis and von Elbe and by Beer and Chigier.

Finally, five journals are particularly useful sources of information: the *AIAA Journal* of the American Institute of Aeronautics and Astronautics; *Combustion and Flame* (published by Elsevier, New York); and *Combustion Science and Technology* (published by Gordon and Breach, New York); and translations of two Soviet journals, *Combustion, Explosion and Shock Waves* (translated and published by Consultants Bureau, New York) and *Soviet Aeronautics* (translated and published by Elsevier, New York).

Beer, J. M. and Chigier, N. A., *Combustion Aerodynamics*, Halsted Press Div., John Wiley & Sons, New York, 1972.

Dolan, F. X. and Runstadler, P. W. Jr., "Pressure Recovery Performance of Conical Diffusers at High Subsonic Mach Numbers," NASA CR-2299, Aug. 1973.

Fifteenth Symposium (International) on Combustion, The Combustion Institute, Pittsburgh, Pa., 1974.

Fourteenth Symposium (International) on Combustion, The Combustion Institute, Pittsburgh, Pa., 1973.

Hawthorne, W. R. and Olson, W. T. (eds.), "Design and Performance of Gas Turbine Power Plants," *High Speed Aerodynamics and Jet Propulsion*, Vol. XI, Princeton University Press, Princeton, N. J., 1960.

Lancaster, O. E. (ed.), "Jet Propulsion Engines," *High Speed Aerodynamics and Jet Propulsion*, Vol. XII, Princeton University Press, Princeton, N. J., 1959.

Lewis, B. and von Elbe, G., *Combustion Flames and Explosions of Gases*, 2nd ed., Academic Press, New York, 1961.

Williams, F. A., *Combustion Theory*, Addison-Wesley Publishing Co. Reading, Mass., 1965.

Zuyev, V. S. and Skubachevskii, L. S., *Combustion Chambers for Jet Propulsion Engines* (translation), The MacMillan Co., New York, 1964.

References

[1]Johnson, R. L. and Cullom, R. R., "Altitude Test of Several Afterburner Configurations on a Turbofan Engine With a Hydrogen Heater to Simulate an Elevated Turbine Discharge Temperature," NASA TP 1068, 1977.

[2]Schetz, J. and Padhye, A., "Penetration and Breakup of Liquids in Subsonic Airstreams," *AIAA Journal*, Vol. 15, Oct. 1977, pp. 1385–1390.

[3]Ingebo, R. D. and Foster, H. H., "National Advisory Committee for Aeronautics," NACA TN 4087, Oct. 1957.

[4]Haddock, G. H., "Flame-Blowoff Studies of Cylindrical Flame Holders in Channeled Flow," Jet Propulsion Laboratory, Pasadena, Calif., Progress Rept. 3-24, May 14, 1951.

[5]Zukoski, E. E. and Marble, F. E., "The Role of Wake Transition in the Process of Flame Stabilization on Bluff Bodies," *Combustion Researches and Reviews 1955*, Butterworths Scientific Publications, London, 1955.

[6]Zukoski, E. E. and Marble, F. E., "Experiments Concerning the Mechanism of Flame Blowoff from Bluff Bodies," *Proceedings of the Gas Dynamics Symposium on Aerothermochemistry*, Northwestern University Press, Evanston, Ill., 1955.

[7]Wright, F. H., "Bluff Body Flame Stabilization: Blockage Effects," *Combustion and Flame*, Vol. 3, 1959, p. 319.

[8]Broman, G. E. and Zukoski, E. E., "Experimental Investigation of Flame Stabilization in a Deflected Jet," *Eighth Symposium (International) on Combustion*, The Williams and Wilkins Co., Baltimore, 1960, p. 944.

[9]Cornell, W. G., "The Flow in a Vee-Gutter Cascade," *Transactions of ASME*, Vol. 78, 1956, p. 573.

[10]Wright, F. H., "Multiple Flame Holder Arrays: Flame Interactions," *ARS Journal*, Feb. 1959.

[11]Potter, A. E. Jr. and Wong, E. L., "Effect of Pressure and Duct Geometry on Bluff Body Flame Stabilization," NASA TN 4381, Sept. 1958.

[12]Mullins, B. P., "A Spontaneous Ignition Theory of Combustion Intensity and Combustion Stability Behind a Baffle," *Combustion Researches and Reviews 1955*, Butterworths Scientific Publications, London, 1955.

[13]Mironenko, V. A., "The Use of Thermal Ignition Theory to Determine General Conditions for Flame Stabilization by Means of a Bluff Body," *Izvestiya VUZ, Aviatsionnaya Tekhnika*, No. 1, 1966, pp. 140–145 (translation).

[14]Solokhin, E. L. and Mironenko, V. A., "Stable Combustion Limits in GTE Reheat Combustion Chambers," *Izvestiya VUZ, Aviatsionnaya Tekhnika*, Vol. 15, No. 1, 1972, pp. 135–141 (translation).

[15]Hottel, H. C., Williams, G. C., Jensen, W. P., Tobey, A. C., and Burrage, P. M. R., "Modeling Studies of Baffle-Type Combustors," *Ninth Symposium (International) on Combustion*, Academic Press, New York, p. 923.

[16]Kosterin, V. A., Dudin, L. A., Motylinskii, I. P., Khismatullin, A. Ya., and Gilyazov, M. Sh., "Correlation of Experimental Data on the Limits of Flame Stabilization," *Izvestiya VUZ, Aviatsionnaya Tekhnika*, Vol. 11, No. 3, 1968, pp. 59–66 (translation).

[17]Marshall, R. L., Canuel, G. E., and Sullivan, D. J., "Augmentation Systems for Turbofan Engines," *Cranfield International Symposium Series*, Vol. 10, Pergamon Press, Ltd., London, 1968, p. 129.

[18]Brown, G. L. and Roshko, A., "On Density Effects and Large Structure in Turbulent Mixing Layers," *Journal of Fluid Mechanics*, Vol. 64, Pt. 4, 1974, pp. 775–816.

[19]Williams, G. C., Hottel, H. C., and Scurlock, A. C., "Flame Stabilization and Propagation in High Velocity Gas Streams," *Third Symposium on Combustion and Flame and Explosion Phenomena*, The Williams and Wilkins Co., Baltimore, 1949, p. 21.

[20]Wright, F. H. and Zukoski, E. E., "Flame Spreading from Bluff Body Flame Holders," *Eighth Symposium (International) on Combustion*, The Williams and Wilkins Co., Baltimore, 1960, p. 933.

[21]Solntsev, V. P., "Stabilization of a Flame and Development of the Process of Combustion in a Turbulent Stream," edited by G. M. Gorbunov, Oborongiz, Moscow, 1961, p. 75.

[22]Lefebvre, A. H. and Reid, R., "The Influence of Turbulence on the Structure

and Propagation of Enclosed Flames," *Combustion and Flame*, Vol. 10, 1966, p. 355.

[23]Wohl, K., Shore, L., Von Rosenberg, H., and Weil, C. W., "The Burning Velocity of Turbulent Flames," *Fourth Symposium (International) on Combustion*, The Williams and Wilkins Co., Baltimore, 1953, p. 620.

[24]Thurston, D. W., "An Experimental Investigation of Flame Spreading from Bluff Body Flameholders," Thesis, California Institute of Technology, Pasadena, 1958.

[25]Tsien, H. S., "Influence of Flame Front on the Flow Field," *Journal of Applied Mechanics*, June 1955, p. 188.

[26]Fabri, J., Siestrunck, R., and Foure, C., "On the Aerodynamic Field of Stabilized Flames," *Fourth Symposium (International) on Combustion*, The Williams and Wilkins Co., Baltimore, 1953, p. 443.

[27]Brown, G. L., "The Entrainment and Large Structure in Turbulent Mixing Layers," *Fifth Australasian Conference on Hydraulics and Fluid Mechanics*, University of Canterbury, Christchurch, New Zealand, 1974, p. 352.

[28]Spalding, D. B., "The Spread of Turbulent Flames Confined in Ducts," *Eleventh Symposium (International) on Combustion*, The Combustion Institute, Pittsburgh, Pa., 1967, p. 807.

[29]McAulay, J. E. and Abdelwahab, M., "Experimental Evaluation of a TF30-P-3 Turbofan Engine in an Altitude Facility: Afterburner Performance and Engine-Afterburner Operating Limits," NASA TN D-6839, July 1972.

[30]Useller, J. W., "Effect of Combustor Length on Afterburner Combustion," *Combustion and Flame*, Vol. 3, 1959, p. 339.

[31]Robinson, K., "Afterburning Regulation Concepts," *Power Plant Controls for Aero-Gas Turbine Engines*, AGARD CP 151, Feb. 1975, p. 1074.

[32]Carrierre, P., "Exhaust Nozzles," *Supersonic Turbo-Jet Propulsion Systems and Components*, AGARDograph 120, 1969, pp. 287–379.

[33]Beheim, M. A. et al., "VIII: Supersonic Exhaust Nozzles," *Aircraft Propulsion*, NASA SP-259, Nov. 1970, p. 233.

[34]Devriese, J. and Young, P. H., "Olympus in Concorde," *Aeronautical Journal*, Vol. 76, No. 774, Dec. 1972, pp. 683–694.

[35]Harrje, D. T. (ed.), *Liquid Propellant Rocket Combustion Instability*, NASA SP-194, 1972.

[36]Marble, F. E. and Candel, S. M., "Acoustic Disturbance from Gas Non-Uniformities Convected Through a Nozzle," *Journal of Sound and Vibration*, Vol. 55, No. 2, 1977, pp. 225–243.

[37]Rogers, D. E. and Marble, F. E., "A Mechanism for High-Frequency Oscillation in Ramjet Combustors and Afterburners," *Jet Propulsion*, Vol. 26, June 1956, pp. 456–462.

[38]Barker, C. L. R., "Experiments Concerning the Occurrence and Mechanism of High Frequency Combustion Instability," Thesis, California Institute of Technology, Pasadena, 1958.